Behavioral/Cognitive

Rewarding Capacity of Optogenetically Activating a Giant GABAergic Central-Brain Interneuron in Larval *Drosophila*

Nino Mancini,[1] Juliane Thoener,[1] Esmeralda Tafani,[1] Dennis Pauls,[2] Oded Mayseless,[4] Martin Strauch,[5] Katharina Eichler,[6] Andrew Champion,[7,8] Oliver Kobler,[9] Denise Weber,[3] Edanur Sen,[1] Aliće Weiglein,[1] Volker Hartenstein,[10] Charalampos-Chrysovalantis Chytoudis-Peroudis,[11] Tihana Jovanic,[11] Andreas S. Thum,[3] Astrid Rohwedder,[3] Michael Schleyer,[1] and Bertram Gerber[1,12,13]

[1]Leibniz Institute for Neurobiology, Department Genetics of Learning and Memory, Magdeburg, 39118, Germany, [2]Department of Animal Physiology, Institute of Biology, Leipzig University, Leipzig, 04103, Germany, [3]Department of Genetics, Institute of Biology, Leipzig University, Leipzig, 04103, Germany, [4]Department of Molecular Cell Biology, Weizmann Institute of Science, Rehovot, 7610001, Israel, [5]Institute of Imaging and Computer Vision, RWTH Aachen University, Aachen, 52074, Germany, [6]Institute of Neurobiology, University of Puerto Rico Medical Science Campus, Old San Juan, Puerto Rico, 00901, [7]Department of Physiology, Development and Neuroscience, Cambridge University, Cambridge, CB2 3EL, United Kingdom, [8]Janelia Research Campus, Howard Hughes Medical Institute, Ashburn, 20147, Virginia, [9]Leibniz Institute for Neurobiology, Combinatorial Neuroimaging Core Facility, Magdeburg, 39118, Germany, [10]University of California, Department of Molecular, Cell and Developmental Biology, Los Angeles, California 90095-1606, [11]Université Paris-Saclay, Centre National de la Recherche Scientifique, Institut des neurosciences Paris-Saclay, Saclay, 91400, France, [12]Center for Behavioral Brain Sciences, Magdeburg, 39106, Germany, and [13]Institute for Biology, Otto von Guericke University, Magdeburg, 39120, Germany

Larvae of the fruit fly *Drosophila melanogaster* are a powerful study case for understanding the neural circuits underlying behavior. Indeed, the numerical simplicity of the larval brain has permitted the reconstruction of its synaptic connectome, and genetic tools for manipulating single, identified neurons allow neural circuit function to be investigated with relative ease and precision. We focus on one of the most complex neurons in the brain of the larva (of either sex), the GABAergic anterior paired lateral neuron (APL). Using behavioral and connectomic analyses, optogenetics, Ca^{2+} imaging, and pharmacology, we study how APL affects associative olfactory memory. We first provide a detailed account of the structure, regional polarity, connectivity, and metamorphic development of APL, and further confirm that optogenetic activation of APL has an inhibiting effect on its main targets, the mushroom body Kenyon cells. All these findings are consistent with the previously identified function of APL in the sparsening of sensory representations. To our surprise, however, we found that optogenetically activating APL can also have a strong rewarding effect. Specifically, APL activation together with odor presentation establishes an odor-specific, appetitive, associative short-term memory, whereas naive olfactory behavior remains unaffected. An acute, systemic inhibition of dopamine synthesis as well as an ablation of the dopaminergic pPAM neurons impair reward learning through APL activation. Our findings provide a study case of complex circuit function in a numerically simple brain, and suggest a previously unrecognized capacity of central-brain GABAergic neurons to engage in dopaminergic reinforcement.

Key words: **dopamine; mushroom body; olfaction; optogenetics; reward**

Received Dec. 17, 2022; revised July 19, 2023; accepted Aug. 26, 2023.

Author contributions: N.M., D.P., O.M., M.S., K.E., O.K., V.H., A.S.T., M.S., and B.G. designed research; N.M., J.T., E.T., D.P., O.M., M.S., K.E., A.C., O.K., D.W., E.S., A.W., V.H., C.C.C.P., T.J., and A.R. performed research; N.M., J.T., E.T., D.P., O.M., M.S., K.E., A.C., O.K., D.W., E.S., A.W., V.H., C.C.C.P., T.J., A.S.T., A.R., M.S., and B.G. analyzed data; N.M. and B.G. wrote the first draft of the paper; N.M., J.T., E.T., D.P., O.M., M.S., K.E., A.C., O.K., D.W., E.S., A.W., V.H., C.C.C.P., T.J., A.S.T., A.R., M.S., and B.G. edited the paper; N.M. and B.G. wrote the paper; A.S.T. and A.R. contributed unpublished reagents/analytic tools.

This work was supported by Otto von Guericke University Magdeburg, Wissenschaftsgemeinschaft Gottfried Wilhelm Leibniz, Leibniz Institute for Neurobiology (LIN), and Deutsche Forschungsgemeinschaft (DFG) (DFG-GE 1091/4-1 and FOR 2705 Mushroom body to B.G.; PA1979/3-1 to D.P.; DFG-TH 1584/8-1 and DFG-TH 1584/7-1 to A.S.T.); German Federal Ministry of Education and Research (BMBF) (BMBF-NSF CRCNS *Encoding reward expectation in Drosophila* to B.G.); National Institutes of Health Grant R01 NS054814 to V.H.; and Agence Nationale de la Recherche ANR-21-NEUC-0002 (CRCNS *DrosoExpect*) and ANR-17-CE37-0019 to T.J. We thank A. Bates (Cambridge) for providing the script allowing compartment boundaries to be generated on the dendrograms; H. Tanimoto (U Tohoku), M. Stopfer (National Institutes of Health), Y. Aso (HHMI Janelia), A. Lin (U Sheffield), O. Schuldiner (Weizmann), C. Duch (U Mainz), G. Tavosanis (U Bonn), A. Khalili (U Göttingen), C. König (LIN), B. Michels (LIN), and N. Toshima (LIN) for discussions; and A. Ciuraszkiewicz (LIN), K. Hartung (LIN), M.L. Rodriguez Lopez (LIN), B. Kracht (LIN), T. Niewalda (LIN), M. Paisios (LIN), H. Reim (LIN), and H. Wickborn (LIN) and the workshop team at the LIN for technical assistance.

N. Mancini's present address: Max Planck Florida Institute for Neuroscience, Jupiter, Florida 33458.

A. Weiglein's present address: Institute of Anatomy, Otto von Guericke University, 39120 Magdeburg, Germany.

O. Mayseless' present address: Biozentrum, University of Basel, 4056 Basel, Switzerland.

M. Schleyer's present address: Hokkaido University, Institute for the Advancement of Higher Education, Hokkaido 060-0808, Japan.

A. Champion's present address: Department of Zoology, University of Cambridge, Cambridge, CB2 3EJ, United Kingdom and MRC Laboratory of Molecular Biology, Cambridge, CB2 0QH, United Kingdom.

K. Eichler's present address: Department of Zoology, University of Cambridge, Cambridge, CB2 3EJ, United Kingdom.

The authors declare no competing financial interests.

Correspondence should be addressed to Nino Mancini at nino.mancini@mpfi.org or Bertram Gerber at bertram.gerber@lin-magdeburg.de.

https://doi.org/10.1523/JNEUROSCI.2310-22.2023

Significance Statement

The single, identified giant anterior paired lateral (APL) neuron is one of the most complex neurons in the insect brain. It is GABAergic and contributes to the sparsening of neuronal activity in the mushroom body, the memory center of insects. We provide the most detailed account yet of the structure of APL in larval *Drosophila* as a neurogenetically accessible study case. We further reveal that, contrary to expectations, the experimental activation of APL can exert a rewarding effect, likely via dopaminergic reward pathways. The present study both provides an example of unexpected circuit complexity in a numerically simple brain, and reports an unexpected effect of activity in central-brain GABAergic circuits.

Introduction

Larvae of the fruit fly *Drosophila melanogaster*, which naturally live on overripe fruit, provide a powerful model for investigating the neurogenetic bases of learning and memory (Gerber and Stocker, 2007; Widmann et al., 2018; Thum and Gerber, 2019; Eschbach and Zlatic, 2020). Their small size and low number of neurons have allowed their chemical synapse connectome to be reconstructed, revealing unexpected complexity. In the mushroom body, which is a higher brain structure for sensory integration and memory in insects (Heisenberg, 2003), more than half of the classes of synaptic connections had previously escaped attention (Fig. 1*D*) (Eichler et al., 2017; Eschbach et al., 2020, 2021; adults: Takemura et al., 2017; F. Li et al., 2020). For instance, dopaminergic mushroom body input neurons (DANs) not only relay ascending information to local compartments along the elongated axonal fibers of the mushroom body intrinsic Kenyon cells (KCs), but also integrate local information from the KCs and recurrent signals originating from mushroom body output neurons (MBONs; these likewise respect compartmental boundaries). Similar complexity is observed for octopaminergic input neurons (OANs) and for input neurons using as yet unidentified signaling (Eichler et al., 2017; Saumweber et al., 2018; Eschbach et al., 2020, 2021; Schleyer et al., 2020). Collectively, this should prepare us for more surprises regarding mushroom body function. Here we study one of the most complex mushroom body neurons of larvae, the anterior paired lateral (APL) neuron.

APL is an embryonic-born and hemispherically unique interneuron that can be identified from the earliest larval stage on, throughout metamorphosis and in adults (Eichler et al., 2017; Mayseless et al., 2018; Saumweber et al., 2018). It receives most of its input from, and provides GABAergic output to, the cholinergic KCs, suggesting a role in sparsening sensory representation within the mushroom body (Masuda-Nakagawa et al., 2014; adults: Honegger et al., 2011; Lin et al., 2014; Amin et al., 2020; Prisco et al., 2021; further insects: Homberg et al., 1987; Grünewald, 1999; Papadopoulou et al., 2011). In contrast to most other aspects of mushroom body connectivity, however, there are major differences in APL connectivity between larvae and adults.

In adults, APL innervates all 15 mushroom body compartments and the calyx, where the KCs receive input from sensory projection neurons (Tanaka et al., 2008; Aso et al., 2014). In larvae, APL also innervates the calyx, but only 6 of the 10 compartments (Fig. 1*B*) (Eichler et al., 2017; Saumweber et al., 2018). In adults, APL connects reciprocally with the KCs in the calyx and in all the compartments (C. L. Wu et al., 2013; Takemura et al., 2017; Zheng et al., 2018; Scheffer et al., 2020), whereas in larvae such reciprocal connections exist only in the calyx, and only KC-to-APL synapses are found otherwise (Masuda-Nakagawa et al., 2014; Eichler et al., 2017; Saumweber et al., 2018). In adults, APL is electrically coupled to the dorsal paired median neuron (DPM), a local interneuron that innervates all the compartments but not the calyx (Pitman et al., 2011; C. L. Wu et al., 2011). DPM is serotonergic, coreleases GABA, and can express the amnesiac peptide (Waddell et al., 2000; Lee et al., 2011; Haynes et al., 2015; Turrel et al., 2018). Strikingly, DPM is absent in larvae (Eichler et al., 2017; Saumweber et al., 2018).

These differences caution against extrapolating between findings on APL in larvae and adults, since functions of APL other than a sparsening of KC activity have been described in adults (Liu et al., 2007; Liu and Davis, 2009; Ren et al., 2012; Y. Wu et al., 2012; Lin et al., 2014). In this context, we provide a comprehensive account of the structure of the larval APL neuron, the spatial arrangement of its synapses, its physiological effect on KC activity, and its metamorphic development. Investigating its role in Pavlovian conditioning, we discover that, surprisingly, optogenetic activation of APL exerts a rewarding effect. This effect is studied in detail and is shown to involve a dopamine-dependent process.

Materials and Methods

Drosophila *strains*

Drosophila melanogaster were kept and maintained on standard medium, in mass culture at 25°C, 60%-70% humidity, in a 12/12 h light/dark cycle. We used randomly chosen third-instar, feeding-stage larvae of both sexes, aged 5 d (120 h) after egg laying, unless mentioned otherwise. The strains used in this study and their genotypes are listed in Table 1.

Full-body fluorescence microscopy

To allow a full-body assessment of transgene expression from the APL-specific split-GAL4 SS01671 driver (henceforth APL-GAL4) (Saumweber et al., 2018), it was crossed to w*; UAS-mCherry-CAAX (abbreviated as UAS-mCherry-CAAX; Bloomington Stock Center #59021) (Sens et al., 2010) to express the mCherry-CAAX reporter. Double-heterozygous third-instar progeny (abbreviated as APL>mCherry-CAAX) were analyzed for fluorescence signals under a light-sheet microscope (see next paragraph). Genetic controls were heterozygous for either the GAL4 element (APL>+) or the UAS element (+>mCherry-CAAX). To obtain the driver control, APL-GAL4 was crossed to y^1w^1 (Bloomington Stock Center #1495). As regards the effector control, a strain lacking the GAL4 domains but containing the two split-GAL4 landing sites (attP40/attP2) (Pfeiffer et al., 2010) was crossed to UAS-mCherry-CAAX.

Experimental procedures follow Kobler et al. (2021). In brief, third-instar larvae were first bleached (4% sodium hypochlorite, Roth, order #9062.1) for 10 min at room temperature. After washing (3 × 5 min in distilled water, dH_2O), they were fixed in 4% PFA in 0.1 M PB at pH 9, with gentle shaking overnight at 4°C. Fixed samples were briefly rinsed 3 × with 0.1 M PB containing 0.2% Triton X-100 (PBT), then washed 2 × 60 min and left overnight at 4°C in PBT at pH 9. Dehydration the following day used a graded ethanol (EtOH) series (60 min in 10% and 25% EtOH, followed by 30 min in 50%, 60%, 80% (all at pH 9), and 2 × 100%

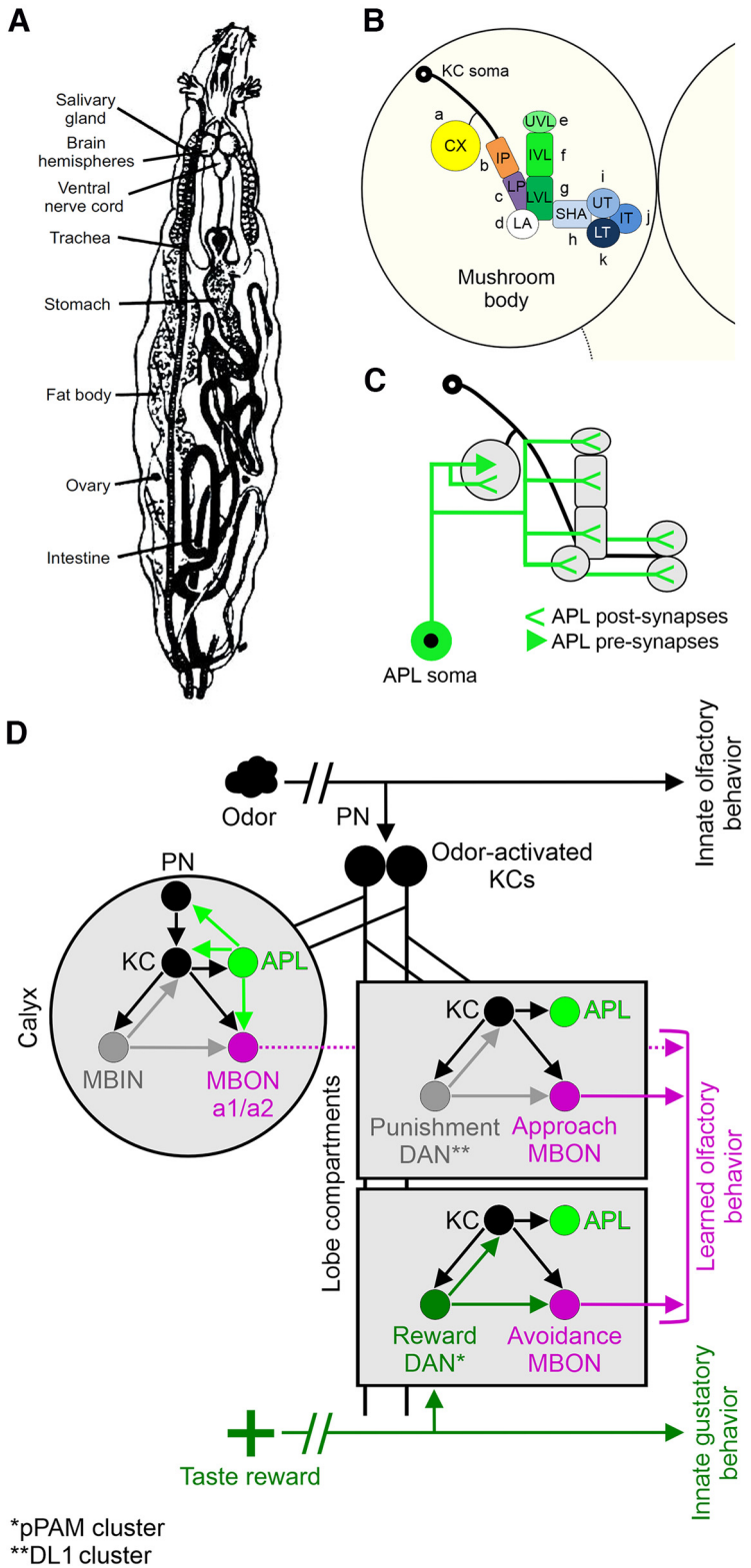

Figure 1. Overview of the larval body and brain and connectivity of the APL neuron in the mushroom body. ***A***, Schematic overview of the larval body, adapted from Demerec and Kaufmann (1940). ***B***, Sketch of one larval brain hemisphere with the mushroom body, highlighting its intrinsic KCs and organization in 10 compartments plus the calyx (letters a-k indicate the suffixes used to indicate the regions innervated by mushroom body extrinsic neurons): CX, Calyx; IP and LP, intermediate and lower peduncle; LA, lateral appendix; UVL, IVL, and LVL: upper, intermediate, and lower vertical lobe; SHA, shaft; UT, IT, and LT, upper, intermediate, and lower toe of the medial lobe. Adapted from Saumweber et al. (2018). ***C***, The larval APL neuron collects input (<) mostly from the KCs both in the calyx and in a subset of the compartments in the lobes, and delivers output (arrowhead) mostly to KCs and almost exclusively in the calyx. Adapted from Saumweber et al. (2018). ***D***, Simplified diagram of the connectivity of APL and of circuits underlying associative odor-reward learning. Within the calyx, a given odor (cloud) leads to the activation of a sparse, odor-specific pattern of KCs established through input from the projection neurons (PN). Within the lobes, a subset of modulatory dopaminergic neurons (Reward DAN) carry taste reward signals to the KCs, which send their axonal projection to avoidance-promoting MBONs (Avoidance MBON). Conversely, a different set of dopaminergic neurons (Punishment DAN) carry aversive signals to the KCs, which send their axonal projection to approach-promoting MBONs (Approach MBON). Reward and punishment DANs belong to the pPAM and DL1 cluster of

EtOH). Samples were then cleared by replacing EtOH with ethyl cinnamate (ECi; ethyl 3-phenyl-2-propenoate; Sigma-Aldrich, order #112372-100G). After 30-60 min, the ECi was refreshed once, and the samples stored at room temperature in black boxes in a desiccator.

The samples were placed ventral side up in ECi-cleared phytagel blocks (1 × 1 × 1 cm, Sigma-Aldrich, P8169). These were placed in a sample holder, which in turn was fixed on a mounting suspension to fit into a high-precision quartz glass cuvette filled with ECi and optically accessible with an UltraMicroscope II light-sheet microscope (Miltenyi Biotec). The microscope was equipped with a Zyla 4.2 PLUS sCMOS camera (Oxford Instruments) and a tube for infinity-corrected objective lenses. An EXW-12 laser (NKT Photonics) was used for excitation through triple-sheet optics to illuminate samples from one side. Excitation and emission filters (AHF Analysentechnik AG) were used as indicated in Figure 2 and Movie 1.

Tiled image stacks were acquired with a LVMI-Fluor 12× objective (Miltenyi Biotec) with a format of 2048 × 2048. Using ImSpector software (version 7.1.4, Miltenyi Biotec), a 10% overlap of tiles was set for stitching.

Image files were processed with Imaris software (version 9.8, Bitplane), including file conversion, stitching, further processing, and rendering. The ortho slicer tool was used to restrict volumes in the *z* direction to improve the representation of structures that were otherwise covered in the context of the whole body. All 3D images were generated using the snapshot function. 2D maximum-intensity projections were generated in Fiji (Schindelin et al., 2012).

Movie 1 was produced in Imaris with the key frame animation tool; Adobe Premiere Pro 2020 (version 14.9.0, Adobe) was used for cutting and labeling.

Immunohistochemistry

All the antibodies used in this study are listed in Table 1.

Transgene expression pattern of the SS01671 driver strain. To validate specific expression in the larval APL neuron of the APL-GAL4 driver strain (Saumweber et al., 2018), it was crossed to UAS-ChR2XXL::tdtomato to express a tomato-tagged version of ChR2XXL (FlyBase ID: FBtp0131815) (Saumweber et al., 2018). Double-heterozygous third-instar progeny (abbreviated as APL>ChR2XXL::tdtomato) were dissected in ice-cold Ringer's solution, and the brains were fixed for 30 min in 10% formaldehyde dissolved in PBS (pH 7.2, P4417, Sigma-Aldrich) at room temperature. After consecutive washing steps (3 × 10 min each) in PBT (0.3% Triton X-100 [CAS: 9036-19-5, Roth] in PBS), the brains were blocked in 5% NGS solution (005-000-121, Jackson ImmunoResearch Laboratories; in PBS) for 2 h at room temperature. To provide a reference staining of fiber tracts (including the mushroom bodies), tissues were incubated overnight at 4°C with a primary monoclonal mouse anti-FASII antibody (AB_528235, DSHB) diluted 1:50 in blocking solution containing 4% NGS in PBS. After six washes (10 min each) in PBS, the tissues were treated overnight at 4°C with a secondary polyclonal goat anti-mouse AlexaFluor-488 antibody (A11001, Invitrogen) diluted 1:200 in PBS. The brains were then washed in PBS (6 × 10 min each) and mounted in Vectashield (Vector Laboratories) on a cover slip. Signal detection from the tomato-tag of ChR2XXL (labeling the APL neuron) did not require antibodies; rather, the tomato fluorescence signal was detected directly under the microscope. Image *z* stacks were acquired with a Leica TCS SP8 confocal microscope (Leica Mikrosysteme Vertrieb) at a format of 1024 × 1024. Image processing was performed using Imaris software (version 9.72, Bitplane).

To visualize the larval APL neuron together with the mushroom bodies, we crossed the APL-GAL4 driver with a recombined effector/enhancer>effector strain that includes a UAS-mIFP-T2A-HO1 effector (abbreviated as mIFP; Bloomington Stock Center #64181) (Yu et al., 2015) recombined with the enhancer>effector construct MB247>mCherry-CAAX (Kobler et al., 2021). Third-instar larval progeny (abbreviated as APL>mIFP/MB247>mCherry-CAAX) were dissected in ice-cold Ca^{2+}-free saline solution and fixed for 24 h in 4% PFA (J19943, Alfa Aesar; in PBS) at 4°C. After six washes (3 × brief; 3 × 10 min) in 0.3% PBT, the brains were mounted in Vectashield (Vector Laboratories) on a cover slip. Signal detection from the mCherry-CAAX reporter (labeling the mushroom bodies) and the mIFP reporter (labeling APL) did not require antibodies for signal amplification. The image *z* stack was acquired with a Leica TCS SP8 confocal microscope (Leica Mikrosysteme Vertrieb) at a format of 1024 × 1024. The corresponding Movie 2 was produced in Imaris (version 9.72, Bitplane).

To examine the interhemispheric symmetry in the morphology of APL, the APL-GAL4 driver was crossed to UAS-mCD8::GFP (Bloomington Stock Center #5137) (Lee and Luo, 1999) as the effector. Third-instar larvae were put on ice and dissected in PBS. The brains were fixed in 4% PFA for 20 min at room temperature. After a succession of washing steps (3 × brief; 1 × 5 min; 3 × 15 min; 1 × 90 min) in 3% PBT (3% Triton X-100 [CAS: 9002-93–1, Sigma-Aldrich] in PBS) on ice, the brains were blocked with 5% NGS (G9023, Sigma-Aldrich) in PBT for 1 h at room temperature and incubated for 48 h with primary antibodies at 4°C. The brains were then washed (2 × brief; 3 × 15 min; 1 × 60 min; on ice; 1 × 30 min at room temperature) in 3% PBT before application of the secondary antibodies for at least 24 h at 4°C. After a final set of washing steps (3 × brief; 3 × 5 min; 2 × 15 min) in 3% PBT, the brains were mounted on poly-L-lysin-coated cover slips (following the Janelia FlyLight recipe), dehydrated by a series of increasing concentrations of EtOH (1× brief in distilled water; 1 × 10 min 30% EtOH; 1 × 10 min 50% EtOH; 1 × 10 min 75% EtOH; 1 × 10 min 95% EtOH; 3 × 10 min 100% EtOH) and cleared (3 × 5 min) in xylene (247642, CAS: 1330-20-7, Sigma-Aldrich). Finally, the brains were mounted in DPX mounting medium (dibutyl phthalate in xylene; 06522, Sigma-Aldrich) and left in darkness for at least 24 h before imaging.

The primary antibody mixture consisted of the following: (1) 2% NGS diluted 1:25 in 3% PBT, (2) a polyclonal rabbit anti-GFP antibody (A6455, Invitrogen) diluted 1:1000 in 3% PBT (for APL staining), (3) a monoclonal mouse 4F3 anti-DLG antibody (AB_528203, Developmental Studies Hybridoma Bank) diluted 1:200 in 3% PBT (for mushroom body staining), and (4) a monoclonal rat anti-N-Cadherin antibody (DN-Ex #8-s, Developmental Studies Hybridoma Bank) diluted 1:50 in 3% PBT (for neuropil staining).

The secondary antibody mixture consisted of the following: (1) 2% NGS diluted 1:25 in 3% PBT, (2) polyclonal goat anti-rabbit AlexaFluor-488 (A11008, Invitrogen), (3) polyclonal goat anti-mouse AlexaFluor-568 (A10037, Invitrogen), and (4) polyclonal goat anti-rat AlexaFluor-647 (712-605-153, Jackson ImmunoResearch Laboratories), all diluted 1:500 in 3% PBT. Confocal microscopy was conducted on a Zeiss LSM800 confocal laser scanning microscope with ZEN 2.3 software. Image *z* stacks were acquired with a LSM800 confocal microscope (Zeiss) at a format of 1024 × 1024. Image processing was performed using Imaris software (version 9.72, Bitplane).

To compare the coverage of the mushroom body calyx and compartments between the APL neuron of each hemisphere, mean pixel intensities were measured using ImageJ (version 1.53c, Fiji ImageJ). Grayscale maximum intensity projections of the GFP-channel (labeling APL membranes) were created, whereas the DLG channel (labeling the mushroom bodies) served as a template for orientation. The mushroom body calyx and compartments were

←

dopaminergic neurons, respectively, as indicated. In addition to its connections with the KCs, the APL neuron establishes synaptic contacts with the calyx MBONs (MBON-a1 and -a2) as well as with a subset of PNs (for additional connections between APL and mushroom body extrinsic neurons that are omitted here, see Figs. 6, 7). During odor-taste reward associative learning, the coincidence between the odor and the reward signal at the KCs is thought to lead to a presynaptic depression of the synapses between the odor-activated KCs and avoidance-promoting MBONs, whereas the synapses of these KCs with approach-promoting MBONs in other compartments remain unchanged (the contribution of MBON-a1/a2 to learned behavior is unclear, as indicated by the stippled lines). Future processing of the learned odor is thus biased in favor of approach. The same rationale is thought to apply for odor-punishment learning, occurring at the synapses between the KCs and approach MBONs. The electron microscopy reconstruction of a first-instar larval nervous system additionally revealed unexpected connections from KCs toward mushroom body input neurons (MBINs), including DANs, as well as MBIN/DAN-to-MBON synapses; KC-to-KC and MBON-to-MBIN connections are not displayed. Arrows indicate synaptic contacts between neurons.

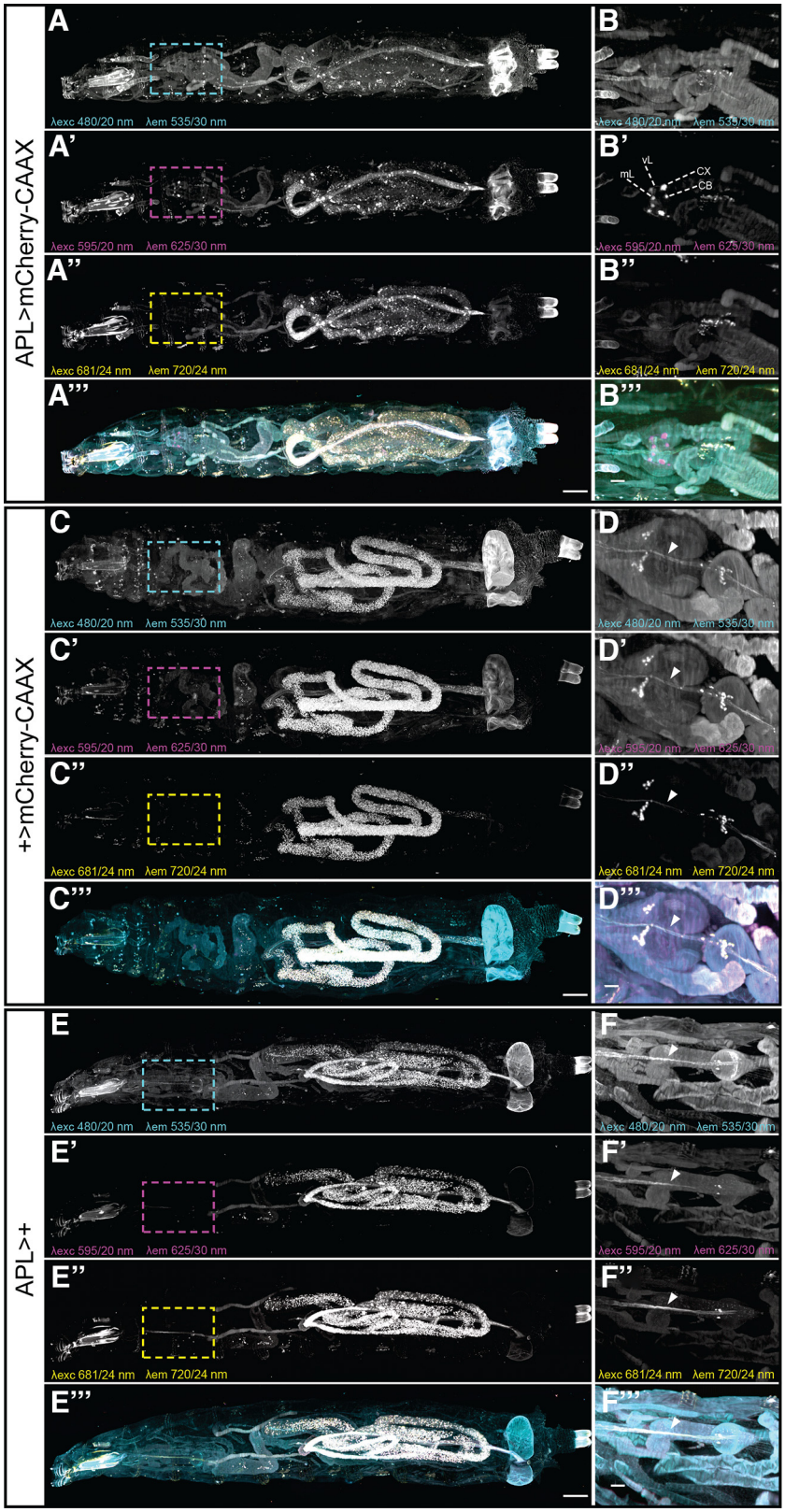

Figure 2. The APL-GAL4 driver does not express outside the brain. ***A–B‴***, Maximum intensity projection of fluorescence signals from an entire larva of the genotype APL>mCherry-CAAX acquired on a light-sheet microscope using a 12× objective (top view, rostral to the left). Dashed boxes represent the CNS, shown enlarged for a volume-restricted view in (***B–B‴***). λ exc and λ em indicate filter band passes used for excitation and emission, respectively (merged in ***A‴***,***B‴***). CX, Mushroom body calyx; CB, cell body of the APL neuron; vL and mL, innervation of APL in the vertical and medial lobe of the mushroom body, respectively. Scale bars: ***A–A‴***, 200 µm; ***B–B‴***, 50 µm. See also Movie 2. ***C–F‴***, Same as in ***A–B‴***, but for the effector control (+>mCherry-CAAX) (***C–D‴***) and driver control (APL>+) (***E–F‴***), respectively. Arrowhead points to autofluorescence signals from the pharynx (visible also in ***B–B‴*** but omitted for clarity). Fluorescence signals that can be observed across wavelengths and genotypes reflect autofluorescence (including from food particles in the gut) and allow bodily detail to be discerned. Fluorescence reflecting the expression of mCherry-CAAX was observed only in the brain and only the APL neuron (***A‴***,***B‴***, magenta signals; Movie 1) (compare ***B′***,***D′***,***F′***).

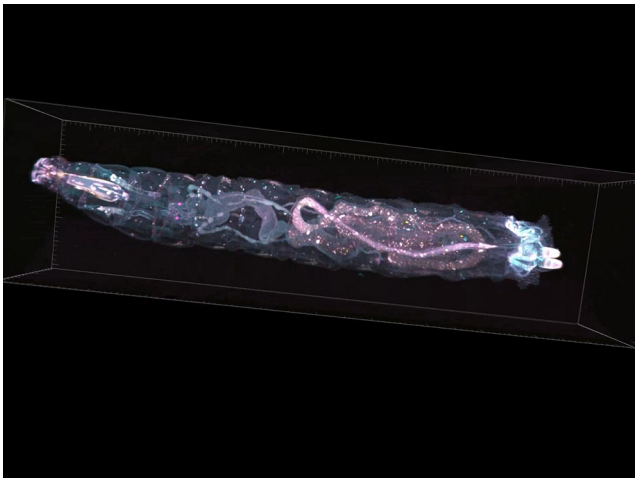

Movie 1. Volume rendering of fluorescence signals in a third-instar larva of the genotype APL>mCherry-CAAX at the indicated combinations of excitation and emission wavelengths (same specimen as in Fig. 2*A–B‴*). The movie starts in the brain region from a dorsal view (rostral to the left), and after rotation zooms out to show the full body. The data were acquired with a 12× objective; grid spacing: 200 μm. [View online]

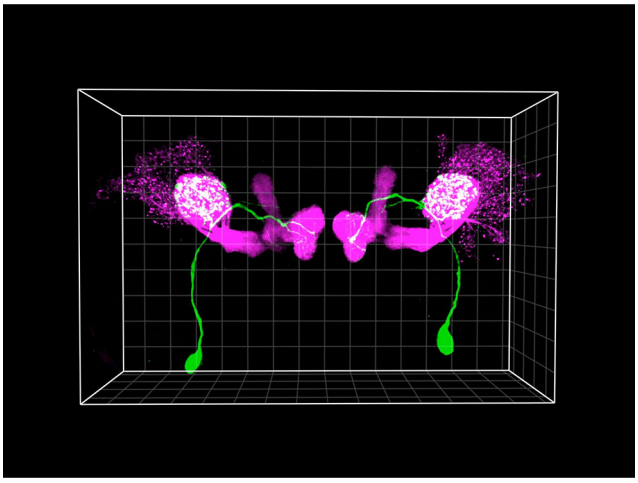

Movie 2. 3D rendering of the APL neuron (green) and the mushroom bodies (magenta) in a third-instar larval brain. Genotype: APL>mIFP/MB247>mCherry-CAAX. The data were acquired with a 40× oil objective; grid spacing: 20 μm. [View online]

selected using the ROI Manager function; mean gray values are documented in Extended Data Figure 3-1.

To validate the expression of the ChR2XXL effector protein used for activating APL, the APL-GAL4 driver was crossed to the UAS-ChR2XXL effector (Bloomington Stock Center #58374) (Dawydow et al., 2014). Following the procedure of Schleyer et al. (2020), brains of third-instar larval progeny (abbreviated as APL>ChR2XXL) were dissected in ice-cold Ca^{2+}-free saline solution and fixed in Bouin's solution (HT10132, Sigma-Aldrich) for 7 min at room temperature. After six successive washing steps (3 × brief; 3 × 15 min) in 0.2% PBT, the brains were incubated overnight at 4°C with a primary monoclonal mouse anti-ChR2 antibody (610180, ProGen Biotechnik) diluted 1:100 in 0.2% PBT. The brains were then washed (3 × 10 min each) in 0.2% PBT and incubated for 1 h at room temperature with a secondary polyclonal donkey anti-mouse Cy3 antibody (715-165-150, Jackson ImmunoResearch Laboratories) diluted 1:300 in 0.2% PBT. Finally, the samples were washed (3 × 10 min each) in 0.2% PBT and mounted in Vectashield (Vector Laboratories) on a cover slip. Image *z* stacks were acquired with a Leica TCS SP8 confocal microscope (Leica Mikrosysteme Vertrieb) at a format of 1024 × 1024. Image processing was performed using Imaris software (version 9.72, Bitplane).

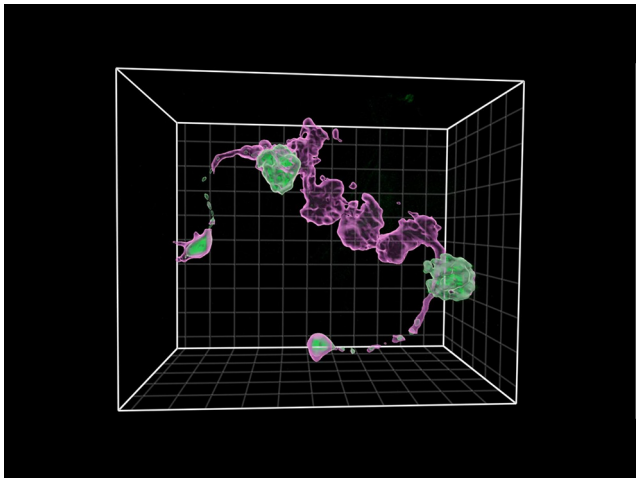

Movie 3. 3D rendering and segmentation of presynaptic (green) and postsynaptic (magenta) regions of the APL neuron in a third-instar larval brain, based on data shown in Figure 4*C–C″*. Genotype: APL>Dsyd-1::GFP/DenMark. The data were acquired with a 63× glycerol objective; grid spacing: 20 μm. [View online]

GABA staining. To confirm the presence of GABA in APL, the APL-GAL4 driver was crossed to a UAS-CsChrimson::mVenus effector (Bloomington Stock Center #55135) (Klapoetke et al., 2014), and third-instar progeny (abbreviated as APL>Chrimson) were dissected in PBS. Signal detection from the mVenus tag of the Chrimson transgene allows visualization of APL membranes without antibodies under the fluorescence microscope. The brains were fixed for 20 min with 4% PFA in 3% PBT on ice. After successive washing steps (2 × brief; 1 × 5 min; 3 × 15 min; 1 × 2 h) in 3% PBT, the brains were blocked for 1-2 h in 2% NGS solution (S-1000, Vector Laboratories; in PBS) on ice. After two overnight incubations at 4°C with the primary antibodies, the brains were rinsed (2 × brief; 1 × 5 min; 3 × 15 min; 1 × 2 h) in 3% PBT and incubated overnight with the secondary antibodies at 4°C. The preparations were finally washed (2 × brief; 1 × 5 min; 5 × 15 min) in 3% PBT, mounted in Vectashield (Vector Laboratories) on a cover slip, and scanned under a LSM510 confocal microscope (Zeiss) at a format of 1024 × 1024. Image processing was performed using Imaris software (version 9.72, Bitplane).

The primary antibody mixture consisted of the following: (1) 2% NGS diluted 1:25 in 3% PBT, (2) a monoclonal rat anti-N-Cadherin antibody (DN-Ex #8-s, Developmental Studies Hybridoma Bank) diluted 1:50 in 3% PBT (for neuropil staining), and (3) a polyclonal rabbit anti-GABA antibody (A2052, Sigma-Aldrich) diluted 1:500 in 3% PBT.

The secondary antibody mixture consisted of the following: (1) 2% NGS diluted 1:25 in 3% PBT, (2) a polyclonal Cy3-conjugated goat anti-rat antibody (A10522, Invitrogen) diluted 1:200 in 3% PBT, and (3) a polyclonal Cy5-conjugated goat anti-rabbit antibody (A10523, Invitrogen) diluted 1:200 in 3% PBT.

APL regional synaptic polarity. To analyze the regional synaptic polarity of the larval APL neuron, the APL-GAL4 driver was crossed to a double effector with both UAS-Dsyd-1::GFP (Owald et al., 2015) and UAS-DenMark (Bloomington Stock Center #33062) (Nicolaï et al., 2010). Third-instar progeny (abbreviated as APL>Dsyd-1::GFP/DenMark) were dissected, fixed, dehydrated, and mounted as described in the preceding section. Image processing was performed, and the corresponding Movie 3 was generated using Imaris software (version 9.72, Bitplane).

The primary antibody mixture consisted of the following: (1) 2% NGS diluted 1:25 in 3% PBT, (2) a monoclonal rat anti-N-Cadherin antibody (DN-Ex #8-s, Developmental Studies Hybridoma Bank) diluted 1:50 in 3% PBT (for neuropil staining), (3) a polyclonal FITC-conjugated goat anti-GFP antibody (ab 6662, Abcam) diluted 1:1000 in 3% PBT (for visualization of the GFP-tag from Dsyd-1::GFP to label presynaptic regions), and (4) a polyclonal rabbit anti-DsRed antibody (632496,

Clontech) diluted 1:200 in 3% PBT (for detecting the DenMark signal to label postsynaptic regions).

The secondary antibody mixture consisted of the following: (1) 2% NGS diluted 1:25 in 3% PBT, (2) a polyclonal Cy3-conjugated goat anti-rat antibody (A10522, Invitrogen) diluted 1:200 in 3% PBT, and (3) a polyclonal Cy5-conjugated goat anti-rabbit antibody (A10523, Invitrogen) diluted 1:200 in 3% PBT.

Chemical tagging for tracking APL development

Chemical tagging provides an alternative method to immunohistochemistry for labeling specific cells and structures in tissues. The tag-based approach uses genetically driven, enzyme-based protein "tags" that are expressed in specific cells and that covalently bind small fluorescent substrates, resulting in fast and specific tissue staining with low background signals (Kohl et al., 2014; Sutcliffe et al., 2017; Meissner et al., 2018).

We used such tagging to track the regional synaptic polarity of APL during development. Specifically, we used the synaptic reporters synaptotagmin fused to the chemical tag SNAPm (Syt1-SNAPm) to label presynaptic regions, and telencephalin fused to CLIPm (TLN-CLIPm) to label postsynaptic regions (Kohl et al., 2014). The effectors UAS-Syt1:SNAP (Bloomington Stock Center #58379) (Kohl et al., 2014), UAS-TLN:CLIP (Bloomington Stock Center #58382) (Kohl et al., 2014), and UAS-mCD8::GFP (for labeling APL) (Lin et al., 2014) were used together with the intersectional driver APLi-GAL4 (NP2631-GAL4, GH146-FLP, tubP-FRT-GAL80-FRT) for specific expression in both larval and adult APL neurons (Lin et al., 2014; Mayseless et al., 2018), since APL-GAL4 does not cover the adult APL neurons (not shown).

Our procedures followed Kohl et al. (2014). In brief, brains of third-instar larvae, pupae (6 or 12 h after puparium formation), and adults of the genotype APLi/Syt1:SNAP>mCD8::GFP/TLN:CLIP were dissected in ice-cold PB (0.1 M) and fixed in 4% PFA at room temperature for 20 min. The brains were permeabilized and washed (3 × 10 min) in PBT (0.3% Triton X-100 in PBS). Chemical tag ligands were then applied in a 300 µl volume on a nutator for 15 min, at room temperature. The chemical substrates were SNAP-tag ligands (SNAP surface 549 - BG 549 [NEB, S9112S]) and CLIP-tag ligands (CLIP surface 647 - BC 647 [NEB, S9234S]) at final concentrations of 1 μM in 0.3% PBT. To minimize cross-reactivity, the SNAP-tag ligands were applied 10 min before the CLIP-tag ligands. To label APL, the brains were immunostained: three consecutive washing steps (10 min each) in 0.3% PBT were followed by 30 min incubation in blocking solution with 5% NGS (005-000-121, Jackson ImmunoResearch Laboratories) in PBT. The brains were then incubated overnight with a primary antibody mixture consisting of the following: (1) 5% NGS diluted in 0.3% PBT and (2) a polyclonal chicken anti-GFP antibody (AB_10000240, Aves Labs) diluted 1:500. After five consecutive washing steps (3 × brief; 2 × 20 min) in 0.3% PBT, the brains were incubated for 2 h at room temperature with a polyclonal secondary FITC-conjugated goat anti-chicken antibody (A16055, Invitrogen) diluted 1:300 in 0.3% PBT. The preparations were mounted on slides in SlowFade (Invitrogen), and examined under a confocal microscope (Zeiss LSM 800). Image processing was performed using Imaris software (version 9.2 Bitplane).

Volume reconstruction of APL from an EM dataset

We added radial volume annotations to an existing skeleton reconstruction of the APL neuron in both hemispheres (Eichler et al., 2017) from an electron microscopy dataset of a 6-h-old first-instar larva (Ohyama et al., 2015). More details of the neuron reconstructions can be found in Eichler et al. (2017). Volume annotations were made manually using the web-based software CATMAID (Saalfeld et al., 2009; Schneider-Mizell et al., 2016), which was extended with a tool to allow for rapid graphical annotations of the radii of contiguous cable segments with similar radius. Radial annotations were used to create a volumetric representation of the cells' morphology as conical frustum compartments. The radii were placed so as to preserve the approximate volume of the irregularly shaped processes while accounting for the anisotropic image resolution of 3.8 nm × 3.8 nm × 50 nm. We defined the axon and dendrite of both APL neurons as the two synapse-rich areas along the arbor separated from the neurite by the high Strahler branch point nearest to the cell body. Reconstructed neurons and their synapses were analyzed using the natverse package (http://natverse.org/) (Bates et al., 2020) in R (version 3.6.2) and plotted using Blender (version 2.79) with the CATMAID-to-Blender plugin (https://github.com/schlegelp/CATMAID-to-Blender) (Schlegel et al., 2016).

Dendrogram representations of APL synapses and branching

Neuron dendrograms are simplified, but topologically correct, 2D representations of neurons with complex morphologies (Strauch et al., 2018). As relative branch lengths and synapse location are preserved, dendrograms can be used to visualize the spatial distribution of synapses in an easily readable way. The APL dendrograms are derived from existing electron microscopy reconstructions (Eichler et al., 2017) and were created following established computational methods (Strauch et al., 2018). Additionally, mushroom body calyx and compartment boundaries were superimposed onto the dendrograms, based on the projection patterns of mushroom body extrinsic neurons (Saumweber et al., 2018). We used the natverse toolbox for R (Bates et al., 2020) and custom code (A. Bates, University of Cambridge) to extract the synaptic coordinates from the CATMAID L1 dataset and to generate an envelope that surrounds the synapses formed by the mushroom body extrinsic neurons belonging to the calyx and each given compartment. Boundaries were plotted onto the dendrograms as hulls around the synapses located within the respective region. When these extended across several dendrogram branches, they were connected by dashed lines.

To analyze the relative distribution of APL-to-KC and KC-to-APL synapses in the calyx, we followed a procedure described in detail in Schleyer et al. (2020). In brief, we computed geodesic distances between synapses (i.e., "cable length" distances along the neuron's branches). Based on the geodesic distances, a clustering algorithm served to partition all synapses, regardless of their type, into local synapse clusters, that is, regions of high synapse density (domains). For each domain, the distances were then evaluated from the APL-to-KC (or KC-to-APL) synapses to the cluster's centroid point, which served as a measure for the spatial distribution of APL-to-KC (or KC-to-APL) within the domain.

Functional imaging

The functional imaging methods follow those described in greater detail previously (Selcho et al., 2017; Lyutova et al., 2019). In brief, to monitor intracellular Ca^{2+} levels of KCs in response to optogenetic activation of the APL neuron, the lexA-lexAop system was used to express the fluorescent Ca^{2+} reporter GCaMP6m in KCs (effector lexAOp-GCaMP6m; Bloomington Stock Center #44276) (Chen et al., 2013); driver R14H06-lexA (Bloomington Stock Center #52482) (Pfeiffer et al., 2010), and the GAL4-UAS system was used to express ChR2-XXL in APL (effector UAS-ChR2XXL; Bloomington Stock Center #58374) (Dawydow et al., 2014); driver R26G02-GAL4 (Bloomington Stock Center #48065) (Saumweber et al., 2018). The R26G02-GAL4 driver covers APL plus additional cells outside the mushroom body; it was chosen because the more specific APL-GAL4 driver, as a split-GAL4 strain, could not be combined with the lexA-lexAop system. Using classical genetics, we generated strains that carried a combination of the drivers (R14H06-lexA/R26G02-GAL4) or the effectors (lexAop-GCaMP6m/UAS-ChR2XXL) (Lyutova et al., 2019). These strains were crossed, and from the progeny (abbreviated as APL_{26G02}>ChR2XXL; KC>GCaMP6m) larval brains were dissected and placed in a Petri dish containing 405 µl hemolymph-like HL3.1 Ringer solution. Images with ROIs around the calyx and KCs were recorded with an Axio Examiner D1 microscope (Zeiss) using a W Plan-Apochromat 20 × 1.0 DIC (UV) VIS-IR objective and a Axiocam 506 camera (Zeiss). We monitored fluorescence intensity on pulsed 475 nM light (Colibri LED, Zeiss) at an intensity of 1.8 mW/cm^2 for a first observation period, followed by pulses at an intensity of 4.1 mW/cm^2 for a second observation period immediately thereafter. The light pulses were of 80 ms duration and were given at a 2 s onset–onset interval. We used larvae without the APL driver as the genetic control (abbreviated as +>ChR2XXL; KC>GCaMP6m).

To see whether APL activation would be potent enough to reduce the very high intracellular Ca^{2+} levels that result from cholinergic stimulation of the KCs, we used carbamylcholine (CAS: 51-83-2, Sigma-

Aldrich). Specifically, we monitored fluorescence intensity under pulsed 475 nm light as described above for a total of 8 min and after the first 2 min manually bath-applied 45 µl carbamylcholine, dissolved in HL3.1 to a final concentration of 10^{-4} M.

We present the fluorescence intensity ($\Delta F/F_0$) across the observation period normalized to the values at its beginning (Normalized $\Delta F/F_0$) as the baseline. To analyze the differences between the experimental conditions, we determined, for each calycal ROI/KC, the maximum difference from the baseline, as well as the normalized area under the curve.

Behavioral assays

Experimental setup. Larvae were trained and tested on Petri dishes (9 cm inner diameter; Sarstedt) filled either with 1% agarose only (CAS: 9012-36-6, Roth) or with 1% agarose containing 2 mol/L D-fructose (99% purity; CAS: 57-48-7, Roth) as the taste reward (+). Once the contents had solidified, the dishes were covered with their lids and left at 4°C until the experiment started, and for a maximum of 2 weeks.

As the odors, *n*-amyl acetate (AM; CAS: 628-63-7, Merck) diluted 1:20 in paraffin oil (CAS: 042-47-5, AppliChem) and 1-octanol (OCT, undiluted; CAS: 111-87-5, Sigma-Aldrich) were used. The paraffin oil is without behavioral effect as an odor (Saumweber et al., 2011). Before the experiments, 10 µl of the respective odor was added to odor containers (5 mm inner diameter) covered by perforated lids (5-10 holes of 0.5 mm diameter each). Larvae were collected from their food vial with a brush, briefly rinsed in tap water, and used immediately for behavioral experiments.

Behavioral assays were conducted in a light-shielded, custom-built box, as described by Schleyer et al. (2020). In brief, the box contained a 24 × 12 LED array light table (Solarox) with a 6-mm-thick Plexiglas diffusion panel placed above it, providing constant light conditions and intensity for the activation of light-gated ion channels expressed in neurons of interest (see Genotypes and methods for optophysiology). Larvae in Petri dishes were placed onto the diffusion panel and were surrounded by a translucent polyethylene ring. The ring featured 30 infrared LEDs mounted behind to deliver light (invisible to the animals) allowing behavioral recording for offline tracking analysis (see Video recording and tracking of locomotion).

Odor-fructose reward association. A two-group, reciprocal conditioning paradigm was used following standard procedures (Scherer et al., 2003; Neuser et al., 2005; Saumweber et al., 2011; for a detailed manual: Michels et al., 2017). In brief, one group of larvae received the odor presented together with the fructose reward (paired training), whereas a second group received separate presentations of the odor alone and the fructose reward alone (unpaired training).

For paired training, a cohort of ~ 30 larvae was placed at the center of a Petri dish filled with agarose that was mixed with fructose as the reward (+). Two containers were filled with the odor (AM+) and placed on opposite sides of the Petri dish. The lid was then closed, and the larvae were allowed to move freely for 2.5 min. The larvae were then removed and placed on a fresh, pure-agarose Petri dish in the presence of two empty containers (EM), the lid was closed, and the larvae could again move freely for 2.5 min. This training cycle was performed once only, unless mentioned otherwise. The sequence of training was alternated across replications: that is, for half of the cases, we started with AM as described above (AM+/EM), and for the other half with EM (EM/AM+). After training, the larvae were tested for their odor preference. Specifically, the animals were transferred to the center of a fresh, pure-agarose Petri dish (i.e., without fructose reward, unless mentioned otherwise) featuring one AM container on one side, and one EM container on the other side. After 3 min, the number of larvae on the AM side (#AM), the EM side (#EM), as well as on the middle "neutral" stripe (10 mm), was counted, and the olfactory preference score (PREF) was calculated as follows:

$$PREF = \frac{\#AM - \#EM}{\#Total} \quad (1)$$

Thus, preference scores may range from 1 to −1, with positive values showing preference for AM, and negative values indicating avoidance of AM. Larvae crawling up onto the lid or onto the odorant containers during the test (<5%) were discarded from the analysis.

For unpaired training, the procedure was the same, except that the odor and the reward were presented separately to the animals. That is, after collection the larvae were placed on a fresh, pure-agarose Petri dish in the presence of two containers both filled with AM. Then, the larvae were transferred onto a fresh agarose Petri dish with fructose added, in the presence of two empty containers (EM+). Again, the training sequence started with AM (AM/EM+) in half of the cases, and in the other half of the cases with EM (EM+/AM). The larvae were then tested for their AM preference, and the olfactory preference score was calculated as for the paired group (Eq. 1).

Associative memory is indicated by a difference in preference for AM after paired training compared with the reciprocal, unpaired training. These differences in AM preference were quantified by the associative memory score as follows:

$$Memory\ score = \frac{PREF\,(Paired) - PREF\,(Unpaired)}{2} \quad (2)$$

Thus, memory scores may range from 1 to −1, with positive values indicating appetitive associative memory, and negative values indicating aversive associative memory. These experiments were combined with optogenetic APL activation (see Genotypes and methods for optophysiology).

Odor-APL association. Based on early results in this study (see Results), we suspected that optogenetic activation of the APL neuron might have a rewarding effect. Therefore, the associative learning paradigm described above was modified by using optogenetic APL activation (+) instead of a fructose reward (i.e., no real reward was presented). In the paired group, AM was presented together with continuous 2.5 min light stimulation to activate APL, whereas empty containers were subsequently presented in darkness, also for 2.5 min (AM+/EM). In the unpaired group, the larvae were exposed to odor and light separately (AM/EM+). This training cycle was performed once only, with the training sequence alternated across repetitions as described in the preceding section. After training, the larvae were tested on a fresh, pure-agarose Petri dish, and their odor preference as well as the memory score were calculated as detailed above (Eqs. 1, 2).

In addition, a differential two-odor version of the paradigm using APL activation as the reinforcer was used. This was performed as described above, except that, instead of using empty containers (EM), the containers were filled with OCT (undiluted). Thus, differential conditioning followed the logical structure of training being either AM+/OCT or in the reciprocal case AM/OCT+ (again, the training sequence was alternated across repetitions of the experiments). The larvae were then tested for their choice between AM and OCT on a fresh, pure-agarose Petri dish, and the data were analyzed, with due adjustment, as detailed above (Eqs. 1, 2). In this case, positive memory score values thus indicate odor-specific appetitive associative memory, whereas negative memory score values indicate odor-specific aversive associative memory.

Whenever variations on the above paradigms were used, these are mentioned in Results.

Innate olfactory behavior. The odor preference of experimentally naive larvae was assayed following standard procedures (Saumweber et al., 2011). Cohorts of ~ 30 animals were transferred onto a pure-agarose plate in the presence of one odor-filled container and another empty container placed on opposite sides of the plate. Odor preference was calculated after 3 min following Equation 1. To probe whether APL activation has an effect on innate olfactory behavior, the test was conducted either without light stimulation, or with light stimulation.

Genotypes and methods for optophysiology. For the experiments on APL activation, we used third-instar transgenic larvae expressing either ChR2XXL or Chrimson in APL. To this end, APL-GAL4 was crossed to UAS-ChR2XXL or to UAS-CsChrimson::mVenus as the effector. Double-heterozygous progeny (abbreviated as APL>ChR2XXL or APL>Chrimson) were used for activation of the APL neuron; larvae heterozygous for either the GAL4 element (APL>+) or the UAS element

(+>ChR2XXL or +>Chrimson) were used as the driver and the effector genetic control, respectively. To obtain the driver controls, APL-GAL4 was crossed to w^{1118} (Bloomington Stock Center #3605, #5905, #6326). As regards the effector controls, a strain lacking the GAL4 domains but containing the two split-GAL4 landing sites (attP40/attP2) was crossed to UAS-ChR2XXL or UAS-CsChrimson::mVenus. For experiments using Chrimson, the flies were raised on food supplemented with all-trans retinal (100 mM final concentration; cat: R2500; CAS: 116-31-4, Sigma-Aldrich), unless mentioned otherwise.

For the experiments on MBON activation, UAS-ChR2XXL was crossed to one of the three following drivers: (1) R36G04-GAL4, covering the two calyx MBONs in each hemisphere, plus additional cells in the ventral nerve cord (Bloomington Stock Center #49940; abbreviated as MBONa1,a2-GAL4) (Saumweber et al., 2018); (2) the split-GAL4 line SS02006, covering only one calyx MBON in each hemisphere (kindly provided by M. Zlatic, University of Cambridge; abbreviated as MBONa1-GAL4) (Eschbach et al., 2021); (3) SS01417, covering one, or in some cases both, of the calyx MBONs in each hemisphere (Extended Data Fig. 16-1; kindly provided by M. Zlatic, University of Cambridge; abbreviated as MBONa2-GAL4) (Eschbach et al., 2021). Again, double-heterozygous progeny (abbreviated as MBONa1,a2>ChR2XXL, MBONa1>ChR2XXL or MBONa2>ChR2XXL) were used for activating the calyx MBONs; driver and effector control larvae were obtained as detailed in the preceding paragraph.

For simultaneous activation of APL and ablation of the pPAM neurons, the lexA-lexAop system was used to express the pro-apoptotic *reaper* gene in the pPAM neurons (effector lexAop-reaper) (Herranz et al., 2014); driver R58E02-lexA (Bloomington Stock Center #52740) (Lyutova et al., 2019), and the GAL4-UAS system was used to express ChR2-XXL in APL (effector UAS-ChR2XXL; Bloomington Stock Center #58374) (Dawydow et al., 2014); driver R55D08-GAL4 (Bloomington Stock Center #39115) (Saumweber et al., 2018). The R55D08-GAL4 driver covers APL plus additional cells outside the mushroom body; it was chosen because the more specific APL-GAL4 driver, as a split-GAL4 strain, could not be combined with the lexA-lexAop system. Using classical genetics, we generated strains that carried a combination of the drivers (R58E02-lexA/R55D08-GAL4) or the effectors (lexAop-reaper/UAS-ChR2XXL) (Lyutova et al., 2019). These strains were crossed, and the progeny obtained (abbreviated as APL_{55D08}>ChR2XXL; pPAM>reaper) were used for the experiment. As regards single effector controls, a strain lacking lexAop-reaper but containing UAS-ChR2XXL was crossed to R58E02-lexA/R55D08-GAL4 (abbreviated as APL_{55D08}>ChR2XXL; pPAM>+). As regards single driver controls, a strain lacking R58E02-lexA but containing R55D08-GAL4 was crossed to lexAop-reaper/UAS-ChR2XXL (abbreviated as APL_{55D08}>ChR2XXL; +>reaper).

The above-mentioned custom-built box (see Experimental setup) was equipped for illumination from a blue LED light table when ChR2XXL was used (wavelength: 470 nm; intensity: 120 $\mu W/cm^2$; Solarox), or from a red LED light table when Chrimson was used (wavelength: 630 nm; intensity: 350 $\mu W/cm^2$; Solarox).

For silencing experiments, the light-gated chloride channel GtACR1 was used. Specifically, APL-GAL4, R36G04-GAL4, SS02006-GAL4, or SS01417-GAL4 was crossed to UAS-GtACR1::YFP (Bloomington Stock Center #9736; kindly provided by R. Kittel, University of Leipzig) (König et al., 2019). Double-heterozygous progeny (APL>GtACR1, MBONa1, a2>GtACR1, MBONa1>GtACR1 or MBONa2>GtACR1) were used for silencing the respective neurons; driver and effector control larvae were obtained as described in the preceding paragraphs. A green LED light table (wavelength: 520 nm; intensity: 2003 $\mu W/cm^2$; Solarox) was used for illumination.

In all cases, the timing of illumination is mentioned for each experiment in Results. As all effectors are sensitive to daylight, the breeding of all transgenic animals was performed in darkness, effectuated by black covers wrapped around the food vials. All behavioral experiments were conducted in parallel for the respective experimental group and genetic controls; investigators were blind with respect to genotypes.

Video recording and tracking of locomotion. For a subset of experiments, larval behavior was video-recorded throughout the test and analyzed as described by Paisios et al. (2017). In brief, four behavioral features were analyzed in relation to odor:

First, the olfactory preference (PREF time, in s) was calculated as follows:

$$PREF\ time = \frac{Time\ spent\ on\ AM\ side - Time\ spent\ on\ EM\ side}{Total\ duration} \quad (3)$$

Thus, preference scores may range from 1 to −1, with positive scores indicating that larvae spent more time on the odor side, and negative values indicating more time spent on the nonodor side, representing approach and avoidance, respectively.

Second, the head cast (HC) rate modulation was calculated as follows:

$$HC\ rate\ modulation = \frac{\#HC/s(away\ from\ AM) - \#HC/s(toward\ AM)}{\#HC/s(away\ from\ AM) + \#HC/s(toward\ AM)} \quad (4)$$

Thus, positive scores indicate odor approach; that is, the larvae make more HCs when crawling away from the odor than when crawling toward it. Conversely, negative scores indicate odor avoidance.

Third, the HC reorientation (°) was calculated as follows:

$$HC\ reorientation = abs(before\ HC) - abs(after\ HC) \quad (5)$$

The absolute heading angle (abs) indicates how the larva's head is oriented relative to the odor. For instance, at abs 180° or 0°, the odor is located behind or in front of the animal, respectively. Thus, positive values indicate odor approach; that is, the HC directs the larva toward the odor instead of away from it. Conversely, negative values indicate odor avoidance.

Fourth, the run speed modulation was calculated as follows:

$$Run\ speed\ modulation = \frac{Run\ speed\ toward\ AM - Run\ speed\ away\ from\ AM}{Run\ speed\ toward\ AM + Run\ speed\ away\ from\ AM} \quad (6)$$

Thus, positive values for run speed modulation indicate that animals slow down whenever they head away from the odor, and speed up whenever they move toward it, indicating approach. Conversely, negative values indicate avoidance.

Pharmacological manipulation of dopamine synthesis

To test whether the dopaminergic system is implicated in odor-APL associative learning, a systemic pharmacological approach was used to disrupt dopamine synthesis (Neckameyer and White, 1993; Kaun et al., 2011; Thoener et al., 2021). This approach was combined with behavioral experiments using optogenetic APL activation as the reinforcer (see Odor-APL association) and followed the procedures described by Thoener et al. (2021). In brief, a 0.5 mg/ml yeast solution was produced and kept for up to 1 week at 4°C. The dopamine synthesis inhibitor 3-iodo-L-tyrosine (3IY; CAS: 70-78-0, Sigma-Aldrich; concentration: 5 mg/ml) was added to samples of 2 ml yeast solution. In the instances mentioned in Results, the dopamine precursor 3,4-dihydroxyphenylalanine (L-DOPA; CAS: 59-92-7, Sigma-Aldrich; concentration: 10 mg/ml) was added to a yeast solution with or without 3IY. After mixing on a shaker for 1 h, the solutions were transferred into vials containing two pieces of PET mesh. Third-instar progeny of the APL-GAL4 driver crossed to UAS-ChR2XXL (APL>ChR2XXL) were transferred from their food vials to the respective yeast solutions. After a feeding period of 4 h at 25°C and 60%-70% relative humidity, the larvae were briefly washed in water and immediately used in behavioral experiments.

Connectivity analyses from an EM dataset

A connectivity analysis was performed using the open-source web-based platform CATMAID (Saalfeld et al., 2009; Schneider-Mizell et al., 2016)

Table 1. Table containing the key reagents (fly strains, antibodies, software) used in this study

Reagent or resource	Source or reference	Identifiers	Additional information
Fly strains			
SS01671-GAL4 (APL-GAL4; split-GAL4 driver covering specifically APL in larvae)	Saumweber et al., 2018		
APLi-GAL4 (intersectional driver covering specifically APL in larvae and adults)	Lin et al., 2014; Mayseless et al., 2018		
R36G04-GAL4 (MBONa1,a2-GAL4; GAL4 driver covering the calyx MBONs, plus additional neurons in the VNC in larvae)	Saumweber et al., 2018	BDSC #49940	Chrs III
SS02006-GAL4 (MBONa1-GAL4; split-GAL4 driver covering specifically one of the two calyx MBONs in larvae)	Eschbach et al., 2020; kindly provided by M. Zlatic, University of Cambridge		
SS01417-GAL4 (MBONa2-GAL4; split-GAL4 driver covering one, or in some cases both calyx MBONs in larvae)	Eschbach et al., 2020; kindly provided by M. Zlatic, University of Cambridge		
R26G02-GAL4 (GAL4 driver covering APL, plus additional neurons in the VNC)	Jenett et al., 2012; Saumweber et al., 2018	BDSC #48065	Chrs III
R55D08-GAL4 (GAL4 driver covering APL, plus additional neurons in the VNC)	Jenett et al., 2012; Saumweber et al., 2018	BDSC #39115	Chrs III
R14H06-LexA (LexA driver covering the KCs in larvae)	Pfeiffer et al., 2010; lexA Driver Collection of Rubin Laboratory at Janelia Farm	BDSC #52482	Chrs II
R58E02-LexA (LexA driver covering the pPAM neurons in larvae)	Pfeiffer et al., 2010; lexA Driver Collection of Rubin Laboratory at Janelia Farm	BDSC #52740	Chrs II
UAS-ChR2-XXL (optogenetic effector)	Dawydow et al., 2014	BDSC #58374	Chrs II
UAS-ChR2-XXL-td::tomato (reporter/optogenetic effector)	Saumweber et al., 2018	FlyBase ID: FBtp0131815	Chrs II
UAS-mCherry-CAAX (reporter effector)	Sens et al., 2010; Kobler et al., 2021	BDSC #59021	Chrs II
UAS-mIFP-T2A-HO1 (reporter effector)	Yu et al., 2015; Kobler et al., 2021	BDSC #64181	Chrs III
UAS-mIFP/MB247>mCherry-CAAX (recombined reporter effector/ enhancer>effector)	Kobler et al., 2021		
UAS-mCD8::GFP (reporter effector)	Lee and Luo, 1999	BDSC #5137	Chrs II
20xUAS-IVS-CsChrimson::mVenus (reporter/optogenetic effector)	Klapoetke et al., 2014	BDSC #55136	Chrs III
UAS-GtACR1::YFP (reporter/optogenetic effector)	Kindly provided by R. Kittel, Würzburg; König et al., 2019	BDSC #9736	Chrs II
lexAop-GCaMP6m (reporter effector)	Chen et al., 2013; Lyutova et al., 2019	BDSC #44276	Chrs III
lexAop-reaper (pro-apoptotic effector)	Herranz et al., 2014; Lyutova et al., 2019		Chrs III
UAS-Dsyd-1::GFP (presynaptic reporter)	Owald et al., 2015		Chrs III
UAS-DenMark (postsynaptic reporter)	Nicolaï et al., 2010	BDSC #33062	Chrs II
UAS-Syt1:SNAP (presynaptic TAG reporter)	Kohl et al., 2014	BDSC #58379	Chrs III
UAS-TLN:CLIP (postsynaptic TAG reporter)	Kohl et al., 2014	BDSC #58382	Chrs III
w1118		BDSC #3605, #5905, #6326	
y1w1		BDSC #1495	
attP40/attP2	Pfeiffer et al., 2010		
Antibodies			
Primary monoclonal mouse anti-FASII	DSHB	1D4 anti-Fasciclin II; AB_528235	1:50
Primary monoclonal mouse anti-ChR2	ProGen Biotechnik	610180	1:100
Primary polyclonal rabbit anti-GFP	Invitrogen	A6455	1:1000
Primary polyclonal FITC-conjugated goat anti-GFP	Abcam	ab 6662	1:1000
Primary monoclonal mouse 4F3 anti-DLG	Hybridoma	AB_528203	1:200
Primary polyclonal rabbit anti-DsRed	Clontech	632496	1:200
Primary monoclonal rat anti-N-Cadherin	Hybridoma	DN-Ex #8-s	1:50
Primary polyclonal rabbit anti-GABA	Sigma-Aldrich	A2052	1:500
Primary polyclonal chicken anti-GFP	Aves Labs	AB_10000240	1:500
Secondary polyclonal goat anti-rabbit AlexaFluor-488	Invitrogen	A11008	1:500
Secondary polyclonal goat anti-mouse AlexaFluor-568	Invitrogen	A10037	1:500
Secondary polyclonal goat anti-rat AlexaFluor-647	Jackson ImmunoResearch Laboratories	712-605-153	1:500
Secondary polyclonal donkey anti-mouse Cy3	Jackson ImmunoResearch Laboratories	715-165-150	1:300
Secondary polyclonal goat anti-mouse AlexaFluor-488	Invitrogen	A11001	1:200
Secondary polyclonal goat anti-rabbit Cy5	Invitrogen	A10523	1:200
Secondary polyclonal goat anti-rat Cy3	Invitrogen	A10522	1:200
Secondary polyclonal FITC-conjugated goat anti-chicken	Invitrogen	A16055	1:300
Chemical TAG ligands (chemical substrates)			
SNAP-tag ligands (SNAP surface 549 - BG 549)	NEB	S9112S	
CLIP-tag ligands (CLIP surface 647 - BC 647)	NEB	S9234S	
Odors			
AM	Merck	628-63-7	
OCT	Sigma-Aldrich	111-87-5	
Drugs			
Carbamylcholine	Sigma-Aldrich	51-83-2	

(*Table continues*)

Table 1. Continued

Reagent or resource	Source or reference	Identifiers	Additional information
3IY	Sigma-Aldrich	70-78-0	
L-DOPA	Sigma-Aldrich	59-92-7	
Software			
Fiji ImageJ 1.53c	National Institutes of Health	SCR_002285	
CATMAID	Saalfeld et al., 2009; Schneider-Mizell et al., 2016		
Imaris 9.72, 9.8	Oxford Instruments	SCR_007370	
ImSpector 7.1.4	Miltenyi Biotec		
R 3.3.2	Development Core Team 2016		
Statistika 13	StatSoft	SCR_014213	
Corel Draw 2019	Corel	SCR_013674	
GraphPad Prism 6	GraphPad Software	SCR_002798	
Adobe Premiere Pro 2020, version 14.9.0	Adobe		

on published EM reconstruction data (Eichler et al., 2017; Eschbach et al., 2021). We used the fractions of inputs (FI) as a measure of the connectomic impact of an upstream neuron on its downstream partner (Ohyama et al., 2015; Schneider-Mizell et al., 2016). To analyze the connections that APL makes, via the KCs, with DANs/OANs/MBINs, we determined these fractions for each APL>KC>DAN/OAN/MBIN connection. For an indirect connection between, for example, neurons A and C via neuron B, the activations from A to B and from B to C were considered as independent; the impact of A on C can therefore be defined as the product of two probabilities (FI). Thus, we determine the total impact of A on C via B as follows:

$$iA > C = FI(B, A) * FI(C, B) \tag{7}$$

We computed the impact of the APLs of each hemisphere for each KC that is connected both to one of the APLs and any one of the DANs/OANs/MBINs (KCn) as follows:

$$i(KC_n)_{APL>DAN/OAN/MBIN} = FI(APL > KC_n) \times FI(KC_n > DAN/OAN/MBIN) \tag{8}$$

We then summed the impact of the respective APL, via the KCs, on each DAN/OAN/MBIN as follows:

$$I(KC_{total})_{APL>DAN/OAN/MBIN} = \Sigma_n i(KC_n)_{APL>DAN/OAN/MBIN} \tag{9}$$

Finally, the impact of the APLs of both hemispheres on DANs/OANs/MBINs of the mushroom body calyx and compartments were summed to compare the impact of APL between compartments and between the medial lobe and vertical lobe systems.

Experimental design and statistical analyses

The source data are included in Extended Data Figure 3-1; the results of all statistical tests, performed in Statistica 13 unless mentioned otherwise (SCR_014213, StatSoft), are included in Table 2. Graphs, figures, and sketches were generated with Statistica 13, Corel Draw 2019 (SCR_013674, Corel), and GraphPad Prism 6 (SCR_002798, GraphPad Software); references are documented in Table 1.

To compare the calycal and compartmental coverage between the APL neuron of each hemisphere (see Fig. 3*E*), a Pearson correlation was performed; the data are displayed as a scatter plot.

The experiments in Figure 5 followed a two-group design with two genotypes (APL_{26G02}>ChR2XXL; KC>GCaMP6m as the experimental genotype and +>ChR2XXL; KC>GCaMP6m as the genetic control). We analyzed changes in fluorescence intensity and plotted mean maximal ΔF/F0 (see Fig. 5*B*,*E*,*H*) and the area under the curve for each experiment after normalization (see Fig. 5*C*,*F*,*I*).

To compare the radii of the neurite, dendrite, and axon of APL in both hemispheres (see Fig. 6*D*), Kruskal–Wallis (KW) tests and Mann-Whitney-Wilcoxon (MWW) tests (total of three MWW tests per APL) were used for multiple and two-group comparisons, respectively (R Core Team, 2016). The Bonferroni–Holm (BH) correction was applied to maintain an error rate<5% (Holm, 1979). The data are displayed as violin plots, with bars showing the mean.

For the experiments in Figures 7, 9-19 and Extended Data Figure 7-4, the data are displayed as box plots, the middle line indicates the median, the box boundaries represent the 25% and 75% quantiles, and the whiskers represent the 10% and 90% quantiles; outliers are not displayed.

To compare the geodesic distances of synapses to the center of their respective center-surround structure on the left-hemisphere APL neuron (see Fig. 7*D*), we performed an MWW test between KC-to-APL and APL-to-KC synapses. Corresponding analyses for the right-hemisphere APL neuron can be found in Extended Data Figure 7-4.

For the behavioral results displayed in Figures 9-18, KW and MWW tests were used for multiple and two-group comparisons, respectively. For comparisons to chance levels (i.e., to zero), one-sample sign tests (OSS; corresponding to binom.test in R version 3.3.2) (R Core Team, 2016) were used. The BH correction was applied to maintain an error rate<5%. Sample sizes (biological replications) were chosen based on previous studies that had revealed moderate to mild effect sizes (Paisios et al., 2017; Saumweber et al., 2018) and are indicated in the figures. A sample size of $N = 1$ included ~30 animals of both sexes for each reciprocally trained group, and ~30 animals of both sexes for all innate preference experiments. All behavioral experiments were performed in parallel for the respective experimental group and genetic controls; experimenters were blind to genotypes.

The experiments in Figures 9*A*, *B*, 12*A*, *C*, *G*, 15*A*, 16*A*, *B*, and 18 followed a three-group design with three genotypes (experimental genotype expressing ChR2XXL or GtACR1 or ChR2XXL/reaper, plus effector and driver controls). In case of significance, a KW test across all groups was followed by pairwise MWW tests between genotypes (three MWW tests in total). Comparisons to chance levels (i.e., to zero) were tested for each group by OSS tests; in Figure 16*A*, *B*, no OSS tests were performed.

The experiments in Figures 9*D*, *F–I* and 15*E* followed a two-group design with two test conditions (the presence or absence of light) for the experimental genotype expressing ChR2XXL (see Fig. 9*D*,*F–I*) or Chrimson (see Fig. 15*E*). MWW tests were performed between the two test conditions; no OSS tests were performed.

The experiment in Figure 10 followed a six-group design with two test conditions (the presence or absence of the fructose reward) for the experimental genotype expressing ChR2XXL. The animals received paired or unpaired odor-fructose training, either not activating APL during training at all, or activating APL during odor presentation, or in the absence of odor. A KW test across all groups was followed by pairwise MWW tests between groups within the same test condition, as well as between test conditions

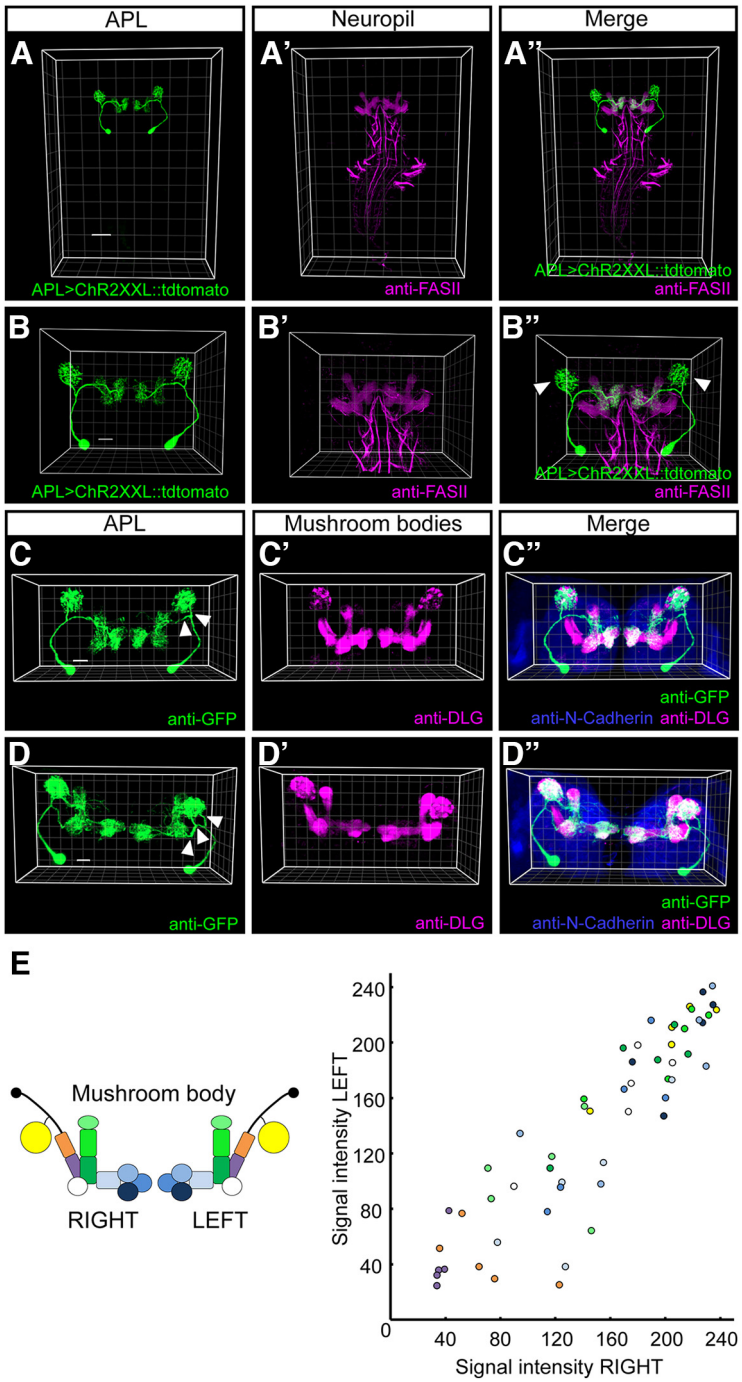

Figure 3. Brain expression of the APL-GAL4 driver is restricted to the APL neuron. ***A–A″***, 3D view of the expression pattern from the APL-GAL4 driver in a third-instar larval brain visualized using the fluorescence signal from the UAS-ChR2XXL::tdtomato effector (APL>ChR2XXL::tdtomato; green). Axon-rich regions of the mushroom body peduncle and lobes can be discerned as references after labeling with a primary monoclonal mouse anti-FASII antibody and a secondary polyclonal goat anti-mouse AlexaFluor-488 antibody (anti-FASII; magenta). Transgene expression is specific to the hemispherically unique APL neuron. The data were acquired with a 20× glycerol objective. Scale bar and grid spacing, 50 µm. ***B–B″***, Same as in ***A–A″***, providing a close-up view of the mushroom bodies. APL sends projections into the calyx and a subset of the compartments of the medial and vertical lobes. ***B″***, White arrowheads point to the calyx, which is innervated by APL but is largely devoid of the axonal FASII marker. The data were acquired with a 63× glycerol objective. Scale bar and grid spacing, 20 µm. ***C–D″***, Same as in ***B–B″***, except that the APL-GAL4 driver was crossed to UAS-mCD8::GFP as the effector. APL membranes can be visualized after labeling with a primary polyclonal rabbit anti-GFP antibody and a secondary polyclonal goat anti-rabbit AlexaFluor-488 antibody (anti-GFP; green). The mushroom bodies are labeled by a primary monoclonal mouse anti-DLG antibody and a secondary polyclonal goat anti-mouse AlexaFluor-568 antibody (anti-DLG; magenta); neuropils can be discerned as a reference by a primary monoclonal rat anti-N-Cadherin antibody and a secondary polyclonal goat anti-rat AlexaFluor-647 antibody (anti-N-Cadherin; blue). Close-up analysis of the APL morphology revealed two, or in one case three, branches (white arrowheads in ***C*** and ***D***, respectively) splitting from the primary neurite; notably, these numbers of branches do not differ between the two hemispheres ($N = 11$ brains). The data were acquired with a 16× glycerol objective. Scale bar and grid spacing, 20 µm. ***E***, For each mushroom body calyx and compartment, the mean pixel intensities of APL labeling in the right hemisphere versus the left hemisphere are plotted (color code in accordance with the mushroom body schematic). The observed correlation indicates no interhemispheric difference in APL morphology. The source data and results of all statistical tests are documented in Extended Data Figure 3-1 and Table 2.

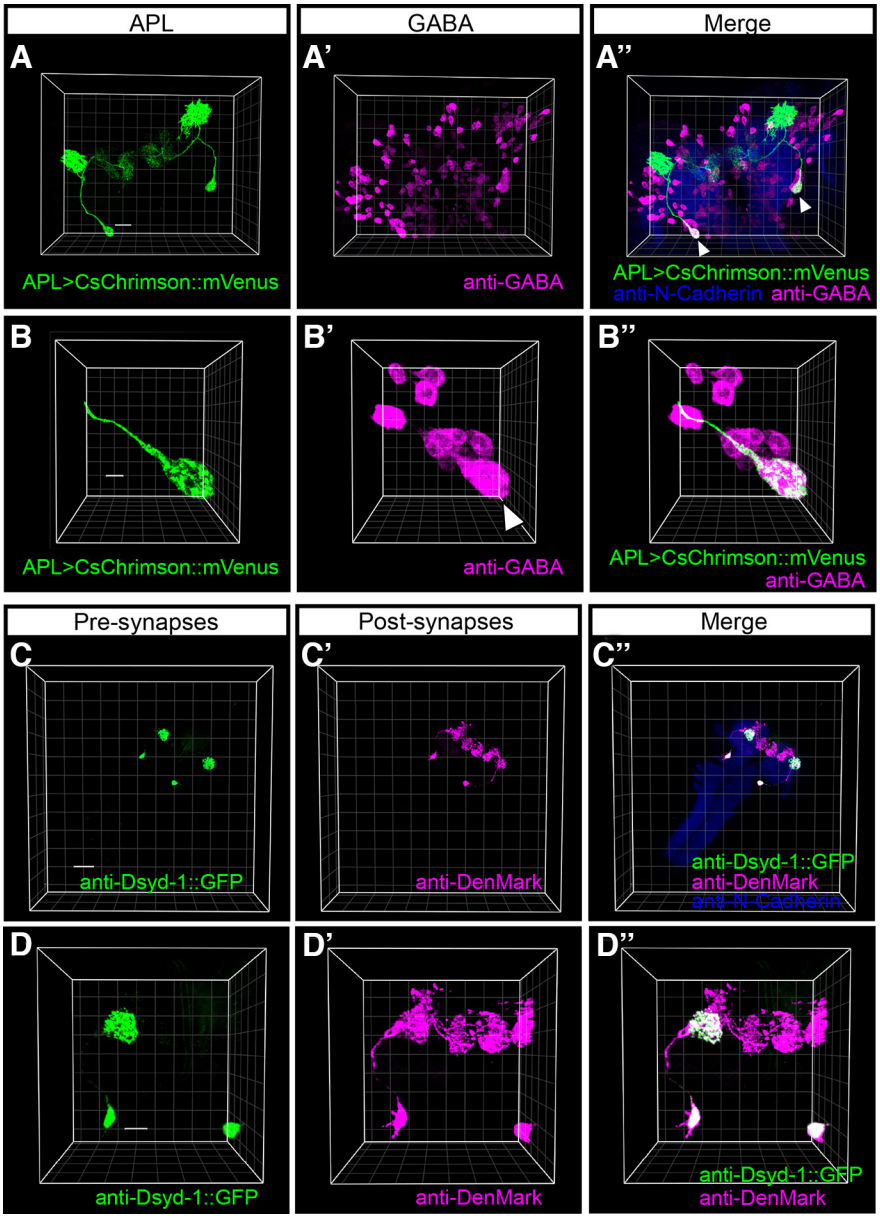

Figure 4. The larval APL neuron is GABAergic and is presynaptic in the calyx and postsynaptic in both the calyx and the lobes. ***A–A″***, 3D view of the expression pattern from the APL-GAL4 driver in the third-instar larval brain visualized using the fluorescence signal from the Chrimson effector (APL>CsChrimson::mVenus; green). GABAergic signals can be visualized after labeling with a polyclonal rabbit anti-GABA antibody and a polyclonal Cy5-conjugated goat anti-rabbit antibody (anti-GABA; magenta). ***A″***, White arrowheads point to an overlap of the GABA signal and the fluorescence signal in the APL soma. Neuropil regions are visualized as a reference by using a primary monoclonal rat anti-N-Cadherin antibody and a secondary polyclonal goat anti-rat Cy3 antibody (anti-N-Cadherin; blue). The data were acquired with a 63× glycerol objective. Scale bar and grid spacing, 20 µm. ***B–B″***, Same as in ***A–A″***, providing a close-up view of the APL soma. ***B′***, White arrowhead points to the APL soma surrounded by additional GABAergic cells. The data were acquired with a 63× glycerol objective. Scale bar and grid spacing, 5 µm. ***C–C″***, The APL-GAL4 driver was crossed to a double effector with both UAS-Dsyd-1::GFP and UAS-DenMark to label the presynaptic and postsynaptic sites of the APL neuron in third-instar larvae. Presynaptic regions of APL can be visualized after labeling with a polyclonal FITC-conjugated goat anti-GFP antibody (anti-Dsyd-1::GFP; green). Postsynaptic regions are revealed after labeling with a primary polyclonal rabbit anti-DsRed antibody and a secondary polyclonal goat anti-rabbit Cy5 antibody (anti-DenMark; magenta). Neuropil regions are visualized as a reference by using a primary monoclonal rat anti-N-Cadherin antibody and a secondary polyclonal goat anti-rat Cy3 antibody (anti-N-Cadherin; blue). The presynaptic marker Dsyd-1 is mainly restricted to the calyx, whereas the postsynaptic marker DenMark localizes to both the calyx and a subset of the compartments in the lobes, confirming the regional synaptic polarities of the larval APL neuron (Masuda-Nakagawa et al., 2014; Eichler et al., 2017). The data were acquired with a 16× glycerol objective. Scale bar and grid spacing, 50 μm. ***D–D″***, Same as in ***C–C″***, providing a close-up view of the presynaptic and postsynaptic regions of APL. Scale bar and grid spacing, 25 μm. For a corresponding movie, see Movie 3.

for a given kind of training regimen (nine MWW tests in total). Differences from chance levels (i.e., from zero) were tested for in each group by OSS tests.

The preference scores shown in Figure 11*A–C* underlie the associative memory scores in Figure 10. The experiment followed a four-group design with two test conditions (the presence or absence of the fructose reward) for the experimental genotype expressing ChR2XXL. A KW test across all groups was followed by pairwise MWW tests between groups that had received paired or unpaired odor-fructose training within the same test condition; in addition, MWW tests were performed between the respectively trained groups that were tested in the absence of fructose and the baseline odor preference scores (four MWW tests in total). Differences from chance levels (i.e., from zero) were tested for in each group by OSS tests.

Figure 11*D* shows pooled preferences from Figure 11*A–C* and follows a three-group design for the experimental genotype expressing

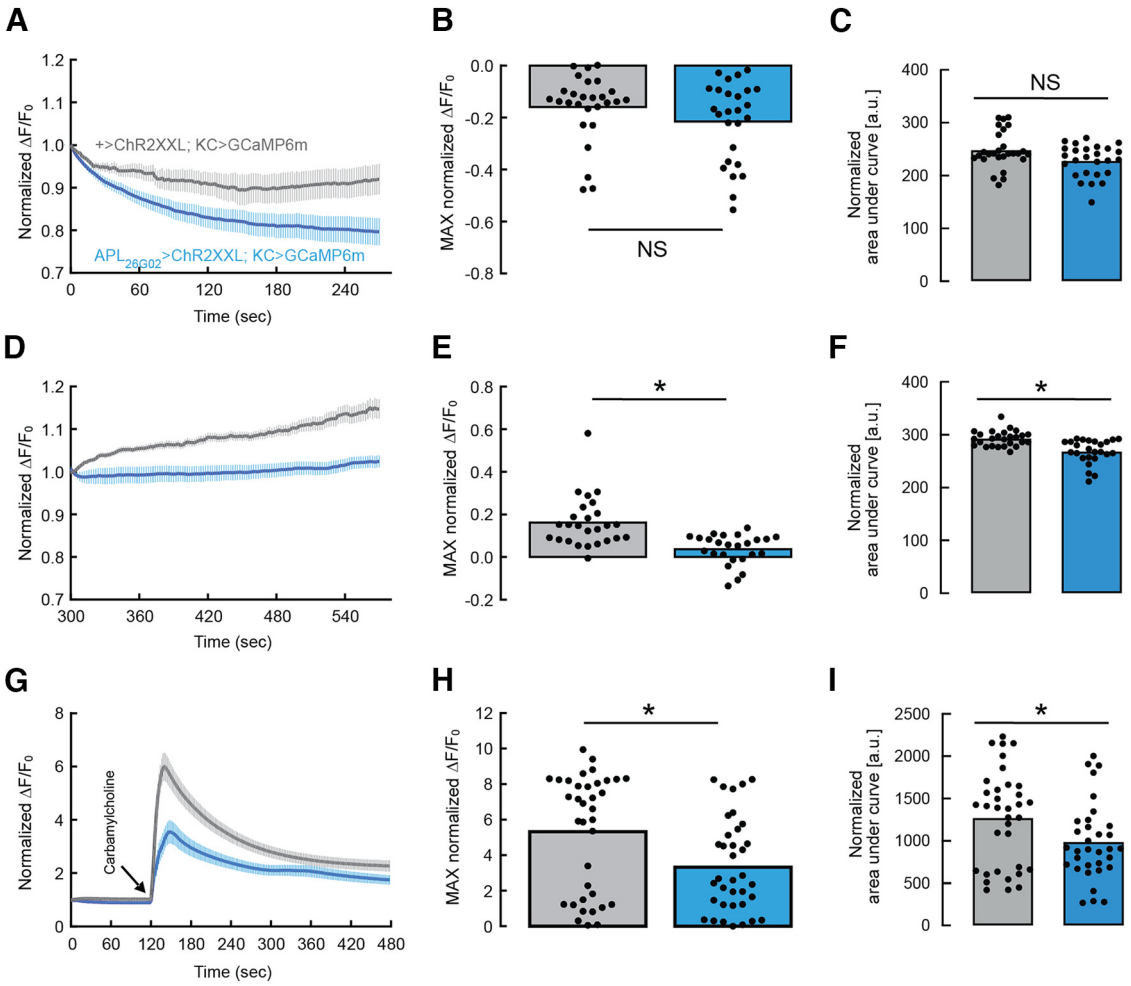

Figure 5. Optogenetic activation of APL can reduce levels of activity in mushroom body KCs. ***A–C***, At relatively low light intensity (from 0 to 270 s), activation of APL in isolated brain preparations of APL_{26G02}>ChR2XXL; KC>GCaMP6m larvae (blue) had no major effect on intracellular Ca^{2+} signals in the calycal ROIs/KCs (Normalized $\Delta F/F_0$) relative to genetic controls (+>ChR2XXL; KC>GCaMP6m) (gray). For each calycal ROI/KC, the data are normalized to the beginning of the indicated observation period as a baseline and are plotted over time in ***A*** (showing mean ± SEM). The maximum difference from the baseline for each calycal ROI/KC is plotted in ***B*** (showing mean and data-point scatter). The area under the curve is shown in ***C*** (showing mean and data-point scatter). ***D–F***, In contrast, compared with genetic controls, activation of APL by a more intense light in the same specimen (from 300 to 570 s) reduced Ca^{2+} signals in the KCs. ***G–I***, Using the same light intensity as in ***D–F***, bath-application of the acetylcholine receptor agonist carbamylcholine (at 120 s) massively increased Ca^{2+} signals in genetic controls (gray), an effect that was reduced to about half under conditions of APL activation (blue). Preparation and imaging according to Selcho et al. (2017) and Lyutova et al. (2019). The number of brains for genetic controls and APL activation, respectively, was 7 and 9 in ***A–F*** and 10 and 8 in ***G–I***; the number of calycal ROIs/KCs was 27 and 26 in ***A–C***, 26 and 25 in ***D–F***, and 36 and 37 in ***G–I***. MWW comparisons: NS, $p > 0.05$; *$p < 0.05$. The source data and results of all statistical tests are documented in Extended Data Figure 3-1 and Table 2.

ChR2XXL. A KW test across all groups was followed by pairwise MWW tests between groups (three MWW tests in total); no OSS tests were performed.

The preference scores shown in Figures 12*B*, *D* and 15*B* underlie the associative memory scores in Figure 12*A*, *C* and Figure 15*A*, respectively. The experiment followed a three-group design for the experimental genotype expressing ChR2XXL (see Fig. 12*B*), GtACR1 (see Fig. 12*C*), or Chrimson (see Fig. 15*B*) and their respective genetic controls. After a KW test across all groups, MWW tests were performed between groups that had received paired or unpaired odor-APL activation training and the baseline odor preference scores (four MWW tests in total).

The experiment in Figure 12*E* followed a four-group design for the experimental genotype expressing ChR2XXL. After a KW test across all groups, MWW tests were performed between the group tested immediately after training (retention interval 0 min) and the groups tested 5, 10, or 20 min after training (three MWW tests in total). Differences from chance levels (i.e., from zero) were tested for in each group by OSS tests.

The experiment in Figure 12*F* followed a nine-group design for the experimental genotype expressing ChR2XXL. A KW test was performed across all groups; no OSS tests were performed.

Figure 13*B* describes the odor preferences of larvae of the experimental genotype expressing ChR2XXL tested after paired or unpaired training, over time. No statistical analyses were performed; rather, the data were collated over time and were statistically compared between the two training groups in Figure 13*C* (see next paragraph).

The experiments in Figures 13*C–F*, 14*C*, 15*C*, *D*, and 17*C* followed a two-group design for the experimental genotype expressing ChR2XXL (see Figs. 13*C–F*, 14*C*, 17*C*) or Chrimson (see Fig. 15*C*,*D*). MWW tests were performed between the two groups. Differences from chance levels (i.e., from zero) were tested for in each group by OSS tests (in Fig. 13*C–F*, no OSS tests were performed).

The experiments in Figure 14*A*, *B*, *E*, *G* followed a six-group design with three genotypes (experimental genotype expressing ChR2XXL, effector, and driver controls) and two test conditions (the presence or absence of light). A KW test across all the groups was performed first. In case of significance, pairwise MWW tests were performed between genotypes within the same test condition, as well as between test conditions for a given genotype (nine MWW tests in total). In Figure 14*A*, *B*, differences from chance levels (i.e., from zero) were tested for in each group by OSS tests; in Figure 14*E*, *G*, no OSS tests were performed.

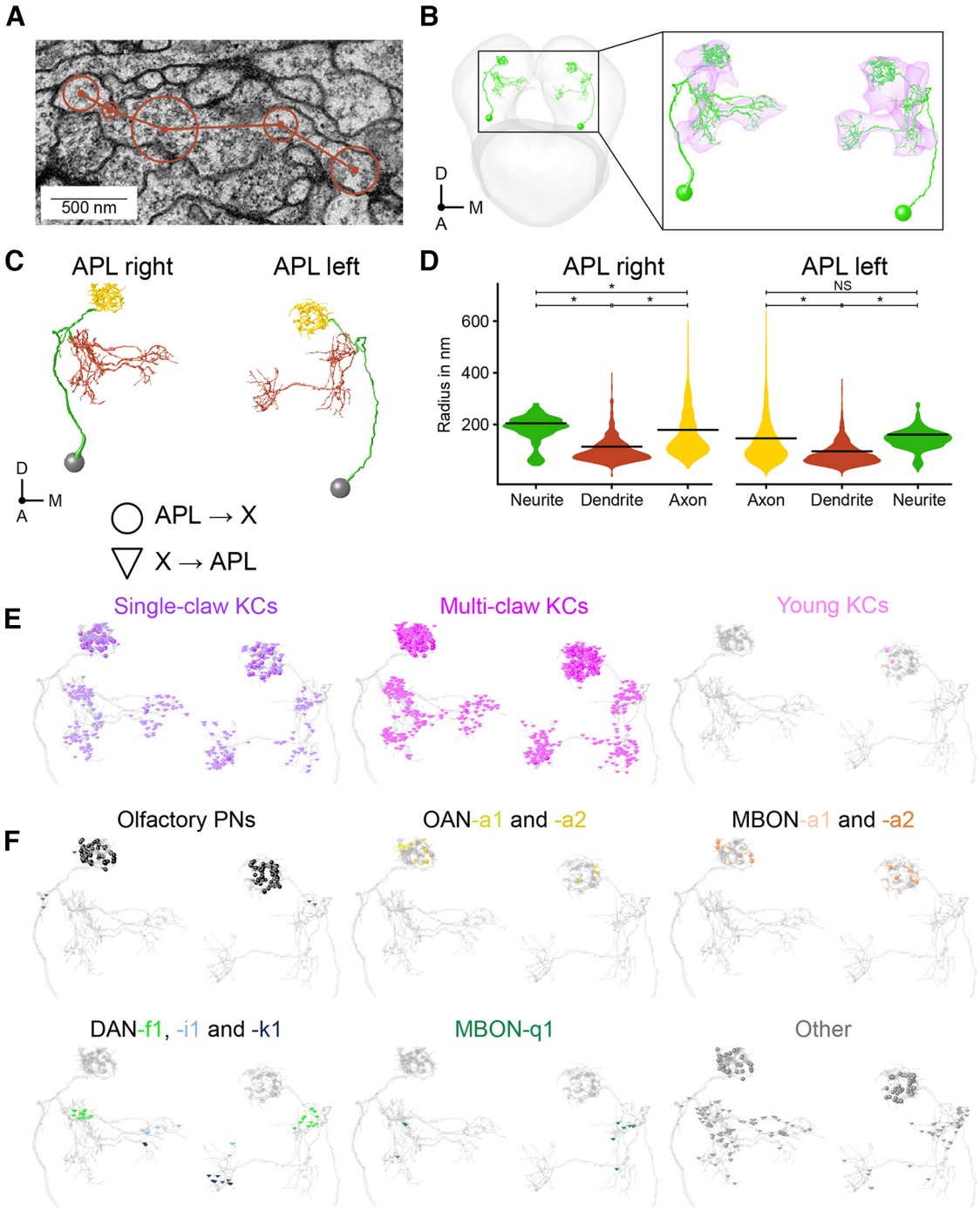

Figure 6. Volume reconstruction of the larval APL neuron. ***A***, Electron microscopy cross-section of the APL neuron in a first-instar larva. Points connected by lines represent the skeletonized reconstruction of the neuron (for details, see Eichler et al., 2017). Circles represent radius annotations for volume reconstruction. Scale bar, 500 nm. ***B***, Reconstructed volume of the left- and the right-hemisphere APL neuron (green) in the context of the complete CNS (left; gray mesh), and in a close-up of the mushroom body region (right; magenta). For a corresponding movie, see Movie 4. ***C***, Reconstructed volume of both APL neurons separated into axonal (yellow) and dendritic (red) regions, and the neurite and its branches (green). ***D***, Quantification of the radii of the APL neurons, showing that the neurite is thicker than the axonal regions (significant only for the right-hemisphere APL neuron), which in turn are thicker than the dendritic regions. The data are displayed as violin plots. Bars represent mean. MWW comparisons between the APL regions with a BH correction: NS, $p > 0.05$; *$p < 0.05$. The source data and results of all statistical tests are documented in Extended Data Figure 3-1 and Table 2. ***E***, ***F***, Dots and triangles represent presynaptic and postsynaptic sites, respectively, selectively for different types of connected neuron, namely: (***E***) single-claw, multiclaw, and young KCs; and (***F***) neurons with connections in the calyx (top row: olfactory PNs; OAN-a1/a2; MBON-a1/a2), as well as neurons that have been studied elsewhere in functional experiments, such as DAN-i1 (Saumweber et al., 2018; Schleyer et al., 2020), DAN-f1 (Eschbach et al., 2020; Weiglein et al., 2021), and DAN-k1 (Saumweber et al., 2018). Neurons with less than two synapses with APL in both hemispheres are shown as "Other." ***B***, ***C***, A, Anterior; D, dorsal; M, medial. Corresponding 3D visualizations can be found in Movies 4, 5, 6.

The experiments in Figure 16*C*, *D* followed a four-group design with two test conditions (the presence or absence of light) for the experimental genotype expressing GtACR1 (see Fig. 16*C*) or ChR2XXL (see Fig. 16*D*). A KW test was performed across all groups; no OSS tests were performed.

The experiments in Figures 14*D* and 17*D* followed a four-group design for the experimental genotype expressing ChR2XXL. In Figure 14*D*, a KW test across all groups was followed by MWW tests performed between the group of larvae trained/tested with AM and (1) the group

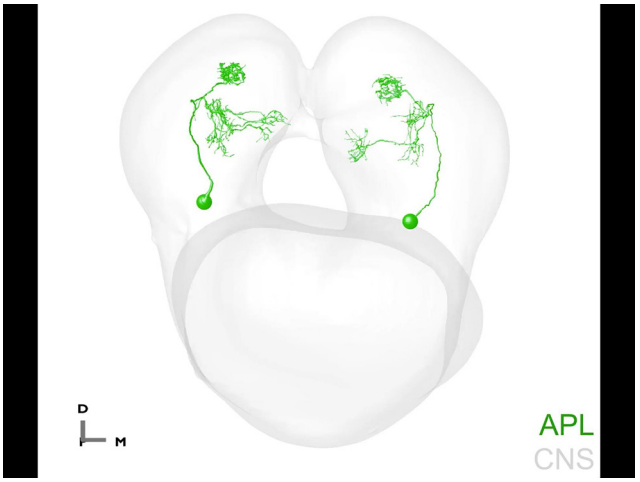

Movie 4. Volume reconstruction of the left- and the right-hemisphere APL neuron (green) in a first-instar larval brain (CNS; gray), with the focus on APL's connectivity within the mushroom bodies (MB; magenta). "X" indicates synapses with any type of partner. Yellow spheres and red pyramids represent the location of presynaptic and postsynaptic sites of both APLs, respectively. A, Anterior; D, dorsal; M, medial. Based on the dataset from Eichler et al. (2017). See also Figure 6*B*. [View online]

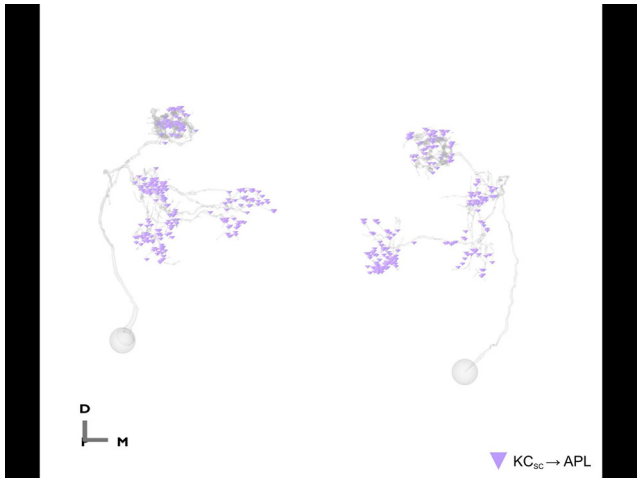

Movie 5. Volume reconstruction of the left- and the right-hemisphere APL neuron in a first-instar larva and sites of presynapses and postsynapses with different subclasses of mushroom body intrinsic neurons (KCs), namely, single-claw, multiclaw, and young KCs. Spheres and pyramids represent presynaptic and postsynaptic sites of APL, respectively. A, Anterior; D, dorsal; M, medial. Based on the dataset from Eichler et al. (2017). See also Figure 6*E*. [View online]

trained with AM/tested with OCT and (2) the group trained/tested with OCT; as well as between the group trained/tested with OCT and the group trained with OCT/tested with AM (three MWW tests in total). Differences from chance levels (i.e., from zero) were tested for in each group by OSS tests. In Figure 17*D*, a KW test across all groups was followed by MWW tests performed between the untreated group and (1) the group fed 3IY, (2) the group fed 3IY plus L-DOPA, and (3) the group fed L-DOPA; as well as between the group fed 3IY and the group fed 3IY plus L-DOPA (four MWW tests in total). Differences from chance levels (i.e., from zero) were tested for in each group by OSS tests.

Results

Organization of the APL neuron

We first investigated the expression pattern of the APL-GAL4 driver in third-instar larvae in the full-body context. This took advantage of a combination of autofluorescence signals with fluorescence from UAS-mCherry-CAAX as the effector construct. These signals can be detected conveniently under a light-sheet microscope on clearing the sample (Kobler et al., 2021). Fluorescence signals that can be observed across wavelengths and in both the experimental genotype (APL>mCherry-CAAX) and the genetic controls (+>mCherry-CAAX and APL>+ as the effector and the driver control, respectively) constitute autofluorescence and allow rich anatomic detail to be discerned (Fig. 2). We note that signals from fluorescent food particles contribute to individually variable signals along the alimentary canal (Kobler et al., 2021). Fluorescence reflecting the expression of mCherry-CAAX, however, was reproducibly seen specifically in a giant pair of cells in the mushroom body region (Fig. 2*B‴*,*D‴*,*F‴*) that can be identified as APL (Movie 1). Thus, to the extent tested here and in the absence of a standard neuroanatomy against which full-body preparations can be systematically registered at high resolution, the effects observed using the APL-GAL4 driver are interpreted without reference to transgene expression elsewhere in the body.

Combining the APL-GAL4 driver with the UAS-ChR2XXL::tdtomato effector and using the resulting fluorescence signal confirm that within the CNS and the mushroom body APL-GAL4 specifically expresses in the APL neuron (Fig. 3*A*-*B″*) (Saumweber et al., 2018). In addition, APL-GAL4 was crossed to UAS-mIFP/MB247>mCherry-CAAX (Kobler et al., 2021) to label APL together with the mushroom body (Movie 2). In both cases, our results confirm that the primary neurite of APL splits to send projections separately into the calyx and the lobes of the mushroom bodies (Fig. 3*B″*; Movie 2) (Masuda-Nakagawa et al., 2014; Mayseless et al., 2018; Saumweber et al., 2018). This morphology was seen in 10 of 11 preparations of third-instar larval brains with the APL-driver and UAS-mCD8::GFP as the effector (Fig. 3*C*–*C″*). Only in one preparation did the primary neurite split into three branches in both hemispheres (Fig. 3*D*–*D″*). This made us wonder whether there is any variability in APL projections to the calyx or different lobe compartments, in particular, in the third-instar larvae

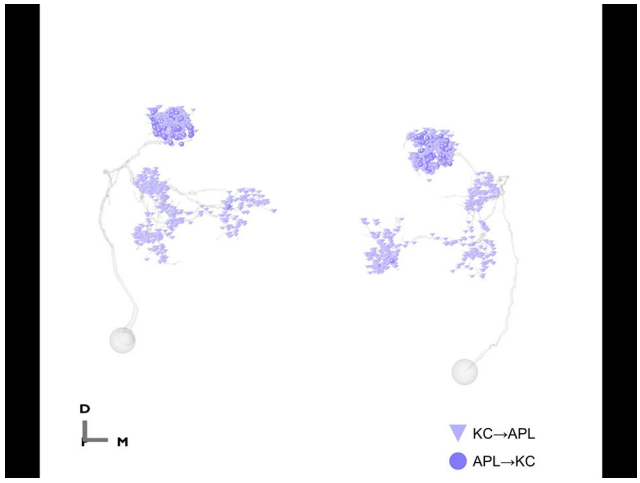

Movie 6. Volume reconstruction of the left- and the right-hemisphere APL neuron in a first-instar larva and sites of presynapses and postsynapses with different types of partner, separated into all subclasses of mushroom body intrinsic neurons (KCs) and the mushroom body extrinsic neurons indicated. Remaining neurons bearing less than two synapses with APL in both hemispheres are shown as "Other"; "X" indicates synapses with non-KCs. Spheres and pyramids represent presynaptic and postsynaptic sites, respectively. A, Anterior; D, dorsal; M, medial. Based on the dataset from Eichler et al. (2017). See also Figure 6*F*. [View online]

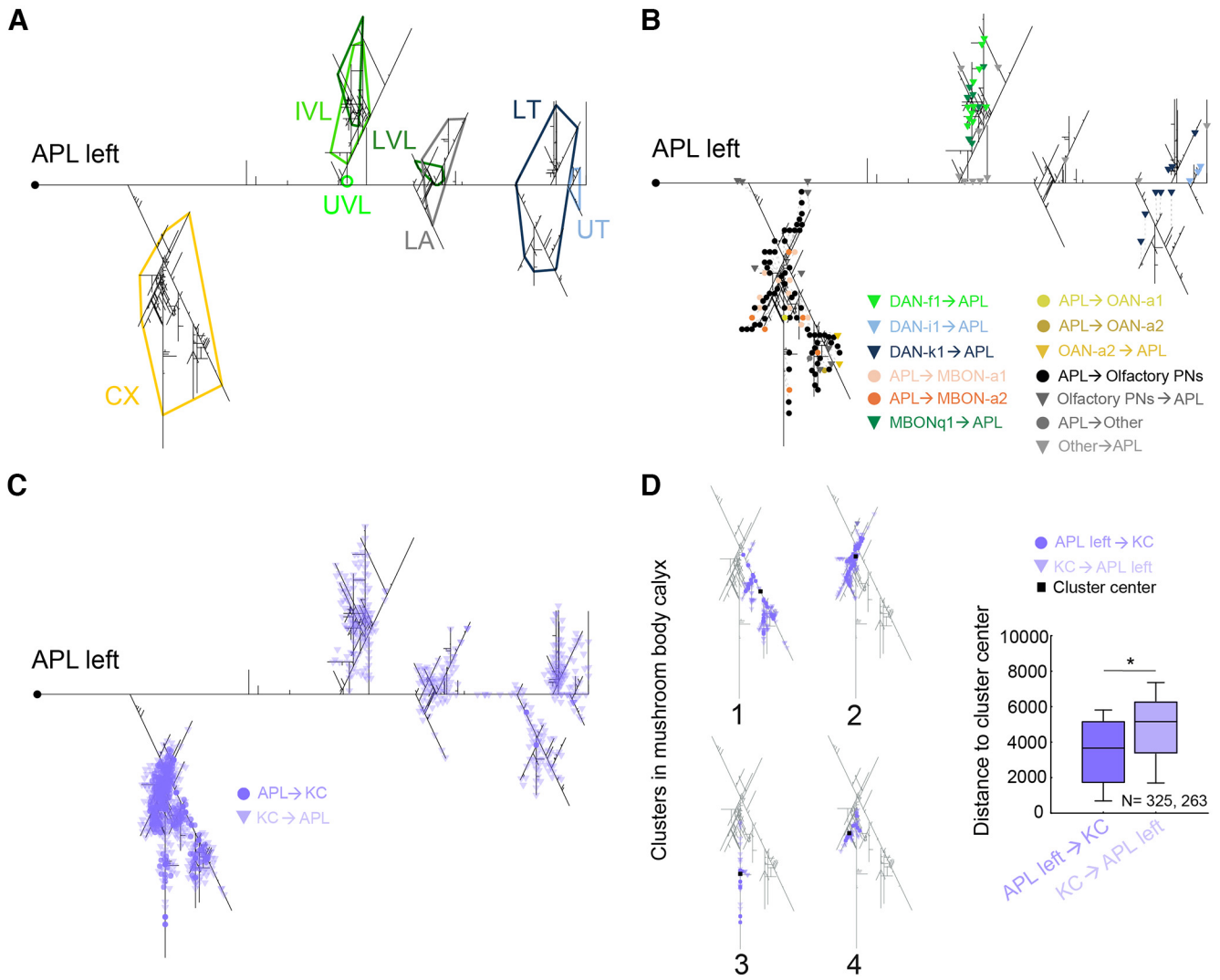

Figure 7. Dendrogram analysis of the larval APL neuron. ***A***, Two-dimensional dendrogram of the APL neuron from the left hemisphere, based on an electron microscope reconstruction in a first-instar larva (data from Eichler et al., 2017). Branch lengths are preserved in a topologically correct manner. Colored envelopes represent the mushroom body calyx and compartments innervated by APL (see also Fig. 1*B*,*C*). High-resolution versions of this figure, for the APL neurons of both hemispheres, can be found in Extended Data Figure 7-1. ***B***, Synapses at their topologically correct site on the left-hemisphere APL neuron with the mushroom body extrinsic neurons indicated. Dots and triangles represent presynaptic and postsynaptic sites of APL, respectively. For better readability, some symbols were displaced and their true locations indicated by a dashed line. High-resolution versions of this figure, for the APL neurons of both hemispheres, can be found in Extended Data Figure 7-2. ***C***, Same as in ***B***, but showing synaptic sites with the mushroom body intrinsic neurons, the KCs. Dark purple dots and bright purple triangles represent APL-to-KC and KC-to-APL synapses, respectively. High-resolution versions of this figure, for the APL neurons of both hemispheres, can be found in Extended Data Figure 7-3. ***D***, Cluster analysis revealed that calycal synaptic sites of the left-hemisphere APL with the KCs are organized in four clusters (1-4). The accompanying quantification shows geodesic distances of synapses to the center of their respective center-surround structure on the left-hemisphere APL neuron. Most of the APL-to-KC synapses (dark purple dots) are observed toward the center of these clusters (dark square), whereas KC-to-APL synapses (bright purple triangles) are observed mainly in the surround. The data are displayed as box plots. Middle line indicates the median. Box boundaries represent the 25% and 75% quantiles. Whiskers represent the 10% and 90% quantiles. The sample sizes (number of synapses) are given within the figure. MWW comparisons between APL-to-KC and KC-to-APL synapses: *$p < 0.05$. The source data and results of all statistical tests are documented in Extended Data Figure 3-1 and Table 2. Corresponding analyses, in the context of the full dendrograms and for the APL neurons of both hemispheres, can be found in Extended Data Figure 7-4.

that we intended to use later in our behavioral analyses. Across five specimens of third-instar larval brains with the APL-driver and UAS-mCD8::GFP as the effector, coverage of the calyx and of the compartments was similar between the APL neuron of each hemisphere (Fig. 3*E*). GFP signals were consistently strong in the calyx, close to absent in the two peduncle compartments, weak in the upper vertical lobe and the shaft of the medial lobe, and moderate to strong in the other compartments (Fig. 3*E*). Taking the present data together with previously published data, we conclude that the larval APL innervates the calyx and 6 of the 10 compartments, namely, the lateral appendix, the upper, intermediate, and lower vertical lobe, as well as the upper and lower toe (Figs. 1*C*, 3) (Masuda-Nakagawa et al., 2014; Eichler et al., 2017; Saumweber et al., 2018).

We next confirmed that APL is GABAergic (Fig. 4*A*–*B*″) (Masuda-Nakagawa et al., 2014) and studied the regional organization of presynaptic and postsynaptic sites of APL using the APL-GAL4 driver together with the double effector UAS-Dsyd-1::GFP/UAS-DenMark (Owald et al., 2015). Our results show that APL is presynaptic in the calyx, whereas it is postsynaptic in both the calyx and the lobes (Fig. 4*C*–*D*″; Movie 3), confirming earlier reports (Masuda-Nakagawa et al., 2014; Eichler et al., 2017). Indeed, we also confirm a functionally inhibitory connection from APL to the KCs in the calyx. Combining transgene

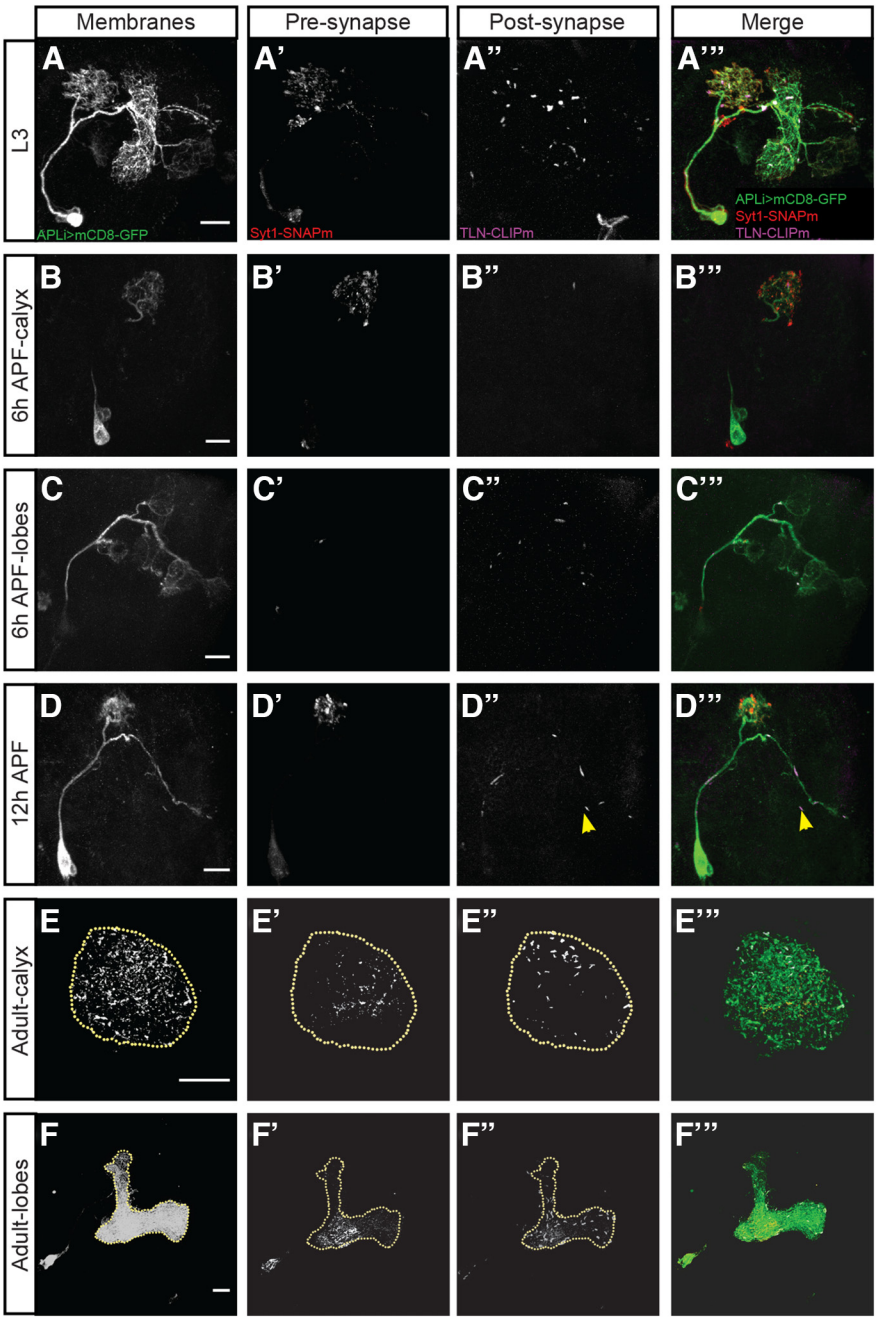

Figure 8. Regional synaptic polarity of APL across metamorphosis. Confocal maximum projection images of stainings for mCD8::GFP, Syt1::SNAP, and TLN::CLIP (Kohl et al., 2014), driven by the APL-specific intersectional driver APLi (Lin et al., 2014; Mayseless et al., 2018) at the following developmental times: (***A–A‴***) third-instar larva (L3); (***B–C‴***) 6 h after puparium formation (6 h APF: calyx: ***B–B‴***; lobes: ***C–C‴***); (***D–D‴***) 12 h APF; (***E–F‴***) adult (calyx: ***E–E‴***; lobes: ***F–F‴***). Brains were stained with a polyclonal chicken anti-GFP antibody to label the APL neuron (***A–F***). To label presynapses (***A′–F′***) and postsynapses (***A″–F″***), the presynaptic reporter synaptotagmin was fused to the chemical tag SNAPm (Syt1-SNAPm), and the postsynaptic reporter telencephalin was fused to CLIPm (TLN-CLIPm), respectively (Kohl et al., 2014). Merged images are shown in ***A‴–F‴***. In the third-instar larva, presynaptic staining was largely restricted to the calyx (***A′***), whereas postsynaptic staining was distributed in both the calyx and the lobes (***A″***). At 6 h APF, both presynaptic and postsynaptic staining are similarly distributed to that in the larvae (***B′–C‴***); notably, presynaptic structures seem to be more punctate (***B′***,***C′***), and fewer postsynaptic structures are detectable (***B″***,***C″***). As late as 12 h APF, both presynaptic and postsynaptic structures are still detectable (***D′***,***D″***); postsynaptic structures appear to be detached from the neurite (***D″***,***D‴***, yellow arrowhead). In adults, both presynaptic and postsynaptic markers are detectable in both the calyx and the lobes (***E–F‴***). The data were acquired with a 40× oil objective. Scale bars, 20 μm.

expression by the GAL4-UAS and the lexA-lexAop systems, we monitored changes in intracellular Ca^{2+} through changes in fluorescence intensity in the KCs of isolated brain preparations of controls (+>ChR2XXL; KC>GCaMP6m) and on optogenetic activation of APL (APL_{26G02}>ChR2XXL; KC>GCaMP6m). At the relatively lower blue-light intensity (80 ms pulses every 2 s, at 1.8 mW/cm^2), the control brains showed no specific response to the light; rather, fluorescence intensity decreased slightly across the recording period (Fig. 5*A*, gray). Activation of APL resulted in a trend for yet further decreased levels of fluorescence (Fig. 5*A–C*, blue). We then exploited the observation that for increased light intensity (4.1 mW/cm^2) fluorescence intensity increased under control conditions (Fig. 5*D*, gray), reflecting the light responsiveness of the KCs themselves or of neurons upstream of the KCs. Relative to these fluorescence signals observed in the controls, signals were reduced by APL activation (Fig. 5*E*,*F*).

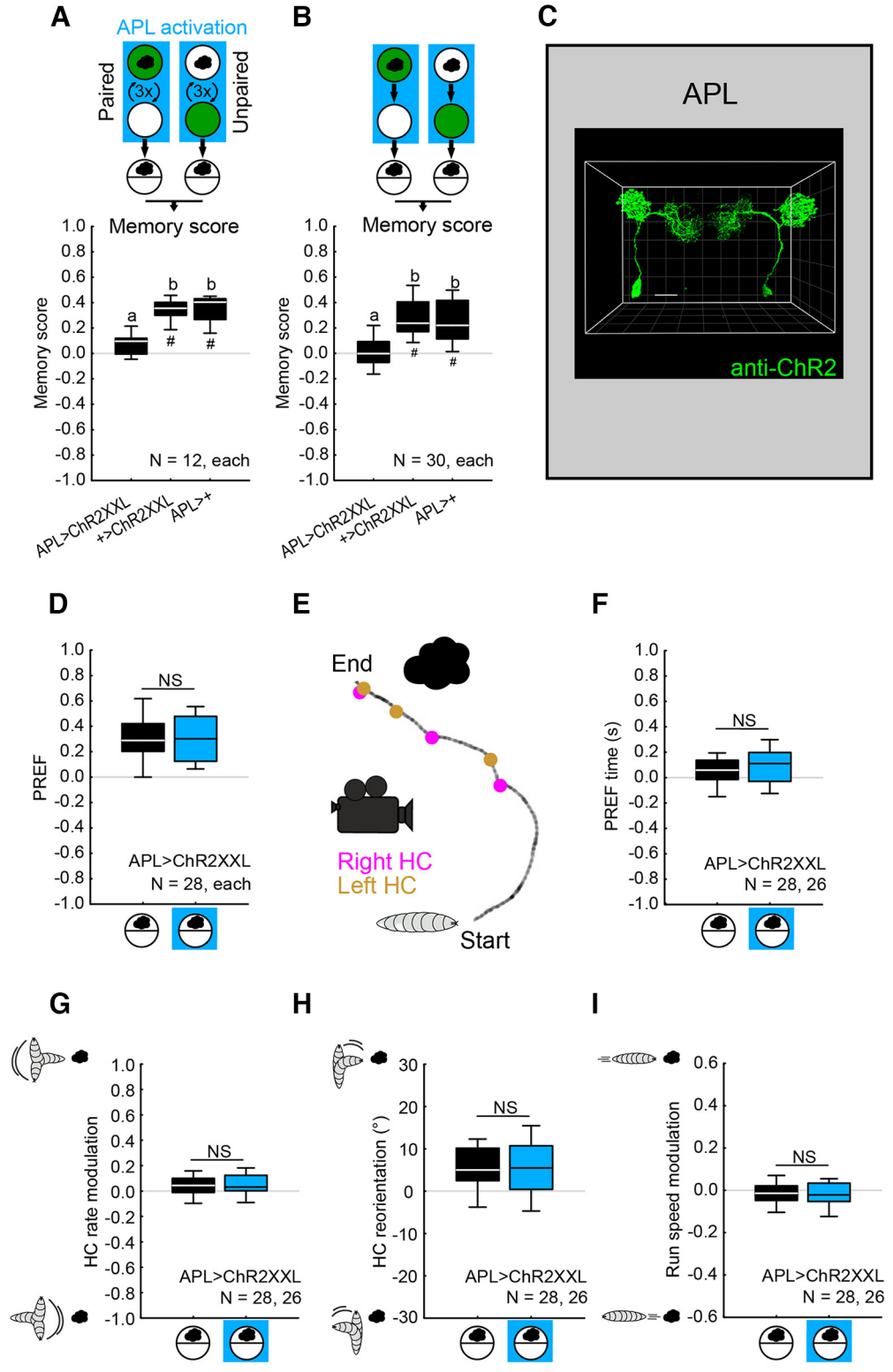

Figure 9. Memory scores are abolished on activation of APL throughout training. ***A***, Larvae were trained such that, in one group of animals, the odor AM (black cloud) was paired with the fructose reward (green fill of circle indicating a Petri dish), alternating with blank trials (open circle), whereas in a reciprocal group, the odor was presented unpaired from the fructose reward; here and throughout this study, the sequence of training events was as depicted in half of the cases, and in the reverse order in the other half of the cases. The APL neuron was optogenetically activated with blue light illumination (blue rectangle) during the complete training phase. The larvae from both groups were then tested for their odor preference, and associative memory was quantified by the memory score as the difference in preference between these reciprocally trained groups of animals. Double-heterozygous animals of the genotype APL>ChR2XXL were used for APL activation; larvae heterozygous for either the GAL4 (APL>+) or the effector (+>ChR2XXL) were used as the genetic controls. Optogenetic activation of the APL neuron during the complete training phase abolished associative memory scores. ***B***, The same effects were observed in a shortened, one-training-cycle version of this experiment. ***C***, Full projection of the expression pattern from the APL-GAL4 driver crossed to UAS-ChR2XXL in the third-instar larval brain. ChR2XXL is visualized by a primary monoclonal mouse anti-ChR2 antibody and a secondary polyclonal donkey anti-mouse Cy3 antibody. Confirming our results from Figures 2-4, this reveals strong and reliable transgene expression in the APL neuron of both hemispheres (anti-ChR2XXL; green). The data were acquired with a 63× glycerol objective. Scale bar and grid spacing, 20 µm. For a corresponding movie, see Movie 7. ***D***, The behavior of experimentally naive

Remarkably, even high levels of fluorescence induced by pharmacologically stimulating KCs via the acetylcholine receptor agonist carbamylcholine in control brains (Fig. 5*G*, gray) were reduced by simultaneous APL activation (Fig. 5*G–I*). Together, these data confirm a functionally inhibitory effect of APL activation on the KCs in the calyx.

In terms of the organization of APL, the above results also match the situation in first-instar larvae, as shown here for a volume reconstruction of APL generated from the electron microscopy reconstruction of the mushroom body in Eichler et al. (2017) (Fig. 6*A*,*B*; Movie 4). Specifically, this volume reconstruction shows that the relatively slender axonal and dendritic branches of APL arise separately from a thicker neurite (Fig. 6*C*,*D*), similar to the locust homolog of APL, called GGN (for giant GABAergic neuron) (Papadopoulou et al., 2011; Ray et al., 2020). The electron microscope dataset of Eichler et al. (2017) further allowed the site of the synapses for the different classes of synaptic partners of APL to be mapped onto its volume reconstruction (Fig. 6*E*,*F*; Movies 5, 6). Furthermore, the connectomics data allowed dendrograms of APL to be derived, that is, 2D representations of APL preserving branch lengths and synaptic locations in a topologically correct manner (Fig. 7). Within such a topology, it can be discerned that, wherever they coexist, the synapses that APL has with mushroom body extrinsic neurons are not segregated from, but are intermingled with, the connections to the mushroom body intrinsic neurons, the KCs (Fig. 7*B*,*C*). In the lobes, the almost exclusively postsynaptic sites of APL are relatively sparse (Fig. 7*B*, *C*) and with some variation in topology between the APL neuron of the left and the right brain hemisphere (for the right-hemisphere APL neuron, see Extended Data Fig. 7-1). In the calyx, an analysis of cable length (geodesic distance between synapses) reveals that reciprocal synapses between APL and the KCs are arranged in four synapse-rich center-surround structures such that APL-to-KC synapses are found toward their center, whereas KC-to-APL synapses are located mainly in the surround (Fig. 7*D*).

Regional synaptic polarity of APL across metamorphosis

Given the conserved regional synaptic polarity of APL across larval stages (see preceding section) and given that APL persists into adulthood yet in adults it is not regionally polarized (C. L. Wu et al., 2013; Lin et al., 2014; Mayseless et al., 2018; Saumweber et al., 2018), we examined how APL develops across metamorphosis. To this end, we used genetically encoded protein

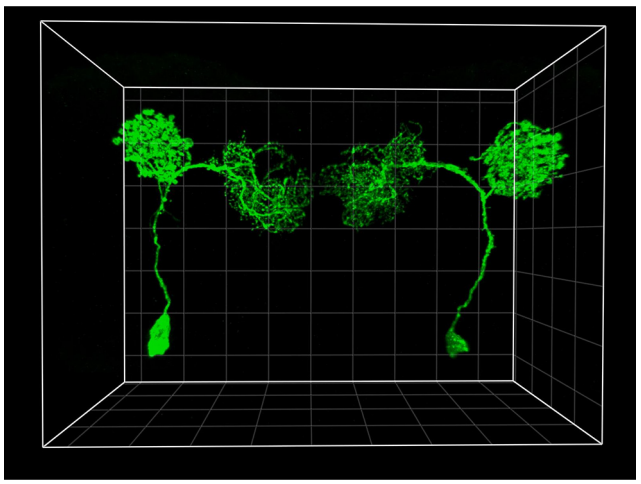

Movie 7. 3D rendering of the expression pattern of ChR2XXL in APL in a third-instar larva, based on data shown in Figure 9*C*. Genotype: APL>ChR2XXL. The data were acquired with a 63× glycerol objective; grid spacing: 20 μm. [View online]

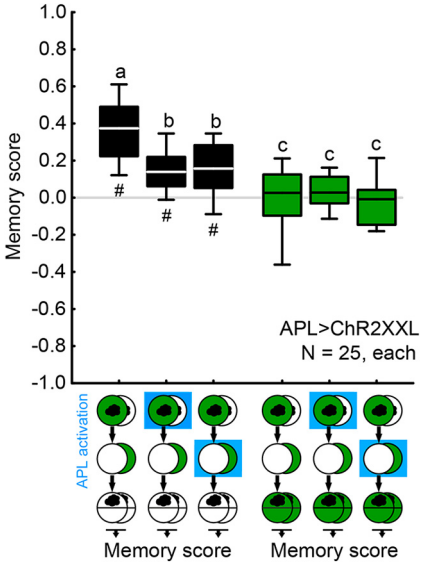

Figure 10. Activation of APL only in the presence or only in the absence of the odor reduces memory scores. Optogenetic activation of APL (blue square) either only when the odor was presented during training, or only when the odor was not presented during training, reduced memory scores to about half the level of control animals that did not receive any APL activation (black-filled box plots). Testing the animals in the presence of the training reward (i.e., fructose) abolished the behavioral expression of memory in all cases (green-filled box plots). The sample sizes and the genotype are given within the figure. $^{\#}$OSS comparisons to chance levels (i.e., to zero) with a BH correction ($^{\#}p< 0.05$); different letters indicate significant differences between groups in MWW comparisons also with a BH correction ($p< 0.05$). The source data and results of all statistical tests are documented in Extended Data Figure 3-1 and Table 2. Other details as in Figure 9.

"tags" coupled with chemical fluorophore ligands (Kohl et al., 2014; Sutcliffe et al., 2017; Meissner et al., 2018). The synaptic reporter synaptotagmin fused to the tag SNAPm (Syt1-SNAPm) allowed us to label presynapses, and the reporter telencephalin fused to the tag CLIPm (TLN-CLIPm) allowed us to label postsynapses (Kohl et al., 2014). These constructs were expressed in APL throughout development using the intersectional driver APLi-GAL4, which specifically expresses in APL of both larvae and adults (Lin et al., 2014; Mayseless et al., 2018) (as stated earlier, APL-GAL4 does not express in adult APLs). In addition, UAS-mCD8::GFP was expressed to visualize APL membranes.

←

larvae of the experimental genotype (APL>ChR2XXL) toward AM (black cloud) was tested, without APL being activated during testing or with APL activated (blue square). Naive odor preference was unaffected by APL activation. ***E–I***, The behavior of larvae in ***D*** was video-recorded and analyzed offline as described by Paisios et al. (2017). ***E***, A short sample from a video recording of a larva with successive runs and HCs. Displayed is the track of the midpoint. Magenta and orange dots represent right and left HCs, respectively. Specifically, four features of locomotion were analyzed in addition to the olfactory preference: that is, the time spent by the larvae on the odor and the nonodor side (***F***), the HC rate modulation (***G***), the HC reorientation (***H***), and the run speed modulation (***I***). In all cases, APL activation had no effect. The data are displayed as box plots. Middle line indicates the median. Box boundaries represent the 25% and 75% quantiles. Whiskers represent the 10% and 90% quantiles. The sample sizes (number of biological replications) and the genotypes are given within the figure. ***A***, ***B***, Different letters indicate significant differences between groups in MWW comparisons with a BH correction ($p< 0.05$), as specified in Experimental design and statistical analyses. ***D***, ***F–I***, NS indicates the absence of significance between groups in MWW comparisons: NS, $p > 0.05$. ***A***, ***B***, OSS comparisons to chance levels (i.e., to zero), also with a BH correction: $^{\#}p< 0.05$. The source data and results of all statistical tests are documented in Extended Data Figure 3-1 and Table 2.

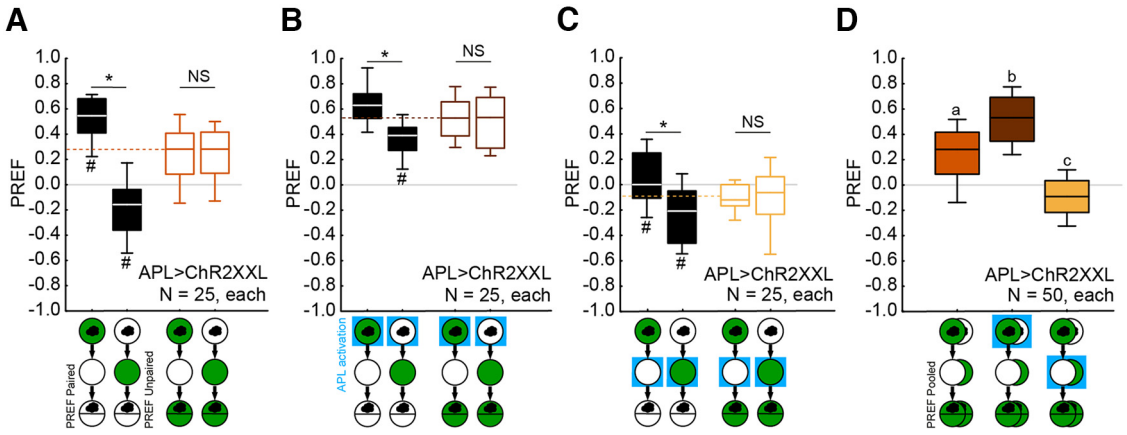

Figure 11. Activation of APL only in the presence or only in the absence of the odor has differential effects on odor preference. ***A***, Examination of the preference scores (PREF) underlying the associative memory scores from Figure 10 reveals that odor preference scores are higher after paired than after unpaired training with odor and fructose reward (black-filled box plots to the left), a difference that is abolished when testing is conducted in the presence of the training reward (right-most colored plots). This is adaptive because learned search for the reward is obsolete in its presence. These preference scores can thus be pooled to serve as the baseline odor preference cleared of associative memory (stippled line). This reveals that odor preference scores are higher than the baseline after paired training and lower than the baseline after unpaired training. ***B***, ***C***, The same on activation of APL during training (blue square), whether only during odor presentation (***B***) or unpaired from odor presentation (***C***). Remarkably, baseline levels of odor preference differ between these three training conditions (***D***): compared with the control condition without APL activation, baseline odor preference scores are increased when APL is activated together with odor presentation, and decreased when APL is activated unpaired from odor presentation. The sample sizes and the genotype are given within the figure. ***A–C***, MWW comparisons between groups with a BH correction: $^{*}p < 0.05$; NS, $p > 0.05$. ***D***, Different letters indicate significant differences between groups in MWW comparisons, also with a BH correction: $p < 0.05$. ***A–C***, MWW comparisons to baseline levels of odor preference, also with a BH correction: $^{\#}p < 0.05$. The source data and results of all statistical tests are documented in Extended Data Figure 3-1 and Table 2. Other details as in Figures 9 and 10.

In third-instar larvae of the genotype APLi/Syt1:SNAP>mCD8::GFP/TLN:CLIP, presynaptic staining was mostly found in the calyx (Fig. 8*A′*), whereas postsynaptic staining was distributed in the calyx and the lobes (Fig. 8*A″*), consistent with previous observations (Fig. 4) (Masuda-Nakagawa et al., 2014). As early as 6 h after puparium formation, we detected presynaptic structures that were more punctate (Fig. 8*B′*,*C′*) and observed fewer postsynaptic structures overall (Fig. 8*B″*,*C″*), consistent with the previously reported pruning of APL secondary neurites during pupal stages (Mayseless et al., 2018). Interestingly, at 12 h after puparium formation, a stage where APL pruning is almost at its peak (Mayseless et al., 2018), we could still detect both presynaptic and postsynaptic structures (Fig. 8*D–D‴*), although some postsynaptic structures were observed detached from the neurite (Fig. 8*D–D″*,*D‴*, yellow arrowhead). Nonetheless, the polarized organization of APL in third-instar larvae was no longer observed in the adult stage, as we detected both presynaptic and postsynaptic markers across both the calyx and the lobes of the adult mushroom bodies (Fig. 8*E–F‴*) (C. L. Wu et al., 2013; Lin et al., 2014).

Together, our results indicate that, whereas APL is regionally polarized throughout larval stages, it undergoes rearrangement during metamorphosis to give rise to a regionally more diffuse organization. In addition, the DPM neuron, one of the main synaptic partners of APL involved in memory consolidation in adults, does not exist in larvae (Pitman et al., 2011; C. L. Wu et al., 2011; Eichler et al., 2017; Saumweber et al., 2018). In light of these differences, and despite the rich insights recently gained into the function of APL in adults (Inada et al., 2017; Zhou et al., 2019; Amin et al., 2020; Apostolopoulou and Lin, 2020; Kanellopoulos et al., 2020; Yamagata et al., 2021), a detailed look into the function of the larval APL neuron seemed warranted.

Memory scores are abolished on activating APL throughout odor-fructose training

We first asked whether the optogenetic activation of APL affects associative memory formation. Third-instar larvae were trained in a standard Pavlovian conditioning paradigm, using an odor (AM) as the conditioned stimulus and a fructose reward as the unconditioned stimulus (Scherer et al., 2003; Neuser et al., 2005; Saumweber et al., 2011; Michels et al., 2017). One group of larvae received the odor presented together with the fructose reward (paired training), whereas a second group received separate presentations of the odor and the fructose reward (unpaired training). After training, both groups were tested for their odor preference. A difference in odor preference between paired and unpaired training thus reflects associative memory, and is quantified by the memory score. According to convention, positive memory scores reflect appetitive associative memory, whereas negative scores reveal aversive memory (Eq. 2; see Materials and Methods). Notably, paired and unpaired training both establish associative memory, yet of opposite "sign." After paired training, the odor predicts the occurrence of the reward, leading to an associative increase in odor preference. In contrast, unpaired training establishes the odor as a predictor of the nonoccurrence of the reward and supports an associative decrease in odor preference (for a detailed discussion, see Schleyer et al., 2018).

We repeated an experiment from Saumweber et al. (2018), in which APL was optogenetically activated throughout odor-fructose training (Fig. 9). Here, we confirmed their report that odor-fructose memory scores in the experimental genotype (APL>ChR2XXL) were reduced to chance levels and were reduced relative to both genetic controls, heterozygous for either only the effector (+>ChR2XXL) or the driver (APL>+) construct alone (Fig. 9*A*). The same abolishment of memory scores was observed in a shortened, one-trial version of this experiment (Fig. 9*B*). For practical reasons, this shortened experimental design was used throughout the rest of our study. In addition, the expression of ChR2XXL in APL was directly confirmed by immunohistochemistry (Fig. 9*C*; Movie 7). Critically, the behavior of experimentally naive larvae toward the odor (i.e., innate odor preference) was unaffected by APL activation (Fig. 9*D*) (Saumweber et al., 2018). Further, as shown here from offline analyses of video tracking data, APL activation did not

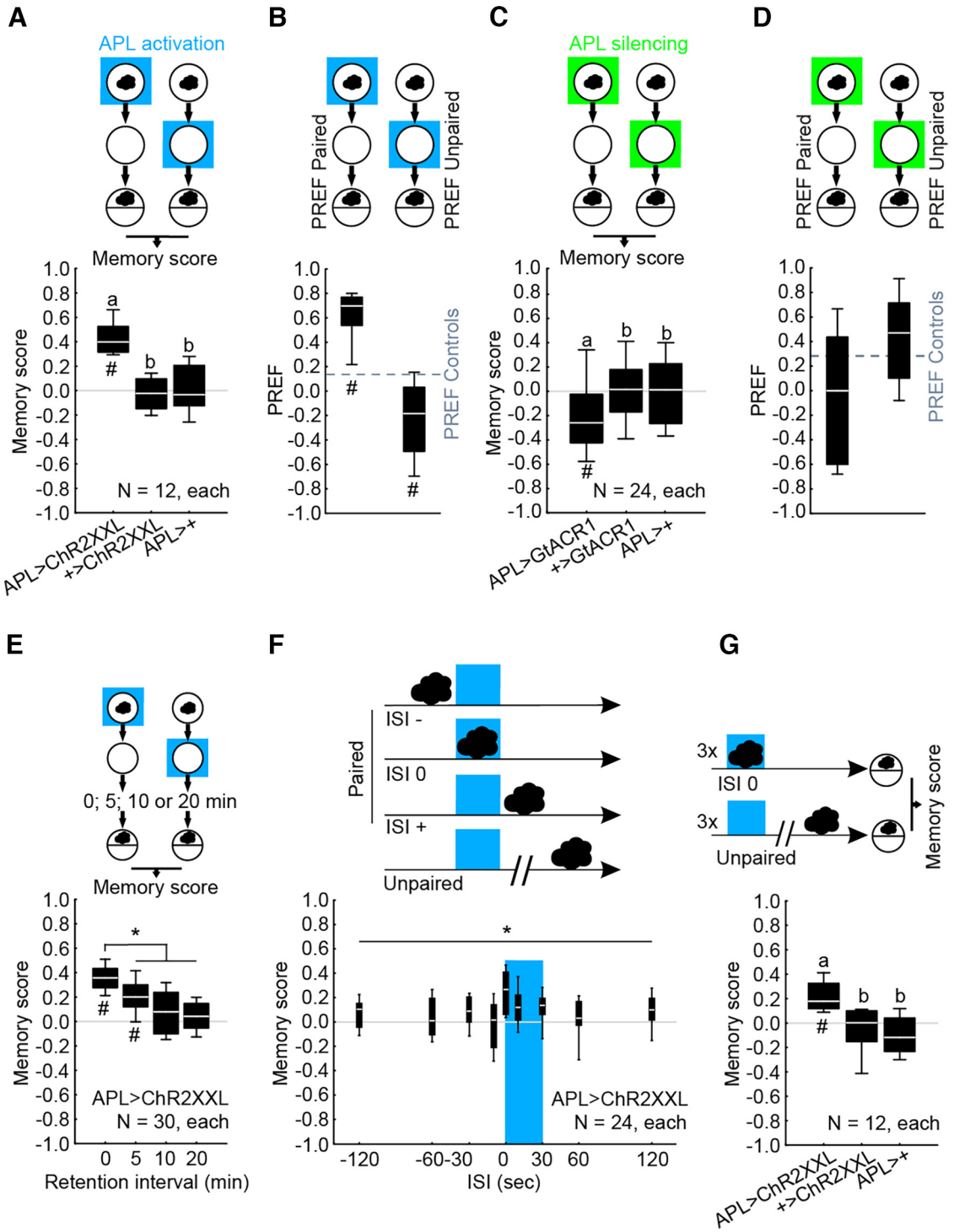

Figure 12. Activating APL has a rewarding effect. ***A***, Animals were trained by presenting odor either paired with, or unpaired from, activation of APL using ChR2XXL as the effector through blue light illumination (blue square). The effect of APL activation as a reward is quantified by positive memory scores, differing significantly from the genetic controls. ***B***, Preference scores (PREF) underlying the associative memory scores in ***A***. Preference scores from the genetic controls were pooled to serve as the baseline preference (stippled line), revealing that preference scores are higher than the baseline after paired training and lower than the baseline after unpaired training. ***C***, Procedure as in ***A***, except that APL was optogenetically silenced using GtACR1 as the effector through green light illumination (green square). The effect of APL silencing as a punishment is quantified by negative memory scores, differing significantly from the genetic controls. ***D***, Preference scores (PREF) underlying the associative memory scores in ***C***. Stippled line indicates the pooled preference scores of the genetic controls as a baseline. ***E***, Larvae of the experimental genotype (APL>ChR2XXL) were trained as described in ***A*** and tested either immediately after training (retention interval 0 min) or 5, 10, or 20 min after training. Expression of odor-APL memory was observed immediately after training and was still detectable at a 5 min retention interval; it was significantly reduced compared with immediate testing when assessed at 5, 10, or 20 min retention intervals. ***F***, Larvae of the experimental genotype (APL>ChR2XXL) were trained as in ***A*** (i.e., paired or unpaired) but with modifications of the paradigm in accordance with Weiglein et al. (2021). Specifically, odor presentation and APL activation lasted for 30 s each with different timings relative to their onset (interstimulus interval [ISI]): the odor was presented before the APL activation (negative ISI values), during the APL activation (ISI 0), or after the APL activation (positive ISI values); in all cases, reciprocal training involved odor presentation unpaired from APL activation. Three training trials were performed, followed by the test of odor preference. Memory scores differed according to the ISI. ***G***, Repetition of the experiment from ***F***, but for simultaneous presentation of odor and APL activation (ISI 0), including genetic controls. Positive memory scores for the experimental genotype (APL>ChR2XXL) indicate that a brief

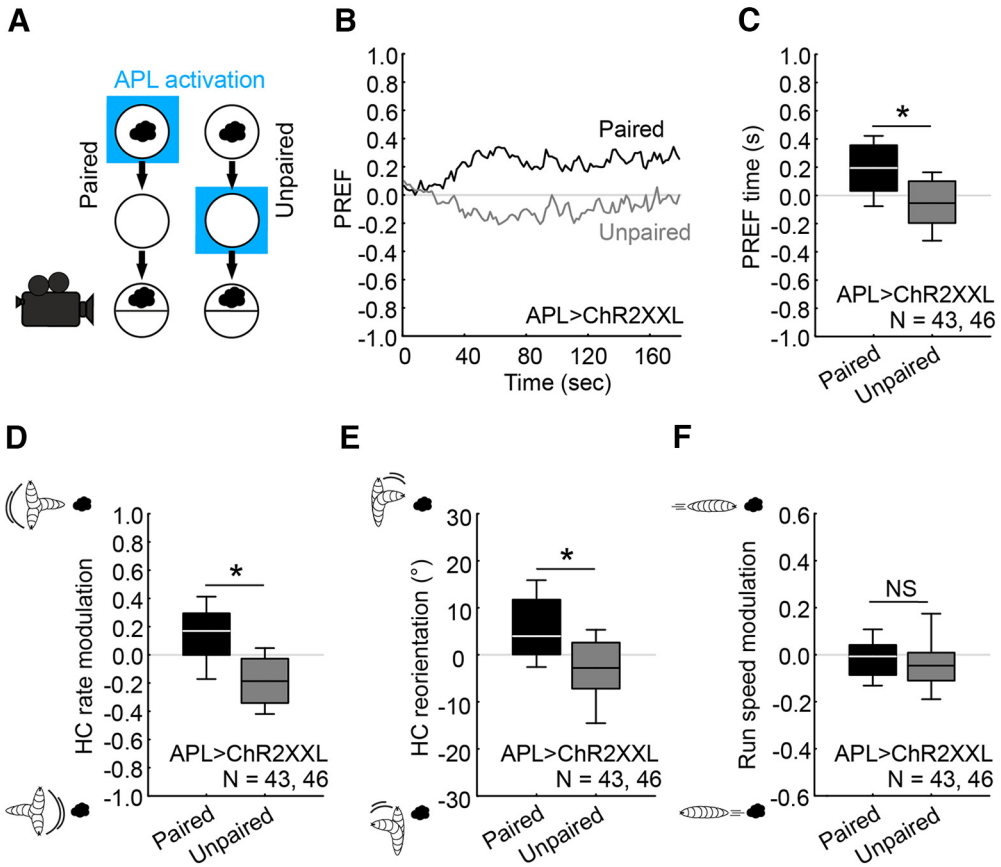

Figure 13. Locomotor "footprint" of odor-APL memory. ***A***, The behavior of larvae of the genotype APL>ChR2XXL was video-recorded after paired or unpaired training with odor and APL activation. ***B***, Larvae showed a higher preference for the odor after paired training than after unpaired training; dataset split into 100 bins (1.8 s, each), showing the median of odor preferences across Petri dishes over time. ***C***, Larvae from the paired group spent more time on the odor side than on the nonodor side during testing, whereas the contrary was observed for the unpaired group. ***D***, Paired-trained larvae exhibited more HCs when crawling away from the odor than when moving toward it; the opposite was observed for the unpaired group. ***E***, Larvae from the paired group oriented their HCs more in the direction of the odor compared with larvae from the unpaired group. ***F***, The run speed when heading toward versus when heading away from the odor did not differ between paired- and unpaired-trained animals. ***B–F***, Analyses are based on data available from the experiments shown in Figures 12*A*, *E* and 14*A*. Similar results were observed using Chrimson as the optogenetic effector (not shown). The sample sizes (number of biological replications) and the genotype are given within the figure. ***C–E***, Significant differences between groups in MWW comparisons: $^{*}p < 0.05$. ***F***, NS indicates the absence of significance between groups in MWW comparisons: NS, $p > 0.05$. The source data and results of all statistical tests are documented in Extended Data Figure 3-1 and Table 2. Other details as in Figures 9-12.

affect the modulation of locomotor patterns by which these odor preferences were realized (i.e., modulations of HC rate and direction, but not of run speed: Fig. 9*E–I*).

Activating APL either in the presence or in the absence of the odor reduces memory scores

As argued in Saumweber et al. (2018), the abolishment of memory scores on activation of APL during the complete training phase (Fig. 9) may arise because APL provides an inhibitory GABAergic signal onto the KCs (Fig. 5) (Masuda-Nakagawa et al., 2014). Taking the argument to the extreme, the activation of APL would silence the KCs, preventing a proper odor representation in the mushroom body and thereby also preventing odor-fructose memory formation thereafter. If so, memory formation should be disrupted when APL is activated while the odor is presented, but should not be disrupted when APL is activated while the odor is not presented. To our surprise, however, in both cases, odor-fructose memory scores were partially reduced compared with a control condition in which APL was not activated at all (Fig. 10). In regard to these residual memory scores, we considered the interpretation of odor-fructose memory as a learned search for the fructose reward (Saumweber et al., 2011; Schleyer et al., 2011). This interpretation implies that memory is behaviorally expressed if the sought-for fructose reward is indeed absent during the test, but that memory is not expressed if the testing is conducted in the presence of the sought-for fructose reward. This was indeed the case in all three conditions, namely (1) when APL was not activated during training at all, and (2) when APL was activated during odor presentation or (3) in the absence of odor (Fig. 10, right); innate olfactory behavior is not changed in the presence of fructose or other tastants (Schleyer et al., 2011). In other words, the residual memory scores after APL activation during either period of the training also reflect a search for the fructose reward.

←

stimulation of APL is sufficient to be rewarding, an effect that was not observed in the genetic controls. The sample sizes and the genotypes are indicated within the figure. ***A***, ***C***, ***G***, Different letters indicate significant differences between groups in MWW comparisons with a BH correction: $p < 0.05$. ***E***, Significant differences between groups in MWW comparisons with a BH correction: $^{*}p < 0.05$. ***F***, KW multiple-group comparison: $^{*}p < 0.05$. ***A***, ***C***, ***E***, ***G***, OSS comparisons to chance levels (i.e., to zero), also with a BH correction: $^{\#}p < 0.05$. ***B***, MWW comparisons to the control baseline (i.e., to the pooled preference scores from the genetic controls), also with a BH correction: $^{\#}p < 0.05$. The source data and results of all statistical tests are documented in Extended Data Figure 3-1 and Table 2. Other details as in Figures 9-11.

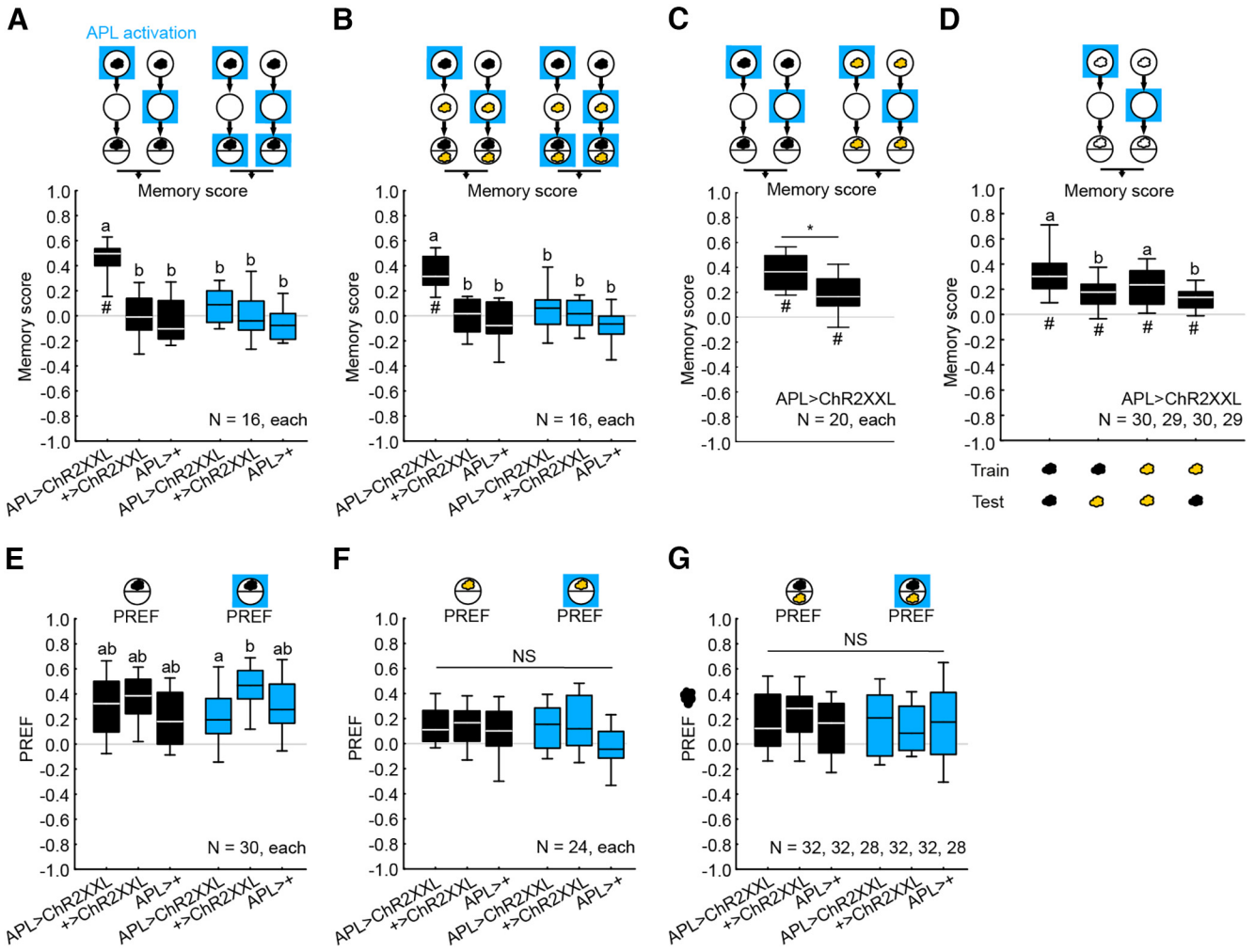

Figure 14. Activation of APL during testing prevents the behavioral expression of appetitive odor-APL memory. ***A***, Repetition of the experiment from Figure 12*A*, confirming that APL activation has a rewarding effect (black-filled box plots). Activating APL during testing as well prevented the behavioral expression of appetitive odor-APL memory (blue-filled box plots). ***B***, Larvae were trained and tested as in ***A***, except that in a differential conditioning protocol, OCT was used as a second odor (yellow cloud) in all training trials in which AM (black cloud) was not presented. Presenting one of the two odors paired with APL activation induced odor-specific appetitive memory; as in ***A***, testing the animals while activating APL prevented the behavioral expression of memory. ***C***, Larvae were trained and tested as in Figure 12*A* either with AM (black cloud) or OCT (yellow cloud) as a single odor. Compared with AM, larvae showed lower appetitive memory scores when OCT was used as a conditioned stimulus. ***D***, Larvae were trained as in ***C*** and tested either with the same trained odor (AM or OCT), or with the respective other novel odor (AM or OCT). Testing larvae with the novel odor led to generalization decrement. ***E***, The behavior of experimentally naive larvae toward AM (black cloud) was tested either without APL activation or with APL activation during the test. Naive odor preference in the experimental group was unaffected by APL activation (APL>ChR2XXL) (see also Fig. 9*D*), with the caveat that it did differ from the effector (+>ChR2XXL), but not from the driver control (APL>+). ***F***, Same as in ***E***, except that OCT was used as a single odor (yellow cloud). Naive odor preference in the experimental group was unaffected by APL activation (APL>ChR2XXL), and did not differ from the genetic controls. ***G***, Same as in ***E***, ***F***, except that OCT was used as a second odor (yellow cloud). Again, naive odor preference in the experimental group was unaffected by APL activation (APL>ChR2XXL) and did not differ from the genetic controls. The sample sizes and the genotypes are given within the figure. ***A–D***, OSS comparisons to chance levels (i.e., to zero) with a BH correction: $^{\#}p < 0.05$. ***A***, ***B***, ***D***, ***E***, Different letters indicate significant differences between groups in MWW comparisons, also with a BH correction: $p < 0.05$. ***C***, Significant differences between groups in MWW comparisons. NS indicates the absence of significance between groups in MWW comparisons with a BH correction in ***F***, and in KW comparisons in ***G*** (NS, $p > 0.05$). The source data and results of all statistical tests are documented in Extended Data Figure 3-1 and Table 2. Other details as in Figures 9-13.

Differential effects of activating APL only in the presence or only in the absence of the odor

As mentioned, it was unexpected that odor-fructose memory was impaired by activation of APL during the odor-absent periods of training. In order to understand this result, we separately analyzed odor preferences underlying the memory scores from Figure 10. In all 3 cases — (1) when APL was not activated at all during training, (2) when it was activated while the odor was presented, and (3) when it was activated while the odor was not presented — odor preference scores after paired versus unpaired training were indistinguishable from each other when the fructose reward was present during testing (Fig. 11*A–C*, open boxes). In other words, in all cases, learned search ceased once the sought-for reward was found. As discussed in detail by Schleyer et al. (2018), this allows the odor preferences after paired and unpaired training to be pooled to determine baseline levels of odor preference, cleared of associative memory (Fig. 11*A–C*, stippled lines). In all 3 cases, these baseline preference scores were intermediate between the paired-trained and the unpaired-trained animals that were tested in the absence of fructose, consistent with earlier reports (Schleyer et al., 2018). This is adaptive because after paired training the larvae search for fructose where the odor is, whereas after unpaired training they search for fructose where the odor is not, and accordingly in either case their search is suppressed in the presence of the sought-for fructose. Important for the

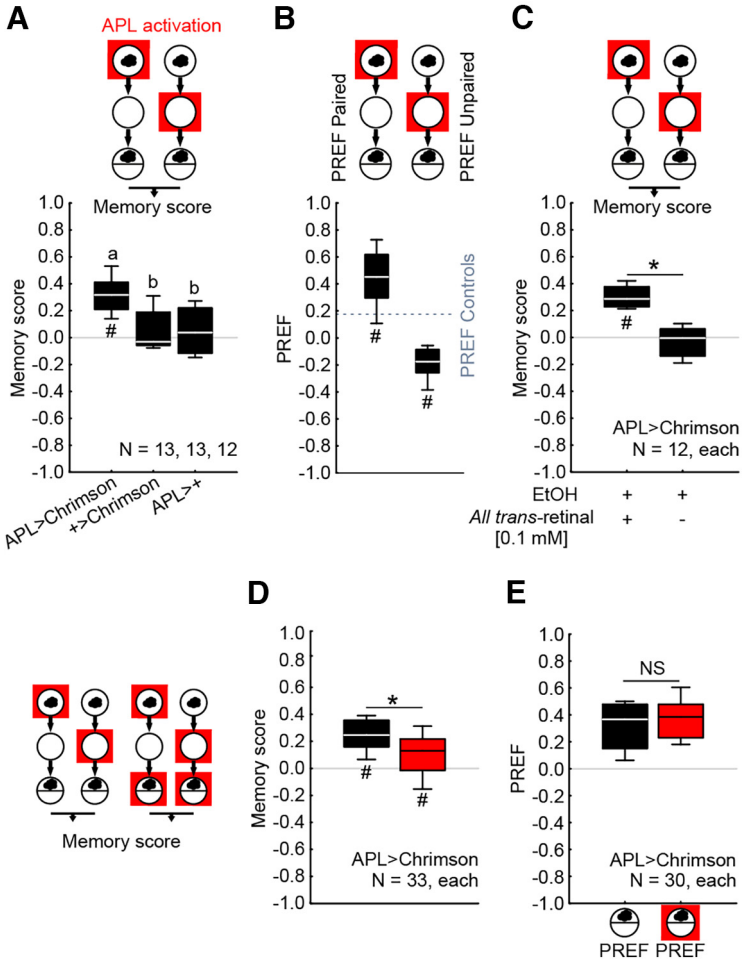

Figure 15. Activating APL with Chrimson has a rewarding effect. ***A***, The rewarding effect of APL activation was confirmed using Chrimson as the effector and red light illumination (red square), and quantified through positive memory scores in the experimental group (APL>Chrimson), differing significantly from the genetic controls. Transgenic flies were raised on standard food supplemented with retinal (100 mM final concentration). ***B***, Preference scores (PREF) underlying the associative memory scores in ***A***. Preference scores from the genetic controls were pooled to serve as the baseline odor preference (stippled line), revealing that preference scores are higher than the baseline after paired training and lower than the baseline after unpaired training. ***C***, Larvae of the experimental genotype (APL>Chrimson) were trained and tested after being raised on food either supplemented with retinal (final concentration in EtOH [99.9%] 100 mM), or without retinal (food medium supplemented with EtOH only). The rewarding effect of APL activation was observed in retinal-fed animals but was not observed without retinal feeding. ***D***, The behavioral expression of odor-APL memory was reduced but not abolished by testing the animals while APL was activated (red-filled box plot). ***E***, The behavior of experimentally naive larvae of the genotype APL>Chrimson toward AM (black cloud) was tested, either without APL activation or with APL activated during testing (red square). Naive odor preference remained unaffected by APL activation. ***A***, ***C***, ***D***, ***E***, The sample sizes and the genotypes are given within the figure. ***A***, Different letters indicate significant differences between groups in MWW comparisons with a BH correction: $p < 0.05$. ***C***, ***D***, Significant differences between groups in MWW comparisons, also with a BH correction: $^{*}p < 0.05$. ***E***, NS indicates the absence of significance between groups in MWW comparisons: NS, $p > 0.05$. ***A***, ***C***, ***D***, OSS comparisons to chance levels (i.e., to zero) with a BH correction: $^{\#}p < 0.05$. ***B***, MWW comparisons to the control baseline (i.e., to the pooled preference scores from the genetic controls), also with a BH correction: $^{\#}p < 0.05$. The source data and results of all statistical tests are documented in Extended Data Figure 3-1 and Table 2. Other details as in Figures 9-14.

current context, however, is that these baseline levels varied strikingly with the contingency between APL activation and odor presentation (Fig. 11*D*): compared with the control baseline scores when APL was not activated at all (stippled line in Fig. 11*A* and plotted in Fig. 11*D*, left), the baseline scores were increased when APL was activated in the presence of the odor (stippled line in Fig. 11*B*; plotted in Fig. 11*D*, middle), and were decreased when APL was activated in the absence of the odor (stippled line in Fig. 11*C*; plotted in Fig. 11*D*, right). In other words, activation of APL paired with odor increased odor preferences, whereas activation of APL unpaired from odor presentation decreased odor preferences (Fig. 11*D*) — as if, above and beyond the fructose that we intended to be the only reward in these experiments, activation of APL also had a rewarding effect. The next experiment tested this hypothesis.

Activating APL has a rewarding effect

To test our hypothesis that optogenetically activating APL has a rewarding effect, animals were trained by presenting the odor either paired or unpaired with APL activation instead of with the fructose reward. This established positive memory scores in the experimental genotype, differing from the genetic controls (Fig. 12*A*). An analysis of the underlying odor preferences showed that these positive memory scores resulted from both an increase in odor preferences after paired training and a decrease in odor preferences after unpaired training, relative to the baseline odor preferences in the genetic controls (Fig. 12*B*). Thus, APL activation during training has a rewarding effect and can establish appetitive, associative memory. In turn, optogenetically silencing APL leads to an aversive memory (Fig. 12*C*); in this case, the apparent trend for opposite effects of paired versus unpaired training did not reach statistical significance (Fig.

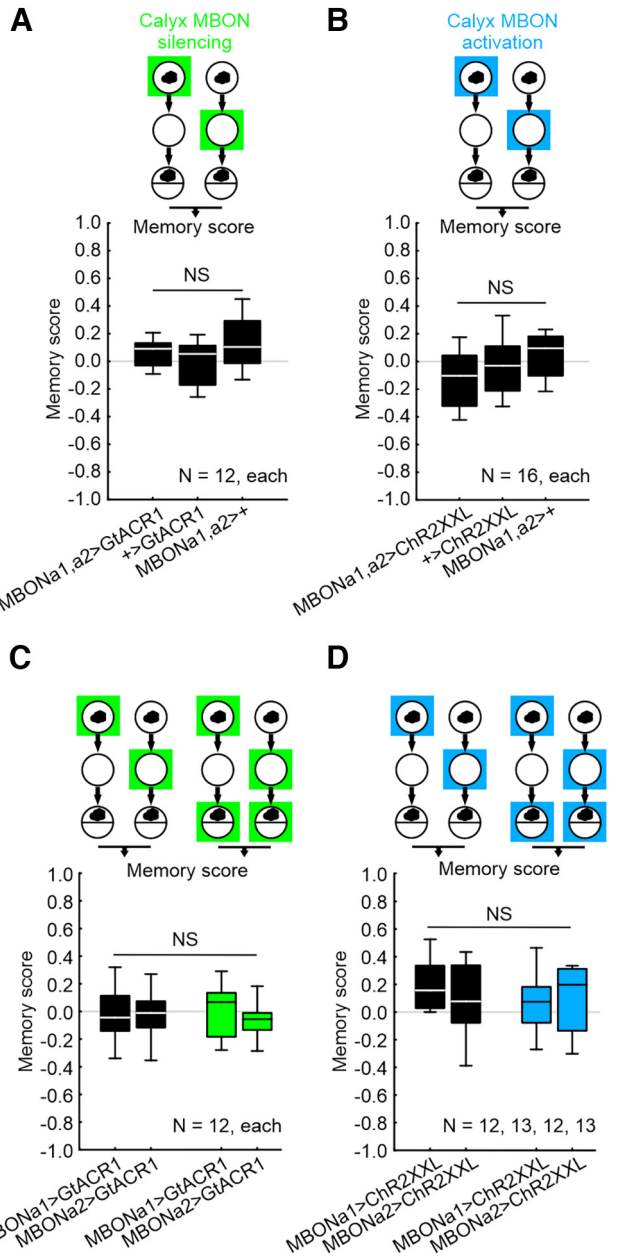

Figure 16. Manipulating activity in the calyx MBONs has no reinforcing effect. ***A***, Larvae were trained such that odor was presented either paired or unpaired with the silencing of the two calyx MBONs, using GtACR1 as the effector and green light illumination (green square). Silencing the two calyx MBONs together was seen to have no rewarding or punishing effect, as larvae of the experimental genotype (MBONa1,a2>GtACR1) did not behave differently from the genetic controls. ***B***, Activating the two calyx MBONs together likewise had no rewarding or punishing effect. ***C***, ***D***, Silencing (***C***) or activating (***D***) the two calyx MBONs separately had no reinforcing effect, either. The sample sizes and the genotypes are given within the figure. NS indicates the absence of significance between groups in MWW comparisons: NS, $p > 0.05$. The source data and results of all statistical tests are documented in Extended Data Figure 3-1 and Table 2. Other details as in Figures 9-15. Expression patterns of the calyx MBON drivers used in ***C***, ***D*** are shown in Extended Data Figure 16-1.

12*D*). Throughout the rest of the study, we decided to focus on the rewarding effect of APL on its activation. We found that odor-APL memory was transient and lasted for<10 min (Fig. 12*E*), as is the case for odor-fructose memory after one training trial (Weiglein et al., 2019) and for appetitive olfactory memories formed by optogenetic activation of large sets of KCs (Lyutova et al., 2019). A rewarding effect of APL activation was likewise observed when a brief-stimulation protocol was used (Fig. 12*F*,*G*). In addition, offline analysis of video-recorded larval locomotion revealed that the same aspects of larval locomotion were modulated by odor-APL memory (Fig. 13) as previously shown for similarly strong odor-taste reward associative memories, namely, the rate of HCs and their orientation but not run speed (Schleyer et al., 2015b, 2020; Paisios et al., 2017; Saumweber et al., 2018; Thane et al., 2019). Inspired by what has been reported on fructose as a taste reward (Schleyer et al., 2015a) (see also Figs. 10, 11), we reasoned that, if odor-APL memory scores reflect a learned search for the training reward (which is APL activation in the present case), these memory scores should be abolished if the sought-for reward is present during the test. We therefore repeated the experiment from Figure 12*A* and added an experimental condition whereby APL was also activated during testing. This prevented the behavioral expression of appetitive odor-APL memory (Fig. 14*A*) (for a similar effect of DAN activation, see Schleyer et al., 2020). The same was observed for a two-odor, differential conditioning version of the paradigm, using OCT as the second odor (Fig. 14*B*). Compared with AM, OCT turned out less salient as a conditioned stimulus (Fig. 14*C*). Interestingly, when these odors were used for training but testing was conducted either with the same trained odor or with the respectively other novel odor, we observed a generalization decrement in both cases (Fig. 14*D*), suggesting that the established memories are at least partially specific for the trained odor. We find it striking that APL activation is effective as a reward, even in differential conditioning, because it implies that an associable, odor-specific representation can be established in the mushroom body under the condition of an optogenetically activated APL neuron. In line with our earlier results from Figure 9*D*, naive odor preferences were unaffected by APL activation (Fig. 14*E*–*G*). Thus, APL activation has two kinds of effect previously reported for taste rewards: it both induces associative memory when paired with odor during training (Figs. 12, 14; with the same locomotor "footprint" as for taste rewards: Fig. 13), and it terminates the search behavior that is based on this memory during the test (Fig. 14). These two effects of reward are adaptive because they help the animals to search for the reward, and prevent them from drifting away from a reward once it is found, respectively. Both of these reward-like effects of APL activation, plus the opposite effects of paired versus unpaired training and the lack of any effect of APL activation on naive odor preference, were confirmed using Chrimson as the effector (Fig. 15*A*–*E*), although the effect of APL activation to terminate search behavior during testing was only partial for Chrimson (Fig. 15*D*).

Manipulating activity in the calyx MBONs has no reinforcing effect

Considering the circuit mechanisms by which APL activation exerts a rewarding effect, we first focused on the calyx MBONs to which APL is presynaptic (MBONa1 and MBONa2; also known as "Odd" neurons: Figs. 6*F*, 7*B*; Movie 6) (Slater et al., 2015; Eichler et al., 2017; Saumweber et al., 2018). We reasoned that, if activation of the GABAergic APL neuron exerts its rewarding effect by inhibiting the calyx MBONs, then optogenetically silencing these MBONs should also have a rewarding effect. Using the chloride channel GtACR1 as the effector, however, this was found not to be the case (Fig. 16*A*). We then

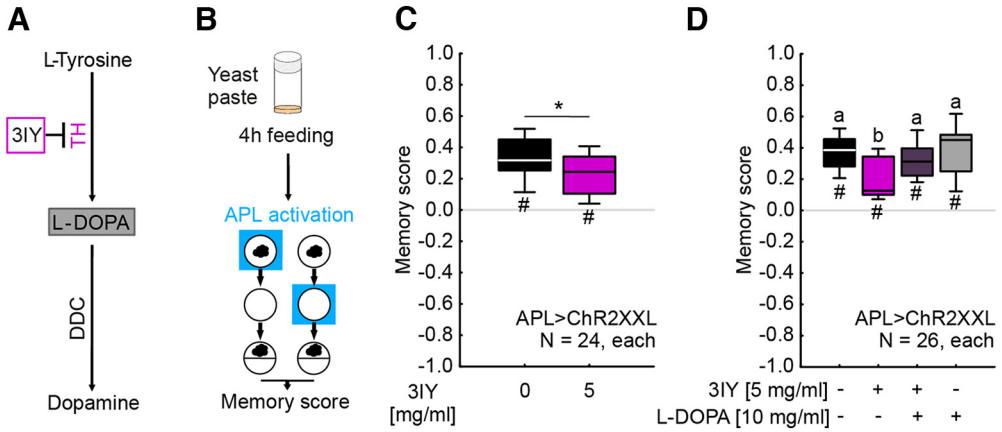

Figure 17. Inhibition of dopamine synthesis impairs odor-APL memory. A systemic pharmacological approach was used to disrupt dopamine synthesis (Thoener et al., 2021). ***A***, Sketch of dopamine biosynthesis. The enzyme tyrosine hydroxylase (TH) converts the amino acid L-tyrosine to L-DOPA. In the next step, the enzyme dopa-decarboxylase (DDC) converts L-DOPA to dopamine. Application of 3IY inhibits the TH enzyme. ***B***, Third-instar APL>ChR2XXL larvae were transferred from their food vials to a yeast solution either without 3IY or supplemented with 3IY. After 4 h of such feeding, the animals were trained and tested as in Figure 12*A*. ***C***, Relative to control larvae, the 3IY-fed larvae exhibited impaired odor-APL memory scores. ***D***, Same as in ***C***, except that the yeast solution was prepared (1) without additional substances, (2) with 3IY added, (3) with 3IY plus L-DOPA (a dopamine precursor), or (4) with L-DOPA only, at the concentrations indicated. Again, relative to control larvae, reduced memory scores were observed in 3IY-fed larvae; feeding them additionally with L-DOPA rescued that memory impairment, leading to scores similar to those of the control animals. L-DOPA alone had no impact on odor-APL memory. The sample sizes and the genotypes are given within the figure. ***C***, ***D***, OSS comparisons to chance levels (i.e., to zero) with a BH correction: $^{\#}p< 0.05$. ***C***, Significant differences between groups in MWW comparisons with a BH correction: $^{*}p< 0.05$. ***D***, Different letters indicate significant differences between groups in MWW comparisons, also with a BH correction ($p< 0.05$). The source data and results of all statistical tests are documented in Extended Data Figure 3-1 and Table 2. Other details as in Figures 9-16.

considered the possibility that, unlike the KCs (Fig. 5), the calyx MBONs might actually be activated rather than inhibited by activation of APL, for example, through GABA-induced chloride spikes as reported for insect motoneurons (Ryglewski et al., 2017) or by yet-to-be-identified excitatory transmitters coreleased by APL. We thus repeated the same experiment, but this time activated the MBONs: again, no rewarding effect was observed on such manipulation (Fig. 16*B*). Before ruling out the involvement of the two calyx MBONs in the rewarding effect of APL, however, it was important to test for the effects of manipulating each of them separately. This is because activation of MBONa1 and MBONa2 induces approach and avoidance, respectively (Eschbach et al., 2021). We therefore reasoned that they might exert a rewarding and punishing effect, respectively, which would sum to zero when both these MBONs were manipulated together. However, neither silencing nor activating either one of the calyx MBONs yielded evidence of such oppositely reinforcing effects (Fig. 16*C*,*D*; Extended Data Fig. 16-1); we included groups tested in the presence of light because we reasoned that, similar to what has been observed for gustatory punishment (Gerber and Hendel, 2006; Selcho et al., 2009; Schleyer et al., 2011; Widmann et al., 2016; Weber et al., 2023), this might promote aversive memory expression. These results suggest that the rewarding effect of APL activation does not involve APL-to-MBONa1/a2 connections. Given the role of dopamine in conveying reward signals in larval *Drosophila* (Selcho et al., 2009; Rohwedder et al., 2016; Thoener et al., 2021), we next inquired into the dopamine dependency of APL's rewarding effect.

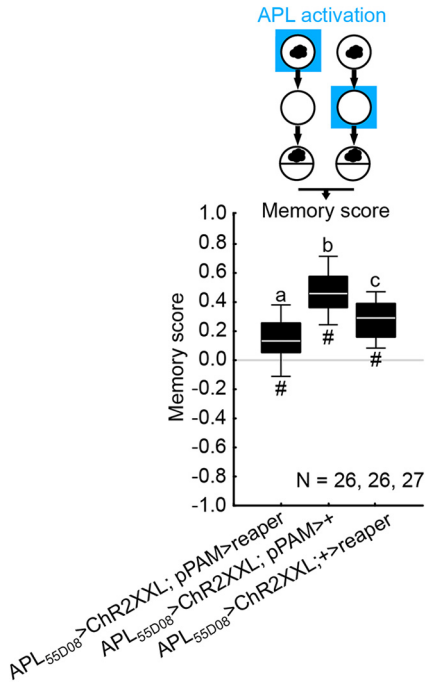

Figure 18. Ablation of dopaminergic pPAM neurons impairs odor-APL memory. Larvae were trained and tested as in Figure 12*A*. Optogenetic activation of APL and simultaneous ablation of the pPAM neurons (APL_{55D08}>ChR2XXL; pPAM>reaper) reduced odor-APL memory scores relative to genetic controls (APL_{55D08}>ChR2XXL; pPAM>+ and APL_{55D08}>ChR2XXL; +>reaper). The sample sizes and the genotypes are given within the figure. Different letters indicate significant differences between groups in MWW comparisons with a BH correction ($p< 0.05$). $^{\#}$OSS comparisons to chance levels (i.e., to zero), also with a BH correction ($^{\#}p< 0.05$). The source data and results of all statistical tests are documented in Extended Data Figure 3-1 and Table 2. Other details as in Figures 9-17.

Inhibition of dopamine synthesis impairs odor-APL memory

We used a systemic pharmacological approach to acutely disrupt dopamine synthesis. This was done by inhibiting the enzyme tyrosine hydroxylase (TH), which is rate-limiting for dopamine synthesis (Neckameyer and White, 1993; Bainton et al., 2000; Fernandez et al., 2017; Thoener et al., 2021). The TH-inhibitor 3IY was added to the larval food at a dose that leaves intact task-relevant behavioral faculties (i.e., innate odor preference and locomotion) (Thoener et al., 2021). When 4 h later the larvae were trained and tested for odor-APL memory, they exhibited reduced memory scores (Fig. 17*A*–

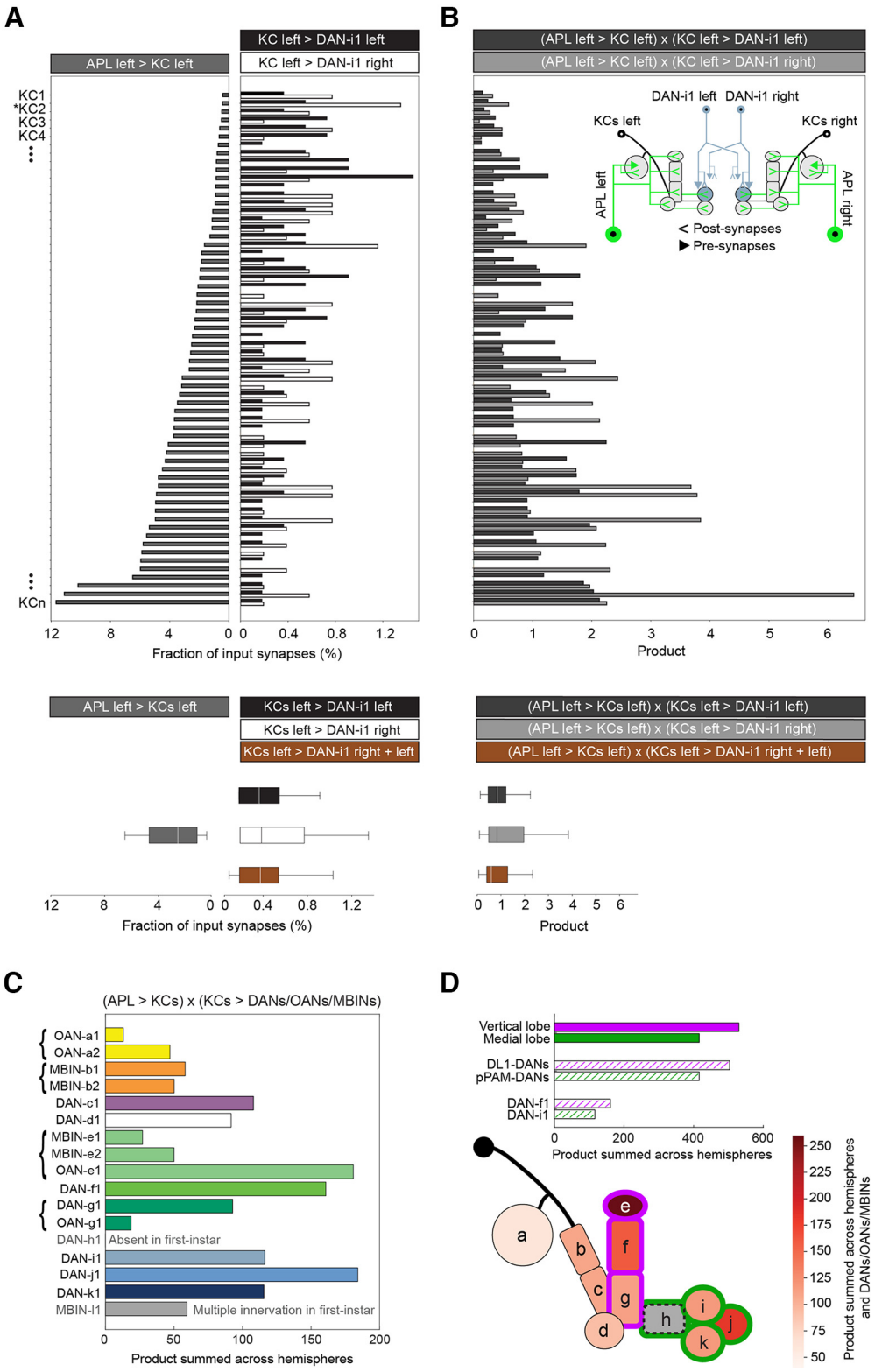

Figure 19. Analysis of connectivity from APL, via KCs, to the DANs/OANs/MBINs. ***A***, Fraction of input synapses from APL left to each left-hemisphere KC (APL left >KC left), and from each of these KCs to DAN-i1 left (KC left >DAN-i1 left) and DAN-i1 right (KC left >DAN-i1 right). All APL-KC connections are ipsilateral, excepting the "freak" KC indicated with *. Bottom, The median fraction of input synapses is shown for the synapses from APL left on KCs (APL left >KCs left), and for the KCs synapsing to either DAN-i1 left (KC left >DAN-i1 left) or DAN-i1 right (KC left >DAN-i1 right), or to both DAN-i1 left and right (KC left >DAN-i1 right + left). ***B***, The impact of APL left on the DAN-i1s via the left-hemisphere KCs is estimated by the product of the FI synapses shown in ***A***. Schematic represents the connectivity between APL, DAN-i1, and the KCs. Bottom, The median of these products is shown. The raw data underlying corresponding analyses of the right-hemisphere APL are shown in Extended Data Figure 3-1. ***C***, Products, summed across KCs and hemispheres, as a proxy of the total possible impact of both APLs, via KCs, on the indicated DANs, OANs, and MBINs. ***D***, Bar graphs and color-coded map of the mushroom body based on the data in ***C***, suggesting a stronger negative impact of APL (1) on activity in the input neurons to the vertical lobe (compartments e, f, g) compared with the medial lobe input neurons (compartments i, j, k) (indicated with bold magenta or green edges and filled bars, respectively); (2) on activity in the DL1-DANs (DAN-c1, -d1, -f1, -g1, and MBIN-e2: Selcho et al., 2009; Rohwedder et al., 2016; Saumweber et al., 2018; but see Eichler et al., 2017) compared

C). In a repetition of this experiment, we showed that this reduction in memory was rescued in larvae that were additionally fed with the dopamine precursor L-DOPA (Fig. 17*D*; notably, L-DOPA alone did not increase memory scores: Fig. 17*D*). These results suggest that the rewarding effect of APL activation involves a dopaminergic process.

Ablation of the dopaminergic pPAM neurons impairs odor-APL memory

We next sought to identify the dopaminergic neurons that mediate the rewarding effect of APL activation. Given the role of the dopaminergic pPAM neurons in larval reward learning (Rohwedder et al., 2016; Saumweber et al., 2018; Schleyer et al., 2020; Thoener et al., 2022), we combined the GAL4/UAS with the lexA/lexAop systems to optogenetically activate APL (APL-GAL4>UAS-ChR2XXL) in animals expressing the pro-apoptotic *reaper* gene in the pPAM neurons, leading to their ablation (pPAM-lexA>lexAop-reaper). Larvae of the experimental group (APL_{55D08}>ChR2XXL; pPAM>reaper) showed reduced odor-APL memory scores relative to genetic controls that lacked either the reaper effector or the pPAM driver for ablation (APL_{55D08}>ChR2XXL; pPAM>+ and APL_{55D08}>ChR2XXL; +>reaper, respectively) (Fig. 18). Together, these results suggest that the rewarding effect of the activation of APL comes about, in part, by engaging a dopaminergic and pPAM-dependent process.

Discussion

The present study consolidates and broadens our knowledge of the morphology of the larval APL, of its GABAergic nature and its capacity to inhibit mushroom body KCs, of the polarity and topology of its chemical synapses, its development through metamorphosis, and of the specificity of a transgenic driver strain for studying it (Figs. 2-8) (Masuda-Nakagawa et al., 2014; Eichler et al., 2017; Saumweber et al., 2018). All these findings are consistent with APL playing a role in the sparsening of neuronal activity across the mushroom body (Masuda-Nakagawa et al., 2014; adults: Lin et al., 2014; Amin et al., 2020) and establish APL as one of the most comprehensively described neurons in *Drosophila*. The present study further uncovers unexpected functional complexity by revealing a rewarding effect of optogenetically activating APL (Fig. 12*A*). Our experiments were then designed to study key features of this effect and how it comes about (Figs. 12*C*-18).

Features of the rewarding effect of APL activation

Optogenetic activation of APL induces associative reward learning about odors after only one training trial (Figs. 12-15). This is similar to odor-sugar associative learning and to the rewarding effect of activating DAN-i1 (Weiglein et al., 2019; Thoener et al., 2022). Likewise, similar to fructose and DAN-i1 as rewards (Saumweber et al., 2011; Schleyer et al., 2011, 2018, 2020), activation of APL leads to an increase in odor preference when it is paired with odor presentation and to a decrease in odor preference when it is unpaired from odor presentation (Figs. 12*B*, 15*B*). In other words, the respective memories are appetitive as they are about the reward: After paired training, the larvae search for the reward where the odor *is*, whereas after unpaired training, adaptively, they search for the reward precisely where the odor is *not*. Associative learning by APL activation has a symmetrical "temporal fingerprint," with a fairly narrow temporal window for presenting the odor (Fig. 12*F*,*G*). This mirrors what was found for DAN-d1 in the aversive domain (Weiglein et al., 2021), adding to the heterogeneity of internal reinforcement signals (Saumweber et al., 2018; Weiglein et al., 2021; Thoener et al., 2022; adults: Aso and Rubin, 2016; König et al., 2018; Handler et al., 2019).

The appetitive memories established by activating APL decay within minutes (Fig. 12*E*), as do memories for odor-fructose, odor-DAN-i1, and odor-KC association (Neuser et al., 2005; Kleber et al., 2016; Lyutova et al., 2019; Weiglein et al., 2019; Thoener et al., 2022). Similar to odor-fructose memories and odor-DAN-i1 memories (Paisios et al., 2017; Schleyer et al., 2020), APL-induced memories are expressed as modulations of turning, but not of run speed (Fig. 13).

In addition to establishing appetitive associative memory during training, the activation of APL can also terminate learned search behavior during testing (Figs. 14*A*,*B*, 15*D*), without affecting task-relevant innate olfactory behavior (Figs. 14*E*–*G*, 15*E*). This is in line with reports on taste rewards (Schleyer et al., 2015a) and on DAN-i1 activation as a reward (Schleyer et al., 2020).

The rewarding effect of APL activation offers a new perspective on the result from Saumweber et al. (2018), who showed that activating APL throughout the complete training phase abolishes odor-fructose memory scores, an effect that we replicated (Fig. 9*A*,*B*). In these experiments, a fructose reward is presented paired with or unpaired from the odor. The protocol of APL activation engages an additional, much stronger reward signal throughout training. Thus, the animals are rewarded regardless of the presence or absence of the odor, which overrides the learning of the relationship between odor and fructose. Thus, the rewarding effect of activating APL is compatible with the previous results from Saumweber et al. (2018), and the resulting appetitive, associative memories resemble those established by DANs or taste reinforcement.

Possible mechanisms of odor-APL learning: notes upfront

Our results confirm that the larval APL neuron is GABAergic (Fig. 4*A*-*B*″) (Masuda-Nakagawa et al., 2014). Tests for the presence of octopamine, acetylcholine, and glutamate in the larval APL turned out negative (Masuda-Nakagawa et al., 2014; Eichler et al., 2017). This matches a recent transcriptome analysis in adults (Aso et al., 2019), whereas two earlier reports had suggested the presence of GABA, octopamine, and glutamate in the adult APL (C. L. Wu et al., 2013; H. Li et al., 2017). In the absence of evidence suggesting otherwise for the larval APL, the following discussion considers only GABAergic signaling.

GABA binding to ionotropic GABA-A receptors and the ensuing chloride influx confer the typical inhibitory effect of GABA on postsynaptic neurons. Accordingly, APL activation reduces activity in KCs (Fig. 5*G*–*I*). However, effects of GABA via metabotropic receptors may also have a role in postsynaptic activity. In motoneurons of pupal *Drosophila*, moreover, GABA-induced spikelets have been observed, arguably because of a relatively positive reversal potential for chloride during this life stage (Ryglewski et al., 2017; mammals: Ben-Ari, 2002). Thus, it cannot be excluded that GABA release from APL leads to

←

with the pPAM-DANs (DAN-i1, -j1, -k1) (magenta or green hatched bars, respectively); and (3) on activity in DAN-f1 compared with DAN-i1 (magenta or green hatched bars, respectively). The absence of DAN-h1 in first-instar larvae is indicated by the gray fill of the h compartment. MBIN-l1 is not considered in these analyses because it innervates multiple compartments in first-instar larvae. Magenta and green represent elements of the system preferentially involved in aversive and appetitive processing, respectively.

Table 2. All statistical results grouped by figure number, figure panel, and statistical tests

Figure	Panel	Data	Statistical test	Result
3	*E*	Mean pixel intensity right (x) vs left (y) hemisphere	Pearson correlation	$r = 0.974$, $p < 0.0001$
5	*B*	+>ChR2XXL; KC>GCaMP6m vs APL_{26G02}>ChR2XXL; KC>GCaMP6m	MWW	$U = 284.5$, $p = 0.238$
	C			$U = 257$, $p = 0.090$
	E			$U = 108$, $p < 0.001$
	F			$U = 119$, $p < 0.001$
	H			$U = 429$, $p < 0.01$
	I			$U = 415$, $p = 0.04$
6	*D*	APL left: axon; dendrite; neurite	KW	H (2, 5924) = 1008.2, $p < 0.001$
		APL left: axon vs dendrite	MWW with BH correction	$U = 1558487$, $p < 0.001$
		APL left: axon vs neurite		$U = 74037$, $p = 0.9821$
		APL left: dendrite vs neurite		$U = 27809$, $p < 0.001$
		APL right: axon; dendrite; neurite	KW	H (2, 8477) = 1940.9, $p < 0.001$
		APL right: axon vs dendrite	MWW with BH correction	$U = 3097808$, $p < 0.001$
		APL right: axon vs neurite		$U = 131161$, $p < 0.01$
		APL right: dendrite vs neurite		$U = 45183$, $p < 0.001$
7; Extended Data Figure 7-4	*D*	APL left ->KC vs KC ->APL left	MWW	$U = 27236.5$, $p < 0.001$
Extended Data Figure 7-4	*D*	APL right ->KC vs KC ->APL right		$U = 50181.5$, $p < 0.001$
9	*A*	APL>ChR2XXL;+>ChR2XXL; APL>+	KW	H (2, 36) = 17.353, $p < 0.001$
		APL>ChR2XXL vs +>ChR2XXL	MWW with BH correction	$U = 5$, $p < 0.001$
		APL>ChR2XXL vs APL>+		$U = 15$, $p = 0.001$
		+>ChR2XXL vs APL>+		$U = 62$, $p = 0.583$
		APL>ChR2XXL vs 0	OSS test with BH correction	$p = 0.146$
		+>ChR2XXL vs 0		$p < 0.001$
		APL>+ vs 0		$p = 0.006$
	B	APL>ChR2XXL;+>ChR2XXL; APL>+	KW	H (2, 90) = 28.063, $p < 0.001$
		APL>ChR2XXL vs +>ChR2XXL	MWW with BH correction	$U = 119$, $p < 0.001$
		APL>ChR2XXL vs APL>+		$U = 165$, $p < 0.001$
		+>ChR2XXL vs APL>+		$U = 421$, $p = 0.673$
		APL>ChR2XXL vs 0	OSS test with BH correction	$p = 1$
		+>ChR2XXL vs 0		$p < 0.001$
		APL>+ vs 0		$p < 0.001$
	D	No light vs light	MWW	$U = 389.5$, $p = 0.974$
	F			$U = 313$, $p = 0.381$
	G			$U = 363$, $p = 0.993$
	H			$U = 363$, $p = 0.993$
	I			$U = 337$, $p = 0.646$
10		No light; light odor trial; light nonodor trial; no light test@fru; light odor trial test@fru; light nonodor trial test@fru	KW	H (5, 150) = 56.412, $p < 0.001$
		No light vs light odor trial	MWW with BH correction	$U = 88$, $p < 0.001$
		No light vs light nonodor trial		$U = 119$, $p < 0.001$
		Light odor trial vs light nonodor trial		$U = 292.5$, $p = 0.705$
		No light test@fru vs light odor trial test@fru		$U = 291$, $p = 0.683$
		No light test@fru vs light nonodor trial test@fru		$U = 292$, $p = 0.700$
		Light odor trial test@fru vs light nonodor trial test@fru		$U = 259$, $p = 0.304$
		No light vs no light test@fru		$U = 54$, $p < 0.001$
		Light odor trial vs light odor trial test@fru		$U = 162$, $p = 0.004$
		Light nonodor trial vs light nonodor trial test@fru		$U = 146$, $p = 0.001$
		No light vs 0	OSS test with BH correction	$p < 0.001$
		Light odor trial vs 0		$p < 0.001$
		Light nonodor trial vs 0		$p = 0.004$
		No light test@fru vs 0		$p = 1$
		Light odor trial test@fru vs 0		$p = 0.690$
		Light nonodor trial test@fru vs 0		$p = 1$
11	*A*	PREF no light; no light test@fru	KW	H (3, 100) = 51.684, $p < 0.001$
		PREF paired vs unpaired no light	MWW with BH correction	$U = 10.5$, $p < 0.001$
		PREF paired vs unpaired light test@fru		$U = 308.5$, $p = 0.946$
		PREF paired no light vs baseline		$U = 228$, $p < 0.001$
		PREF unpaired no light vs baseline		$U = 155$, $p < 0.001$
	B	PREF light odor trial; light odor trial test@fru	KW	H (3, 100) = 22.014, $p < 0.001$
		PREF paired vs unpaired light odor trial	MWW with BH correction	$U = 73$, $p < 0.001$
		PREF paired vs unpaired light odor trial test@fru		$U = 272$, $p = 0.438$
		PREF paired light odor trial vs baseline		$U = 431$, $p = 0.029$
		PREF unpaired light odor trial vs baseline		$U = 358$, $p = 0.002$
	C	PREF light nonodor trial; light nonodor trial test@fru	KW	H (3, 100) = 14.67, $p = 0.002$

(*Table continues*)

Table 2. Continued

Figure	Panel	Data	Statistical test	Result
		PREF paired vs unpaired light nonodor trial	MWW with BH correction	$U = 137$, $p < 0.001$
		PREF paired vs unpaired light nonodor trial test@fru		$U = 264.5$, $p = 0.356$
		PREF paired light nonodor trial vs baseline		$U = 419.5$, $p = 0.021$
		PREF unpaired light nonodor trial vs baseline		$U = 408$, $p = 0.015$
	D	PREF no light test@fru; light odor trial test@fru; light nonodor trial test@fru	KW	H (2, 150) = 88.073, $p < 0.001$
		No light test@fru vs light odor trial test@fru	MWW with BH correction	$U = 513$, $p < 0.001$
		No light test@fru vs light nonodor trial test@fru		$U = 376$, $p < 0.001$
		Light odor trial test@fru vs light nonodor trial test@fru		$U = 20.5$, $p < 0.001$
12	*A*	APL>ChR2XXL;+>ChR2XXL; APL>+	KW	H (2, 36) = 22.524, $p < 0.001$
		APL>ChR2XXL vs +>ChR2XXL	MWW with BH correction	$U = 0$, $p < 0.001$
		APL>ChR2XXL vs APL>+		$U = 3$, $p < 0.001$
		+>ChR2XXL vs APL>+		$U = 64$, $p = 0.665$
		APL>ChR2XXL vs 0	OSS test with BH correction	$p < 0.001$
		+>ChR2XXL vs 0		$p = 0.387$
		APL>+ vs 0		$p = 1$
	B	APL>ChR2XXL paired; APL>ChR2XXL unpaired; +>ChR2XXL paired; +>ChR2XXL unpaired; APL>+ paired; APL>+ unpaired	KW	H (5, 72) = 30.41, $p < 0.0001$
		APL>ChR2XXL paired vs baseline	MWW with BH correction	$U = 49$, $p < 0.0001$
		APL>ChR2XXL unpaired vs baseline		$U = 117.5$, $p < 0.002$
		+>ChR2XXL paired vs +>ChR2XXL unpaired		$U = 64.00$, $p = 0.665$
		APL>+ paired vs APL>+ unpaired		$U = 69.50$, $p = 0.908$
	C	APL>GtACR1;+>GtACR1; APL>+	KW	H (2, 72) =7.756, $p = 0.02$
		APL>GtACR1 vs +>GtACR1	MWW with BH correction	$U = 165$, $p = 0.011$
		APL>GtACR1 vs APL>+		$U = 178$, $p = 0.023$
		+>GtACR1vs APL>+		$U = 287.5$, $p = 0.990$
		APL>GtACR1 vs 0	OSS test with BH correction	$p < 0.01$
		+>GtACR1 vs 0		$p = 0.840$
		APL>+ vs 0		$p = 0.670$
	D	APL>GtACR1 paired; APL>GtACR1 unpaired; +>GtACR1 paired; +>GtACR1 unpaired; APL>+ paired; APL>+ unpaired	KW	H (5, 144) = 10.650, $p = 0.059$
	E	Retention interval 0; 5; 10; 20 min	KW	H (3, 120) = 51.554, $p < 0.001$
		0 vs 5 min	MWW with BH correction	$U = 207$, $p < 0.001$
		0 vs 10 min		$U = 93$, $p < 0.001$
		0 vs 20 min		$U = 24$, $p < 0.001$
		0 min vs 0	OSS test with BH correction	$p < 0.001$
		5 min vs 0		$p < 0.001$
		10 min vs 0		$p = 0.585$
		20 min vs 0		$p = 0.585$
	F	ISI −120; −60; −30; −10; 0; 10; 30; 60; 120	KW	H (8, 216) = 23.4, $p = 0.003$
	G	APL>ChR2XXL;+>ChR2XXL; APL>+	KW	H (2, 36) = 13.839, $p = 0.001$
		APL>ChR2XXL vs +>ChR2XXL	MWW with BH correction	$U = 21$, $p = 0.003$
		APL>ChR2XXL vs APL>+		$U = 14$, $p < 0.001$
		+>ChR2XXL vs APL>+		$U = 58$, $p = 0.436$
		APL>ChR2XXL vs 0	OSS test with BH correction	$p = 0.006$
		+>ChR2XXL vs 0		$p = 1$
		APL>+ vs 0		$p = 0.388$
13	*C*	Paired vs unpaired	MWW	$U = 399$, $p < 0.001$
	D			$U = 270$, $p < 0.001$
	E			$U = 419$, $p < 0.001$
	F			$U = 791$, $p = 0.104$
14	*A*	APL>ChR2XXL;+>ChR2XXL; APL>+; APL>ChR2XXL test@light;+>ChR2XXL test@light; APL>+ test@light	KW	H (5, 96) = 37.772, $p < 0.001$
		APL>ChR2XXL vs +>ChR2XXL	MWW with BH correction	$U = 7$, $p < 0.001$
		APL>ChR2XXL vs APL>+		$U = 17$, $p < 0.001$
		+>ChR2XXL vs APL>+		$U = 103$, $p = 0.356$
		APL>ChR2XXL test@light vs +>ChR2XXL test@light		$U = 94$, $p = 0.207$
		APL>ChR2XXL test@light vs APL>+ test@light		$U = 68$, $p = 0.025$
		+>ChR2XXL test@light vs APL>+ test@light.		$U = 103$, $p = 0.356$
		APL>ChR2XXL vs APL>ChR2XXL test@light		$U = 10$, $p < 0.001$
		+>ChR2XXL vs +>ChR2XXL test@light		$U = 122$, $p = 0.836$
		APL>+ vs APL>+ test@light		$U = 127$, $p = 0.985$
		APL>ChR2XXL vs 0	OSS test with BH correction	$p < 0.001$
		+>ChR2XXL vs 0		$p = 0.804$
		APL>+ vs 0		$p = 0.210$

(*Table continues*)

Table 2. Continued

Figure	Panel	Data	Statistical test	Result
		APL>ChR2XXL test@light vs 0		$p = 0.210$
		+>ChR2XXL test@light vs 0		$p = 0.210$
		APL>+ test@light vs 0		$p = 0.210$
	B	APL>ChR2XXL;+>ChR2XXL; APL>+; APL>ChR2XXL test@light;+>ChR2XXL test@light; APL>+ test@light	KW	H (5, 96) = 30.782, $p < 0.001$
		APL>ChR2XXL vs +>ChR2XXL	MWW with BH correction	$U = 15$, $p < 0.001$
		APL>ChR2XXL vs APL>+		$U = 12$, $p < 0.001$
		+>ChR2XXL vs APL>+		$U = 109$, $p = 0.486$
		APL>ChR2XXL test@light vs +>ChR2XXL test@light		$U = 121$, $p = 0.806$
		APL>ChR2XXL test@light vs APL>+ test@light		$U = 88$, $p = 0.136$
		+>ChR2XXL test@light vs APL>+ test@light		$U = 90$, $p = 0.157$
		APL>ChR2XXL vs APL>ChR2XXL test@light		$U = 38$, $p < 0.001$
		+>ChR2XXL vs +>ChR2XXL test@light		$U = 119$, $p = 0.749$
		APL>+ vs APL>+ test@light		$U = 126$, $p = 0.955$
		APL>ChR2XXL vs 0	OSS test with BH correction	$p < 0.001$
		+>ChR2XXL vs 0		$p = 0.804$
		APL>+ vs 0		$p = 0.454$
		APL>ChR2XXL test@light vs 0		$p = 0.804$
		+>ChR2XXL test@light vs 0		$p = 1$
		APL>+ test@light vs 0		$p = 0.077$
	C	AM/AM vs OCT/OCT	MWW	$U = 85$, $p = 0.0019$
		AM/AM vs 0	OSS test with BH correction	$p < 0.0001$
		OCT/OCT vs 0		$p = 0.0118$
	D	AM/AM; OCT/OCT; AM/OCT; OCT/AM	KW	H (3, 118) =19.34, $p < 0.001$
		AM/AM vs OCT/OCT	MWW with BH correction	$U = 319.00$, $p = 0.054$
		AM/AM vs AM/OCT		$U = 241.00$, $p = 0.003$
		OCT/OCT vs OCT/AM		$U = 280.00$, $p = 0.019$
		AM/AM vs 0	OSS test with BH correction	$p < 0.0001$
		OCT/OCT vs 0		$p < 0.0001$
		AM/OCT vs 0		$p = 0.0009$
		OCT/AM vs 0		$p = 0.0002$
	E	APL>ChR2XXL; +>ChR2XXL; APL>+; APL>ChR2XXL test@light; +>ChR2XXL test@light; APL>+ test@light	KW	H (5, 180) = 17.99, $p < 0.01$
		APL>ChR2XXL vs +>ChR2XXL	MWW with BH correction	$U = 391.5$, $p = 0.391$
		APL>ChR2XXL vs APL>+		$U = 361$, $p = 0.191$
		+>ChR2XXL vs APL>+		$U = 289$, $p = 0.017$
		APL>ChR2XXL test@light vs +>ChR2XXL test@light		$U = 239$, $p = 0.002$
		APL>ChR2XXL test@light vs APL>+ test@light		$U = 388$, $p = 0.363$
		+>ChR2XXL test@light vs APL>+ test@light		$U = 285.5$, $p = 0.015$
		APL>ChR2XXL vs APL>ChR2XXL test@light		$U = 398$, $p = 0.761$
		+>ChR2XXL vs +>ChR2XXL test@light		$U = 360$, $p = 0.188$
		APL>+ vs APL>+ test@light		$U = 331.5$, $p = 0.081$
	F	APL>ChR2XXL; +>ChR2XXL; APL>+; APL>ChR2XXL test@light; +>ChR2XXL test@light; APL>+ test@light	KW	H (5, 144) = 12.59, $p = 0.027$
		APL>ChR2XXL vs +>ChR2XXL	MWW with BH correction	$U = 264$, $p = 0.628$
		APL>ChR2XXL vs APL>+		$U = 269.5$, $p = 0.710$
		+>ChR2XXL vs APL>+		$U = 244.5$, $p = 0.375$
		APL>ChR2XXL test@light vs +>ChR2XXL test@light		$U = 277.5$, $p = 0.836$
		APL>ChR2XXL test@light vs APL>+ test@light		$U = 162$, $p < 0.01$
		+>ChR2XXL test@light vs APL>+ test@light		$U = 167$, $p = 0.013$
		APL>ChR2XXL vs APL>ChR2XXL test@light		$U = 275.5$, $p = 0.804$
		+>ChR2XXL vs +>ChR2XXL test@light		$U = 208.5$, $p = 0.885$
		APL>+ vs APL>+ test@light		$U = 184.5$, $p = 0.033$
	G	APL>ChR2XXL; +>ChR2XXL; APL>+; APL>ChR2XXL test@light; +>ChR2XXL test@light; APL>+ test@light	KW	H (5, 184) = 4.43, $p = 0.489$
15	*A*	APL>Chrimson; +>Chrimson; APL>+	KW	H (2, 38) = 12.204, $p = 0.002$
		APL>Chrimson vs +>Chrimson	MWW with BH correction	$U = 24$, $p = 0.002$
		APL>Chrimson vs APL>+		$U = 25$, $p = 0.004$
		+>Chrimson vs APL>+		$U = 74$, $p = 0.849$
		APL>Chrimson vs 0	OSS test with BH correction	$p = 0.003$
		+>Chrimson vs 0		$p = 0.581$
		APL>+ vs 0		$p = 0.774$
	B	APL>Chrimson paired; APL>Chrimson unpaired; +>Chrimson paired; +>Chrimson unpaired; APL>+ paired; APL>+ unpaired	KW	H (5, 76) = 26.67, $p < 0.001$

(*Table continues*)

Table 2. Continued

Figure	Panel	Data	Statistical test	Result
		APL>Chrimson paired vs baseline	MWW with BH correction	$U = 175.50$, $p = 0.011$
		APL>Chrimson unpaired vs baseline		$U = 81.50$, $p < 0.0001$
		+>Chrimson paired vs +>Chrimson unpaired		$U = 67.00$, $p = 0.383$
		APL>+ paired vs APL>+ unpaired		$U = 65.00$, $p = 0.707$
	C	Retinal vs EtOH	MWW	$U = 5$, $p < 0.001$
		Retinal vs 0	OSS test with BH correction	$p < 0.001$
		EtOH vs 0		$p = 1$
	D	APL>Chrimson vs APL>Chrimson test@light	MWW	$U = 290$, $p = 0.001$
		APL>Chrimson vs 0	OSS test with BH correction	$p < 0.001$
		APL>Chrimson test@light vs 0		$p = 0.013$
	E	APL>Chrimson test@dark vs APL>Chrimson test@light	MWW	$U = 370$, $p = 0.239$
16	*A*	MBONa1,a2>GtACR1; +>GtACR1; MBONa1,a2>+	KW	H (2, 36) = 0.758, $p = 0.684$
	B	MBONa1,a2>ChR2XXL; +>ChR2XXL; MBONa1,a2>+		H (2, 48) = 4.844, $p = 0.088$
	C	MBONa1>GtACR1; MBONa2>GtACR1; MBONa1>GtACR1 test@light; MBONa2>GtACR1 test@light		H (3, 48) = 0.404, $p = 0.939$
	D	MBONa1>ChR2XXL; MBONa2>ChR2XXL; MBONa1>ChR2XXL test@light; MBONa2>ChR2XXL test@light		H (1, 50) = 0.0377, $p = 0.846$
17	*C*	3IY [0 mg.ml^{-1}] vs [5 mg.ml^{-1}]	MWW	$U = 180$, $p = 0.026$
		3IY [0 mg.ml^{-1}] vs 0	OSS test with BH correction	$p < 0.001$
		3IY [5 mg.ml^{-1}] vs 0		$p < 0.001$
	D	Control; 3IY [5 mg.ml^{-1}]; 3IY [5 mg.ml^{-1}] + L-DOPA [10 mg.ml^{-1}]; L-DOPA [10 mg.ml^{-1}]	KW	H (3, 104) = 20.974, $p < 0.001$
		Control vs 3IY [5 mg.ml^{-1}]	MWW	$U = 122$, $p < 0.001$
		Control vs 3IY [5 mg.ml^{-1}] + L-DOPA [10 mg.ml^{-1}]		$U = 267$, $p = 0.196$
		Control vs L-DOPA [10 mg.ml^{-1}]		$U = 309$, $p = 0.60$
		3IY [5 mg.ml^{-1}] vs 3IY [5 mg.ml^{-1}] + L-DOPA [10 mg.ml^{-1}]		$U = 171$, $p = 0.002$
		Control vs 0	OSS test with BH correction	$p < 0.001$
		3IY [5 mg.ml^{-1}] vs 0		$p < 0.001$
		3IY [5 mg.ml^{-1}] + L-DOPA [10 mg.ml^{-1}] vs 0		$p < 0.001$
		L-DOPA [10 mg.ml^{-1}] vs 0		$p < 0.001$
18		APL55D08>ChR2XXL; pPAM>reaper | APL55D08>ChR2XXL; pPAM>+ | APL55D08>ChR2XXL; +>reaper	KW	H (2, 79) =30.85, $p < 0.001$
		APL55D08>ChR2XXL; pPAM>reaper vs APL55D08>ChR2XXL; pPAM>+	MWW with BH correction	$U = 60$, $p < 0.0001$
		APL55D08>ChR2XXL; pPAM>reaper vs APL55D08>ChR2XXL; +>reaper		$U = 180.5$, $p = 0.002$
		APL55D08>ChR2XXL; pPAM>+ vs APL55D08>ChR2XXL; +>reaper		$U = 159$, $p < 0.001$
		APL55D08>ChR2XXL; pPAM>reaper vs 0	OSS test with BH correction	$p = 0.009$
		APL55D08>ChR2XXL; pPAM>+ vs 0		$p < 0.001$
		APL55D08>ChR2XXL; +>reaper vs 0		$p < 0.001$

excitatory effects in a minority of KCs or in non-KC targets of APL. Furthermore, a postinhibitory rebound activation may occur in the target neurons of APL, a widely observed physiological phenomenon (Huguenard and McCormick, 2007; for evidence in adult *Drosophila* after days of APL activation: Apostolopoulou and Lin, 2020). With these caveats in mind, the discussion below maintains the conventional notion of GABA as mediating inhibition.

The fact that activation of APL can establish appetitive memory for an associated odor means that, even under conditions of GABAergic, inhibitory input, an associable odor representation can be established across the KCs. Indeed, these representations can be odor-specific (Fig. 14*B*,*D*). The scenario could be that, under baseline conditions, odors strongly activate "their" subset of KCs while the other KCs are inactive or mildly inhibited. Upon optogenetic APL activation, however, odors only mildly activate an even sparser set of KCs while most other KCs would be strongly inhibited. Interestingly, associable odor representations can be established also under conditions of optogenetically increased levels of activity across the KCs (Lyutova et al., 2019).

We are not aware of data suggesting that GABA can have a direct associative memory-trace-inducing effect. Rather, our results suggest that the rewarding effect of APL activation comes about, at least in part, by engaging a dopaminergic reward signal from the pPAM neurons (Figs. 17, 18). We will therefore focus on plausible pathways from APL toward these pPAM neurons.

From APL to dopaminergic pPAM neurons?

The larval APL has presynapses only in the calyx (Figs. 4, 6-8; Movie 3). The postsynaptic partners of APL include the KCs (see next paragraph) and the two calyx MBONs (Eichler et al., 2017; Saumweber et al., 2018). One of these calyx MBONs promotes approach when optogenetically activated (MBON-a1), whereas the other promotes avoidance (MBON-a2) (Eschbach et al., 2021). Both calyx MBONs give rise to indirect feedback to DANs, including to the punishing DAN-d1 and the rewarding DAN-i1 neuron of the pPAM cluster (Eschbach et al., 2020). However, presenting an odor together with activating or silencing the two calyx MBONs, alone or in combination, did not establish either appetitive or aversive associative odor memory (Fig. 16). Thus, although it is a connectomic possibility, there is no evidence for a reinforcing APL-MBONa1/a2-pPAM loop. What about a loop from APL via the KCs to the pPAM neurons?

A first intuition is that an APL-KC-pPAM loop is an unlikely candidate. This is because, bearing the discussed caveats in mind, APL inhibits KCs, while KCs in turn excite DANs (Lyutova et al., 2019; adults: Cervantes-Sandoval et al., 2017). Thus, APL activation should reduce KC activity, which in turn reduces drive to the pPAMs. However, it might not be the absolute level of activity in the pPAM neurons that matters, but rather whether these are relatively less affected than the punishing DANs. In other words, is the negative impact that APL exerts on DAN activity

stronger for the punishing DANs than for the rewarding DANs? We therefore queried the larval connectome for the possible impact of APL, via the KCs, on the input neurons of the mushroom body (Fig. 19). It turns out that APL can indeed impact the inputs to the vertical lobe more strongly than those to the medial lobe, suggesting a stronger negative impact of APL on activity in the aversive than the appetitive lobe system (Eschbach et al., 2020). Considering the impact on DL1-DANs versus pPAM-DANs (Rohwedder et al., 2016), as well as comparing the impact on DAN-f1 versus DAN-i1 (Thoener et al., 2022), reveals a similar picture of a stronger impact on aversive pathways.

An alternative could be that, similar to the situation in adults for APL and the DPM neuron (C. L. Wu et al., 2011), there is direct signaling from APL to rewarding pPAM-DANs via electrical synapses in the lobes (Figs. 3, 4, 6, 7) and that fewer or no such electrical synapses exist for the punishing DANs.

In conclusion, we report a case of complex circuit function in a numerically simple brain, and demonstrate the capacity of a central-brain GABAergic neuron to engage dopaminergic reward signaling when optogenetically activated.

References

Amin H, Apostolopoulou AA, Suárez-Grimalt R, Vrontou E, Lin AC (2020) Localized inhibition in the *Drosophila* mushroom body. Elife 9:e56954.

Apostolopoulou AA, Lin AC (2020) Mechanisms underlying homeostatic plasticity in the *Drosophila* mushroom body in vivo. Proc Natl Acad Sci USA 117:16606–16615.

Aso Y, Rubin GM (2016) Dopaminergic neurons write and update memories with cell-type-specific rules. Elife 5:e16135.

Aso Y, Hattori D, Yu Y, Johnston RM, Iyer NA, Ngo TT, Dionne H, Abbott LF, Axel R, Tanimoto H, Rubin GM (2014) The neuronal architecture of the mushroom body provides a logic for associative learning. Elife 3: e04577.

Aso Y, Ray RP, Long X, Bushey D, Cichewicz K, Ngo TT, Sharp B, Christoforou C, Hu A, Lemire AL, Tillberg P, Hirsh J, Litwin-Kumar A, Rubin GM (2019) Nitric oxide acts as a cotransmitter in a subset of dopaminergic neurons to diversify memory dynamics. Elife 8:e49257.

Bainton RJ, Tsai LT, Singh CM, Moore MS, Neckameyer WS, Heberlein U (2000) Dopamine modulates acute responses to cocaine, nicotine and ethanol in *Drosophila*. Curr Biol 10:187–194.

Bates AS, Manton JD, Jagannathan SR, Costa M, Schlegel P, Rohlfing T, Jefferis GS (2020) The natverse, a versatile toolbox for combining and analysing neuroanatomical data. Elife 9:e53350.

Ben-Ari Y (2002) Excitatory actions of GABA during development: the nature of the nurture. Nat Rev Neurosci 3:728–739.

Cervantes-Sandoval I, Phan A, Chakraborty M, Davis RL (2017) Reciprocal synapses between mushroom body and dopamine neurons form a positive feedback loop required for learning. Elife 6:e23789.

Chen TW, Wardill TJ, Sun Y, Pulver SR, Renninger SL, Baohan A, Schreiter ER, Kerr RA, Orger MB, Jayaraman V, Looger LL, Svoboda K, Kim DS (2013) Ultrasensitive fluorescent proteins for imaging neuronal activity. Nature 499:295–300.

Dawydow A, Gueta R, Ljaschenko D, Ullrich S, Hermann M, Ehmann N, Gao S, Fiala A, Langenhan T, Nagel G, Kittel RJ (2014) Channelrhodopsin-2-XXL, a powerful optogenetic tool for low-light applications. Proc Natl Acad Sci USA 111:13972–13977.

Demerec M, Kaufmann BP (1940) Drosophila guide: introduction to the genetics and cytology of Drosophila melanogaster. Washington, DC: Carnegie Institution of Washington.

Eichler K, Li F, Litwin-Kumar A, Park Y, Andrade I, Schneider-Mizell CM, Saumweber T, Huser A, Eschbach C, Gerber B, Fetter RD, Truman JW, Priebe CE, Abbott LF, Thum AS, Zlatic M, Cardona A (2017) The complete connectome of a learning and memory centre in an insect brain. Nature 548:175–182.

Eschbach C, Zlatic M (2020) Useful road maps: studying *Drosophila* larva's central nervous system with the help of connectomics. Curr Opin Neurobiol 65:129–137.

Eschbach C, Fushiki A, Winding M, Schneider-Mizell CM, Shao M, Arruda R, Eichler K, Valdes-Aleman J, Ohyama T, Thum AS, Gerber B, Fetter RD, Truman JW, Litwin-Kumar A, Cardona A, Zlatic M (2020) Recurrent architecture for adaptive regulation of learning in the insect brain. Nat Neurosci 23:544–555.

Eschbach C, Fushiki A, Winding M, Afonso B, Andrade IV, Cocanougher BT, Eichler K, Gepner R, Si G, Valdes-Aleman J, Fetter RD, Gershow M, Jefferis GS, Samuel A, Truman JW, Cardona A, Zlatic M (2021) Circuits for integrating learned and innate valences in the insect brain. Elife 10: e62567.

Fernandez RW, Akinleye AA, Nurilov M, Feliciano O, Lollar M, Aijuri RR, O'Donnell JM, Simon AF (2017) Modulation of social space by dopamine in *Drosophila melanogaster*, but no effect on the avoidance of the *Drosophila* stress odorant. Biol Lett 13:20170369.

Gerber B, Hendel T (2006) Outcome expectations drive learned behaviour in larval *Drosophila*. Proc Biol Sci 273:2965–2968.

Gerber B, Stocker RF (2007) The Drosophila larva as a model for studying chemosensation and chemosensory learning: A review. Chem Senses 32: 65–89.

Grünewald B (1999) Morphology of feedback neurons in the mushroom body of the honeybee, *Apis mellifera*. J Comp Neurol 404:114–126.

Handler A, Graham TG, Cohn R, Morantte I, Siliciano AF, Zeng J, Li Y, Ruta V (2019) Distinct dopamine receptor pathways underlie the temporal sensitivity of associative learning. Cell 178:60–75.e19.

Haynes PR, Christmann BL, Griffith LC (2015) A single pair of neurons links sleep to memory consolidation in *Drosophila melanogaster*. Elife 4:e03868.

Heisenberg M (2003) Mushroom body memoir: from maps to models. Nat Rev Neurosci 4:266–275.

Herranz H, Weng R, Cohen SM (2014) Crosstalk between epithelial and mesenchymal tissues in tumorigenesis and imaginal disc development. Curr Biol 24:1476–1484.

Homberg U, Kingan TG, Hildebrand JG (1987) Immunocytochemistry of GABA in the brain and suboesophageal ganglion of *Manduca sexta*. Cell Tissue Res 248:1–24.

Honegger KS, Campbell RA, Turner GC (2011) Cellular-resolution population imaging reveals robust sparse coding in the *Drosophila* mushroom body. J Neurosci 31:11772–11785.

Huguenard JR, McCormick DA (2007) Thalamic synchrony and dynamic regulation of global forebrain oscillations. Trends Neurosci 30:350–356.

Inada K, Tsuchimoto Y, Kazama H (2017) Origins of cell-type-specific olfactory processing in the *Drosophila* mushroom body circuit. Neuron 95:357–367.e4.

Jenett A, Rubin GM, Ngo TT, Shepherd D, Murphy C, Dionne H, Pfeiffer BD, Cavallaro A, Hall D, Jeter J, Iyer N (2012) A GAL4-driver line resource for Drosophila neurobiology. Cell Rep 2:991–1001.

Kanellopoulos AK, Mariano V, Spinazzi M, Woo YJ, McLean C, Pech U, Li KW, Armstrong JD, Giangrande A, Callaerts P, Smit AB, Abrahams BS, Fiala A, Achsel T, Bagni C (2020) Aralar sequesters GABA into hyperactive mitochondria, causing social behavior deficits. Cell 180:1178–1197.e20.

Kaun KR, Azanchi R, Maung Z, Hirsh J, Heberlein U (2011) A *Drosophila* model for alcohol reward. Nat Neurosci 14:612–619.

Klapoetke NC, et al. (2014) Independent optical excitation of distinct neural populations. Nat Methods 11:338–346.

Kleber J, Chen Y, Michels B, Saumweber T, Schleyer M, Kähne T, Buchner E, Gerber B (2016) Synapsin is required to 'boost' memory strength for highly salient events. Learn Mem 23:9–20.

Kobler O, Weiglein A, Hartung K, Chen YC, Gerber B, Thomas U (2021) A quick and versatile protocol for the 3D visualization of transgene expression across the whole body of larval *Drosophila*. J Neurogenet 35:306–319.

Kohl J, Ng J, Cachero S, Ciabatti E, Dolan MJ, Sutcliffe B, Tozer A, Ruehle S, Krueger D, Frechter S, Branco T, Tripodi M, Jefferis GS (2014) Ultrafast tissue staining with chemical tags. Proc Natl Acad Sci USA 111:E3805–E3814.

König C, Khalili A, Ganesan M, Nishu AP, Gomez AP, Niewalda T, Gerber B, Aso Y, Yarali A (2018) Reinforcement signalling of punishment vs. relief in fruit flies. Learn Mem 25:247–257.

König C, Khalili A, Niewalda T, Gao S, Gerber B (2019) An optogenetic analogue of second-order reinforcement in *Drosophila*. Biol Lett 15:20190084.

Lee PT, Lin HW, Chang YH, Fu TF, Dubnau J, Hirsh J, Lee T, Chiang AS (2011) Serotonin-mushroom body circuit modulating the formation of anesthesia-resistant memory in *Drosophila*. Proc Natl Acad Sci USA 108:13794–13799.

Lee T, Luo L (1999) Mosaic analysis with a repressible cell marker for studies of gene function in neuronal morphogenesis. Neuron 22:451–461.
Li F, et al. (2020) The connectome of the adult *Drosophila* mushroom body provides insights into function. Elife 9:e62576.
Li H, Horns F, Wu B, Xie Q, Li J, Li T, Luginbuhl DJ, Quake SR, Luo L (2017) Classifying *Drosophila* olfactory projection neuron subtypes by single-cell RNA sequencing. Cell 171:1206–1220.e22.
Lin AC, Bygrave AM, de Calignon A, Lee T, Miesenböck G (2014) Sparse, decorrelated odor coding in the mushroom body enhances learned odor discrimination. Nat Neurosci 17:559–568.
Liu X, Davis RL (2009) The GABAergic anterior paired lateral neuron suppresses and is suppressed by olfactory learning. Nat Neurosci 12:53–59.
Liu X, Krause WC, Davis RL (2007) GABAA receptor RDL inhibits *Drosophila* olfactory associative learning. Neuron 56:1090–1102.
Lyutova R, Selcho M, Pfeuffer M, Segebarth D, Habenstein J, Rohwedder A, Frantzmann F, Wegener C, Thum AS, Pauls D (2019) Reward signaling in a recurrent circuit of dopaminergic neurons and peptidergic Kenyon cells. Nat Commun 10:3097.
Masuda-Nakagawa LM, Ito K, Awasaki T, O'Kane CJ (2014) A single GABAergic neuron mediates feedback of odor-evoked signals in the mushroom body of larval *Drosophila*. Front Neural Circuits 8:35.
Mayseless O, Berns DS, Yu XM, Riemensperger T, Fiala A, Schuldiner O (2018) Developmental coordination during olfactory circuit remodeling in *Drosophila*. Neuron 99:1204–1215.e5.
Meissner GW, Grimm JB, Johnston RM, Sutcliffe B, Ng J, Jefferis GS, Cachero S, Lavis LD, Malkesman O (2018) Optimization of fluorophores for chemical tagging and immunohistochemistry of *Drosophila* neurons. PLoS One 13:e0200759.
Michels B, Saumweber T, Biernacki R, Thum J, Glasgow RD, Schleyer M, Chen YC, Eschbach C, Stocker RF, Toshima N, Tanimura T, Louis M, Arias-Gil G, Marescotti M, Benfenati F, Gerber B (2017) Pavlovian conditioning of larval *Drosophila*: an illustrated, multilingual, hands-on manual for odor-taste associative learning in maggots. Front Behav Neurosci 11:45.
Neckameyer WS, White K (1993) *Drosophila* tyrosine hydroxylase is encoded by the pale locus. J Neurogenet 8:189–199.
Neuser K, Husse J, Stock P, Gerber B (2005) Appetitive olfactory learning in *Drosophila* larvae: effects of repetition, reward strength, age, gender, assay type and memory span. Anim Behav 69:891–898.
Nicolaï LJ, Ramaekers A, Raemaekers T, Drozdzecki A, Mauss AS, Yan J, Landgraf M, Annaert W, Hassan BA (2010) Genetically encoded dendritic marker sheds light on neuronal connectivity in *Drosophila*. Proc Natl Acad Sci USA 107:20553–20558.
Ohyama T, Schneider-Mizell CM, Fetter RD, Aleman JV, Franconville R, Rivera-Alba M, Mensh BD, Branson KM, Simpson JH, Truman JW, Cardona A, Zlatic M (2015) A multilevel multimodal circuit enhances action selection in *Drosophila*. Nature 520:633–639.
Owald D, Felsenberg J, Talbot CB, Das G, Perisse E, Huetteroth W, Waddell S (2015) Activity of defined mushroom body output neurons underlies learned olfactory behavior in *Drosophila*. Neuron 86:417–427.
Paisios E, Rjosk A, Pamir E, Schleyer M (2017) Common microbehavioral 'footprint' of two distinct classes of conditioned aversion. Learn Mem 24:191–198.
Papadopoulou M, Cassenaer S, Nowotny T, Laurent G (2011) Normalization for sparse encoding of odors by a wide-field interneuron. Science 332:721–725.
Pfeiffer BD, Ngo TT, Hibbard KL, Murphy C, Jenett A, Truman JW, Rubin GM (2010) Refinement of tools for targeted gene expression in *Drosophila*. Genetics 186:735–755.
Pitman JL, Huetteroth W, Burke CJ, Krashes MJ, Lai SL, Lee T, Waddell S (2011) A pair of inhibitory neurons are required to sustain labile memory in the *Drosophila* mushroom body. Curr Biol 21:855–861.
Prisco L, Deimel SH, Yeliseyeva H, Fiala A, Tavosanis G (2021) The anterior paired lateral neuron normalizes odour-evoked activity in the *Drosophila* mushroom body calyx. Elife 10:e74172.
R Core Team (2016) R: a language and environment for statistical computing. Vienna: R Foundation for Statistical Computing. Available at https://www.R-project.org/.
Ray S, Aldworth ZN, Stopfer MA (2020) Feedback inhibition and its control in an insect olfactory circuit. Elife 9:e53281.
Ren Q, Li H, Wu Y, Ren J, Guo A (2012) A GABAergic inhibitory neural circuit regulates visual reversal learning in *Drosophila*. J Neurosci 32:11524–11538.
Rohwedder A, Wenz NL, Stehle B, Huser A, Yamagata N, Zlatic M, Truman JW, Tanimoto H, Saumweber T, Gerber B, Thum AS (2016) Four individually identified paired dopamine neurons signal reward in larval *Drosophila*. Curr Biol 26:661–669.
Ryglewski S, Vonhoff F, Scheckel K, Duch C (2017) Intra-neuronal competition for synaptic partners conserves the amount of dendritic building material. Neuron 93:632–645.e6.
Saalfeld S, Cardona A, Hartenstein V, Tomancak P (2009) CATMAID: collaborative annotation toolkit for massive amounts of image data. Bioinformatics 25:1984–1986.
Saumweber T, Husse J, Gerber B (2011) Innate attractiveness and associative learnability of odors can be dissociated in larval *Drosophila*. Chem Senses 36:223–235.
Saumweber T, Rohwedder A, Schleyer M, Eichler K, Chen YC, Aso Y, Cardona A, Eschbach C, Kobler O, Voigt A, Durairaja A, Mancini N, Zlatic M, Truman JW, Thum AS, Gerber B (2018) Functional architecture of reward learning in mushroom body extrinsic neurons of larval *Drosophila*. Nat Commun 9:1104.
Scheffer LK, et al. (2020) A connectome and analysis of the adult *Drosophila* central brain. Elife 9:e57443.
Scherer S, Stocker RF, Gerber B (2003) Olfactory learning in individually assayed *Drosophila* larvae. Learn Mem 10:217–225.
Schindelin J, et al. (2012) Fiji: an open-source platform for biological-image analysis. Nat Methods 9:676–682.
Schlegel P, Texada MJ, Miroschnikow A, Schoofs A, Hückesfeld S, Peters M, Schneider-Mizell CM, Lacin H, Li F, Fetter RD, Truman JW, Cardona A, Pankratz MJ (2016) Synaptic transmission parallels neuromodulation in a central food-intake circuit. Elife 5:e16799.
Schleyer M, Saumweber T, Nahrendorf W, Fischer B, von Alpen D, Pauls D, Thum A, Gerber B (2011) A behavior-based circuit model of how outcome expectations organize learned behavior in larval *Drosophila*. Learn Mem 18:639–653.
Schleyer M, Miura D, Tanimura T, Gerber B (2015a) Learning the specific quality of taste reinforcement in larval *Drosophila*. Elife 4:e04711.
Schleyer M, Reid SF, Pamir E, Saumweber T, Paisios E, Davies A, Gerber B, Louis M (2015b) The impact of odor–reward memory on chemotaxis in larval *Drosophila*. Learn Mem 22:267–277.
Schleyer M, Fendt M, Schuller S, Gerber B (2018) Associative learning of stimuli paired and unpaired with reinforcement: evaluating evidence from maggots, flies, bees, and rats. Front Psychol 9:1494.
Schleyer M, Weiglein A, Thoener J, Strauch M, Hartenstein V, Kantar Weigelt M, Schuller S, Saumweber T, Eichler K, Rohwedder A, Merhof D, Zlatic M, Thum AS, Gerber B (2020) Identification of dopaminergic neurons that can both establish associative memory and acutely terminate its behavioral expression. J Neurosci 40:5990–6006.
Schneider-Mizell CM, Gerhard S, Longair M, Kazimiers T, Li F, Zwart MF, Champion A, Midgley FM, Fetter RD, Saalfeld S, Cardona A (2016) Quantitative neuroanatomy for connectomics in *Drosophila*. Elife 5:e12059.
Selcho M, Pauls D, Han KA, Stocker RF, Thum AS (2009) The role of dopamine in *Drosophila* larval classical olfactory conditioning. PLoS One 4:e5897.
Selcho M, Millán C, Palacios-Muñoz A, Ruf F, Ubillo L, Chen J, Bergmann G, Ito C, Silva V, Wegener C, Ewer J (2017) Central and peripheral clocks are coupled by a neuropeptide pathway in *Drosophila*. Nat Commun 8:15563.
Sens KL, Zhang S, Jin P, Duan R, Zhang G, Luo F, Parachini L, Chen EH (2010) An invasive podosome-like structure promotes fusion pore formation during myoblast fusion. J Cell Biol 191:1013–1027.
Slater G, Levy P, Chan KL, Larsen C (2015) A central neural pathway controlling odor tracking in *Drosophila*. J Neurosci 35:1831–1848.
Strauch M, Hartenstein V, Andrade IV, Cardona A, Merhof D (2018) Annotated dendrograms for neurons from the larval fruit fly brain. In: Eurographics workshop on visual computing for biology and medicine (Puig Puig A, Schultz T, Vilanova A, eds). Goslar: Eurographics.
Sutcliffe B, Ng J, Auer TO, Pasche M, Benton R, Jefferis GS, Cachero S (2017) Second-generation *Drosophila* chemical tags: sensitivity, versatility, and speed. Genetics 205:1399–1408.

Takemura SY, et al. (2017) A connectome of a learning and memory center in the adult *Drosophila* brain. Elife 6:e26975.

Tanaka NK, Tanimoto H, Ito K (2008) Neuronal assemblies of the *Drosophila* mushroom body. J Comp Neurol 508:711–755.

Thane M, Viswanathan V, Meyer TC, Paisios E, Schleyer M (2019) Modulations of microbehaviour by associative memory strength in *Drosophila* larvae. PLoS One 14:e0224154.

Thum AS, Gerber B (2019) Connectomics and function of a memory network: the mushroom body of larval *Drosophila*. Curr Opin Neurobiol 54:146–154.

Thoener J, König C, Weiglein A, Toshima N, Mancini N, Amin F, Schleyer M (2021) Associative learning in larval and adult *Drosophila* is impaired by the dopamine synthesis inhibitor 3-Iodo-L-tyrosine. Biol Open 10: bio058198.

Thoener J, Weiglein A, Gerber B, Schleyer M (2022) Optogenetically induced reward and 'frustration' memory in larval *Drosophila*. J Exp Biol 225: jeb244565.

Turrel O, Goguel V, Preat T (2018) Amnesiac is required in the adult mushroom body for memory formation. J Neurosci 38:9202–9214.

Waddell S, Armstrong JD, Kitamoto T, Kaiser K, Quinn WG (2000) The amnesiac gene product is expressed in two neurons in the *Drosophila* brain that are critical for memory. Cell 103:805–813.

Weber D, Richter V, Rohwedder A, Großjohann A, Thum AS (2023) The analysis of aversive olfactory–taste learning and memory in *Drosophila* larvae. Cold Spring Harb Protoc 2023:108050.

Weiglein A, Gerstner F, Mancini N, Schleyer M, Gerber B (2019) One-trial learning in larval *Drosophila*. Learn Mem 26:109–120.

Weiglein A, Thoener J, Feldbruegge I, Warzog L, Mancini N, Schleyer M, Gerber B (2021) Aversive teaching signals from individual dopamine neurons in larval *Drosophila* show qualitative differences in their temporal 'fingerprint.' J Comp Neurol 529:1553–1570.

Widmann A, Artinger M, Biesinger L, Boepple K, Peters C, Schlechter J, Selcho M, Thum AS (2016) Genetic dissection of aversive associative olfactory learning and memory in *Drosophila* larvae. PLoS Genet 12: e1006378.

Widmann A, Eichler K, Selcho M, Thum AS, Pauls D (2018) Odor-taste learning in *Drosophila* larvae. J Insect Physiol 106:47–54.

Wu CL, Shih MF, Lai JS, Yang HT, Turner GC, Chen L, Chiang AS (2011) Heterotypic gap junctions between two neurons in the *Drosophila* brain are critical for memory. Curr Biol 21:848–854.

Wu CL, Shih MF, Lee PT, Chiang AS (2013) An octopamine-mushroom body circuit modulates the formation of anesthesia-resistant memory in *Drosophila*. Curr Biol 23:2346–2354.

Wu Y, Ren Q, Li H, Guo A (2012) The GABAergic anterior paired lateral neurons facilitate olfactory reversal learning in *Drosophila*. Learn Mem 19:478–486.

Yamagata N, Ezaki T, Takahashi T, Wu H, Tanimoto H (2021) Presynaptic inhibition of dopamine neurons controls optimistic bias. Elife 10:e64907.

Yu D, Baird MA, Allen JR, Howe ES, Klassen MP, Reade A, Makhijani K, Song Y, Liu S, Murthy Z, Zhang SQ, Weiner OD, Kornberg TB, Jan YN, Davidson MW, Shu X (2015) A naturally monomeric infrared fluorescent protein for protein labeling in vivo. Nat Methods 12:763–765.

Zheng Z, et al. (2018) A complete electron microscopy volume of the brain of adult *Drosophila melanogaster*. Cell 174:730–743.e22.

Zhou M, Chen N, Tian J, Zeng J, Zhang Y, Zhang X, Guo J, Sun J, Li Y, Guo A, Li Y (2019) Suppression of GABAergic neurons through D2-like receptor secures efficient conditioning in *Drosophila* aversive olfactory learning. Proc Natl Acad Sci USA 116:5118–5125.